STRENGTH AND DEFORMATION BEHAVIOUR OF ECCENTRICALLY LOADED SQUARE CONCRETE FILLED STEEL TUBULAR COLUMNS

RUBIEYAT BIN ALI

MASTER OF SCIENCE IN CIVIL ENGINERING (STRUCTURAL)

DEPARTMENT OF CIVIL ENGINEERING

BANGLADESH UNIVERSITY OF ENGINEERING AND TECHNOLOGY

DHAKA, BANGLADESH

SEPTEMBER 2019

STRENGTH AND DEFORMATION BEHAVIOUR OF ECCENTRICALLY LOADED SQUARE CONCRETE FILLED STEEL TUBULAR COLUMNS

by

RUBIEYAT BIN ALI

(Student No: 0417042326F)

A thesis submitted to the Department of Civil Engineering of Bangladesh University of Engineering and Technology, Dhaka in partial fulfillment of the requirement for the degree of
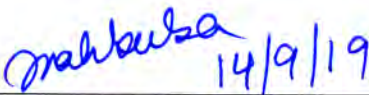
MASTER OF SCIENCE IN CIVIL ENGINERING (STRUCTURAL)

DEPARTMENT OF CIVIL ENGINEERING

BANGLADESH UNIVERSITY OF ENGINEERING AND TECHNOLOGY

DHAKA, BANGLADESH

SEPTEMBER 2019

CERTIFICATE OF APPROVAL

The thesis titled **"Strength and Deformation Behaviour of Eccentrically Loaded Square Concrete Filled Steel Tubular Columns"** submitted by Rubieyat Bin Ali, Student Number: 0417042326F, Session: April, 2017 has been accepted as satisfactory in partial fulfillment of the requirement for the degree of Master of Science in Civil Engineering (Structural) on 14th September, 2019.

BOARD OF EXAMINERS
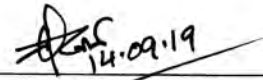
1. **Dr. Mahbuba Begum**
    Professor
    Department of Civil Engineering
    BUET, Dhaka-1000

    Chairman
    (Supervisor)

2. **Dr. Ahsanul Kabir**
    Professor and Head
    Department of Civil Engineering
    BUET, Dhaka-1000

    Member
    (Ex-Officio)

3. **Dr. Raquib Ahsan**
    Professor
    Department of Civil Engineering
    BUET, Dhaka-1000

    Member

4. **Dr. Md. Nazrul Islam**
    Professor
    Department of Civil Engineering
    DUET, Gazipur-1707

    Member
    (External)

DECLARATION

Except for the contents where specific references have been made to the work of others, the studies embodied in this dissertation are the outcome of the research conducted by the author. No part of this dissertation has been submitted to any other University or other educational establishment for a Degree, Diploma or other qualification (except for publication).

Rubieyat Bin Ali
14.09.19

Rubieyat Bin Ali

Dedicated

To

My Beloved Parents

ACKNOWLEDGEMENT

ABSTRACT

Concrete filled steel tubular (CFST) column, comprising a hollow steel tube infilled with concrete with or without additional reinforcements or steel section, has been widely used in high rise building construction. The main advantage of CFST column is that the local buckling of the outer steel tube is delayed or even prevented by the concrete core while the inner concrete core is confined by the steel tube providing enhancement in strength and ductility under high compressive load. Extensive experimental and numerical studies have been carried out by several researchers on concentrically and eccentrically loaded CFST columns with various geometric and material properties. Most of this research work has been performed on CFST columns constructed with available standard tube shapes. However, limited research has been found on CFST columns in built-up steel sections. Current design rules for CFST columns are specified in AISC-LRFD (2010), Eurocode 4 (1994), ACI 318R (2014), British standard BS 5400 (2005) and Canadian Standard Association CSA (2009). But the design of eccentrically loaded CFST column is highly conservative in the available design codes due to the lacking of experimental research. CFST column is a new system for the construction industry of Bangladesh. In the upcoming version of Bangladesh National Building Code (BNBC 2017), the design guidelines for CFST columns are included which is adopted from AISC 2005 specifications. The applicability of these design provisions in the construction environment of Bangladesh needs to be explored. To this end, an attempt has been made in this study to investigate the strength and failure behaviour of the eccentrically loaded square CFST columns constructed with built-up steel section and locally available materials.

This paper presents an experimental investigation on the behaviour of eccentrically loaded CFST columns regarding four parameters: concrete compressive strength (f_c'): 27 Mpa to 44 Mpa; cross sectional slenderness ratio (B/t): 25 to 42; global slenderness ratio (L/B): 3 to 10 and load eccentricity ratio (e/B): 0 to 0.45. Total eleven CFST columns with square cross section were tested under uniaxial eccentric compression. The influences of these parameters on the failure mode, load-strain response, peak load, ultimate moment, mid-height deflection and performance indexes of the square CFST column were investigated. Finally, the design approaches adopted in (Eurocode 4 and AISC-LRFD 2010) were reviewed and applied to calculate the ultimate axial strength and moment of the tests columns. Subsequently, the predicted values were compared with the experimental results obtained from the experiments.

Based on the results, it was observed that concrete compressive strength (f_c'), cross sectional slenderness ratio (B/t), global slenderness ratio (L/B) and load eccentricity ratio (e/B) have significant effects on the load and deformation behavior of eccentrically loaded CFST columns. Stiffness and ultimate capacity of the tested column decreased with the increase of cross-sectional width to tube thickness ratio and load eccentricity ratio, whilst they increased with the increase of concrete compressive strength and the decrease of global slenderness ratio of the specimen. On the other hand, Axial strain at peak load and ductility index of the tested specimen decreased with the increase of concrete compressive strength, B/t ratio and L/B ratio but increased with the increase of e/B ratio of the specimen. However, Ultimate bending moment of the tested column increased with the increase of f_c' and e/B ratio, but decreased with the increase of B/t ratio and L/B ratio of the specimen. Eurocode 4 (2005) somewhat overestimated the ultimate axial strengths, but underestimated the ultimate bending moments of the tested square CFST columns in built-up steel sections, whilst AISC-LFRD (2010) presented the best and safe prediction for both of them. Eurocode 4 (2005) predicted higher capacity than the experimental results about 6%. In general, both codes showed good agreement with the experimental results.

TABLE OF CONTENTS

LIST OF TABLES

LIST OF FIGURES

ABBREVIATION

ACI   American Concrete Institute

AISC   American Institute of Steel Construction

AS   Australian code

B   Width of column

BNBC   Bangladesh National Building Code

BS   British standard

CES   Concrete encased steel

CFDST   Concrete filled double skin steel tubular column

CFST   Concrete filled steel tube

CFT   Concrete filled tube

CHS   Circular hollow section

CSA   Canadian Standard Association

EC4   Eurocode 4

H   Cross-sectional height of column

HPS   High performance steel

HST   Hollow steel tube

HT   Hollow tube

L   Length of column

LVDT   Linear variable differential transducer

OPC   Ordinary Portland cement

RC   Reinforced concrete

RHS   Rectangular hollow section

S-CFT   Stiffened concrete filled slender steel tube

SHS   Square hollow section

SRC   Steel reinforced concrete

TSRC   Tubed steel reinforced concrete

UTM   Universal testing machine

NOTATION

A_c	Area of concrete
A_s	Area of steel
B/t	Column cross-sectional slenderness ratio
e	Eccentricity
e/B	Load eccentricity ratio
E_c	Elasticity modulus of concrete
EI_{eff}	Effective stiffness of composite section
E_s	Modulus of elasticity of steel
$f_c^{/}$	Concrete compressive strength
f_u	Ultimate stress
f_y	Yield stress
f_y	Specified minimum yield stress of steel section
f_{ysr}	Specified minimum yield stress of reinforcing bars
K	Effective length factor
L	Laterally unbraced length of the member
L/B	Column global slenderness ratio
M_{um}	Ultimate moment
P_u	Ultimate load of the tested column
t	Thickness of steel
W_c	Weight of concrete per unit volume
α_c	Strength reduction factor
δ_m	Mid-height deflection at peak load
ε_u	Ultimate strain
ε_y	Yield strain
λ	Slenderness reduction factor
ξ_c	Concrete contribution ratio

ξ_s Steel contribution ratio

p_e Elastic critical buckling load

p_{no} Nominal compressive strength of axially loaded composite member

Chapter 1

INTRODUCTION

1.1   General

Concrete filled steel tubular (CFST) column, comprising a hollow steel tube infilled with concrete with or without additional reinforcements or steel section, has been widely used in high rise building construction. The main advantage of CFST column is that the local buckling of the outer steel tube is delayed or even prevented by the concrete core while the inner concrete core is confined by the steel tube providing enhancement in strength and ductility under high compressive load. The steel tube can serve as permanent formwork for concrete casting and thus it eliminates the need of additional work and leads to fast track construction. The CFST columns have various composite cross-sections as shown in Figure 1.1. Circular, square and rectangular sections are commonly adopted while polygonal or elliptical sections also may be used for architectural and functional requirements. Conventionally, only plain concrete is filled into the hollow steel sections. Nowadays, the concrete core may be reinforced by fibres or steel bars to enhance ductility and fire resistance of the column. For convenience, the reinforcements can be replaced by an internal steel tube which can provide higher confinement to the concrete core. Other steel sections, such as solid steel section or H-section, can be inserted into the concrete core to further enhance the compression resistance and thus reduce the column size. For columns subjected to high flexural loading, concrete filled double-tube sections can be used to increase the flexural stiffness with less material used. Actually Figure 1.1 (a) depicts three typical column cross-sections, where the concrete is filled in a circular hollow section (CHS), a square hollow section (SHS) or a rectangular hollow section (RHS), where D and B are the outer dimensions of the steel tube and t is the wall thickness of the tube. It is noted that the circular cross section provides the strongest confinement to the core concrete, and the local buckling is more likely to occur in square or rectangular cross-sections. However, the concrete-filled steel tubes with SHS and RHS are still increasingly used in construction, for the reasons of being easier in beam-to-column connection design, high cross-sectional bending

stiffness and for aesthetic reasons. Other cross-sectional shapes have also been used for aesthetical purposes, such as polygon, round-ended rectangular and elliptical shapes, as shown in Figure 1.1 (b).

(a)

(b)
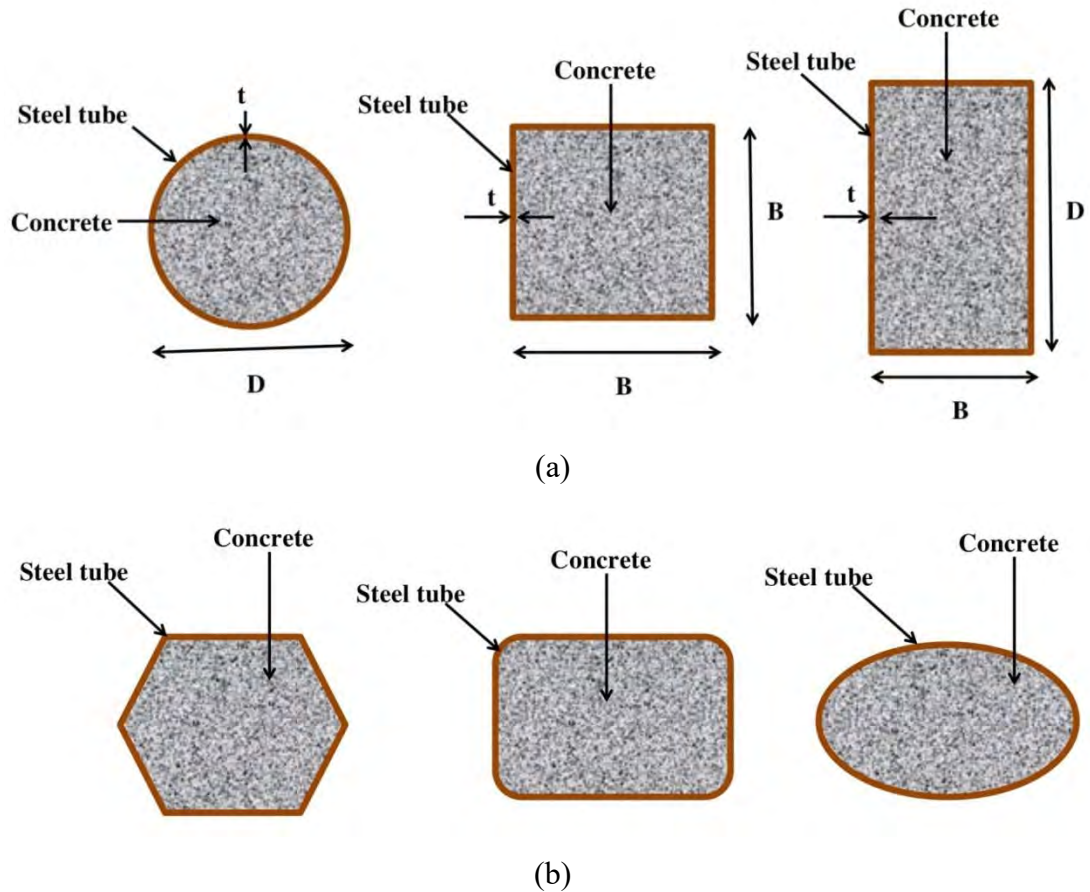
Figure 1.1 Typical concrete filled steel tubular cross sections

In the case of steel and concrete, the best properties would be the tensile capacity of the steel and the compressive capacity of the concrete. A reinforced concrete (RC) structure is a typical application to utilize the advantage of concrete in compression and steel in tension. In addition, a steel-concrete composite structure integrates the respective advantages of both steel and concrete. For example, concrete-filled steel tubes (CFSTs), one of the typical steel-concrete composite structures, combine the full advantages of concrete and steel. Concrete filled steel tube (CFST) column consists of a hollow steel tube filled with concrete. This composite section offers numerous structural benefits over reinforced concrete and steel only sections, including high strength, high ductility and large energy absorption capacities.

During concreting, there is no need for the use of shuttering in CFST structures; hence, the construction cost and time are reduced. In CFST columns the steel tube not only serves as formwork but also provides continuous confinement to concrete core resulting in enhanced strength and ductility of concrete. CFST column reduces the traditional columns" section size. And its seismic behaviour, fire resistance capability and construction ability are excellent. And the long-term behavior of this column is also good. Here long-term behavior means creep and shrinkage of concrete. These advantages have been widely exploited and have led to the extensive use of concrete-filled tubular structures in high rise buildings, bridges and offshore structures (Sakino et al., 2004; Shanmugam and Lakshmi, 2001; Susantha et al., 2001).

The CFST columns increase earthquake resistant capabilities due to the concrete filling inside the steel tubes and are particularly suitable for buildings subjected to large axial compressive stress. Moreover, the columns are also fire resistant and reduce the thickness of or even eliminate the need for, traditional fire-resistant coating. Thus simplifying the construction process and increasing interior space in a building. As a result, the CFST column method is seen as the fourth construction method, which will improve the performance of the conventional Reinforced Concrete (RC), Steel-Reinforced Concrete (SRC) and Steel (S) columns.

Conventional structures like RC, SRC and S structures can be replaced by CFST structure system with a high degree of generality and at the same time reducing costs to a minimum. It is especially useful in high-rise buildings where high work speed is required and flexibility of open space is desired for a maximum range of applications. CFST columns may be used in a situation where the cross sections of RC columns are unacceptably large. There are numerous applications for which some of composite columns provide excellent solution to structural problems when compared with steel column. The composite column has superior load retention at higher temperature, more resistance to local buckling, greater stiffness and abrasion resistance when compared with RC column. The composite column supports more thrust than any other traditional reinforced concrete column of the same dimension.

Extensive experimental and numerical studies have been carried out by several researchers (Han et al., 2014; Sakino et al., 2004; Susantha et al., 2001; Xiamuxi and Hasegawa, 2012; Zeghiche and Chaoui, 2005; Zhu et al., 2010) on concentrically and eccentrically loaded CFST columns with various geometric and material properties. Most of this research work has been performed on CFST columns constructed with available standard tube shapes. However, limited research has been found on CFST columns in built-up steel sections. Current design rules for CFST columns are specified in AISC-LRFD (2010), ACI 318R (2014), Eurocode 4 (1994), British standard BS 5400 (2005) and Canadian Standard Association CSA (2009). But the design of eccentrically loaded CFST column is highly conservative in the available design codes due to the lacking of experimental research. CFST column is a new system for the construction industry of Bangladesh. In the upcoming version of Bangladesh National Building Code (BNBC 2017), the design guidelines for CFST columns are included which is adopted from AISC 2005 specifications. The applicability of these design provisions in the construction environment of Bangladesh needs to be explored. To this end, an attempt has been made in this study to investigate the strength and failure behaviour of the eccentrically loaded square CFST columns constructed with built-up steel section and locally available materials.

1.2   Objectives and Scope of the Study

The objectives of this study are listed below:
  i.   To investigate the strength and behaviour of square CFST columns under eccentric axial load.
  ii.   To study the effect of concrete strength, plate slenderness ratio, column overall slenderness ratio and the variation of eccentricities on the strength and ductility of CFST columns.
  iii. To compare the experimental results with the code predicted capacities for CFST columns subjected to eccentric axial load.

To achieve the above objectives, total 11 square CFST column specimens were tested under uniaxial eccentric loading condition. The test columns had cross-

sectional dimensions of 100 mm x 100 mm, 125 mm x 125 mm and 150 mm x 150 mm and lengths of 1000 mm, 500 mm and 300 mm. These sections were built-up with two channel sections. The tube was fabricated by joining two channels through continuous welding. Two steel plates (200 mm x 200 mm x 25mm) were welded to the bottom and top of each specimen for uniform distribution of the applied load. Concrete was poured vertically into these hollow tubes and vibrator was used for proper compaction of concrete. Specimens with different values of concrete compressive strength ($f_c^{/} = 27$, 35 and 44 MPa), width to thickness ratio (B/t ranging from 25 to 42), length to width ratio (L/B ranging from 3 to 10) and eccentricity to width ratio (e/B = 0, 0.30 and 0.45) were constructed and tested under eccentric axial load by both end knife edge setups under a universal testing machine (UTM). The effects of these parameters on the strength and failure behaviour of CFST columns were investigated. Finally, the experimental results were compared with the code predicted capacities.

1.3   Organization of the Thesis

This thesis is divided into six chapters. An overview of each chapter follows.

Chapter 1 It includes the research background, objectives and the scope of the study.

Chapter 2 presents a brief review on the literature related to both concentrically and eccentrically loaded CFST columns and explores in relative detail research works carried out on CFST columns.

Chapter 3 contains the details of description of experimental specimens, material properties, fabrication of specimens and test module. A description of the instrumentation, end fixtures and loading condition is also included.

Chapter 4 represents all the output of this study which includes the failure mode, load-strain response, mid-height deflection and performance indexes of tested columns.

The design guidelines along with the capacity and moment prediction equations for eccentrically loaded CFST columns are presented in **Chapter 5**. This chapter also includes the comparison of experimental and code predicted results with the two design codes AISC-LRFD (2010) and Eurocode 4 (2005).

Finally, the summary and conclusions of the work along with the recommendations for future research have been included in **Chapter 6**.

Chapter 2
LITERATURE REVIEW

2.1   Introduction

Concrete Filled Steel Tube (CFST) is the composite section formed by filling concrete into a hollow steel tube. The CFST section resists applied load through the composite action of concrete and steel, this advantageous interactive behaviour between steel tubes and concrete increases the strength of CFST section. Hence, it has become popular in recent days and is being used in structures such as bridges, electricity towers, buildings etc. Extensive works carried out on CFST columns in past years have indicated that the CFST sections possess high ductility, strength and stiffness properties. These properties are considered to be important, especially for the multi-storied buildings required to be erected in earthquake-prone areas. Therefore, the behaviour of CFST sections needs to be studied. The research work on concrete-filled steel tubular structures can generally be classified as the research dealing with members, connections/joints and structural systems. The general research framework of CFST column is illustrated in Figure 2.1.
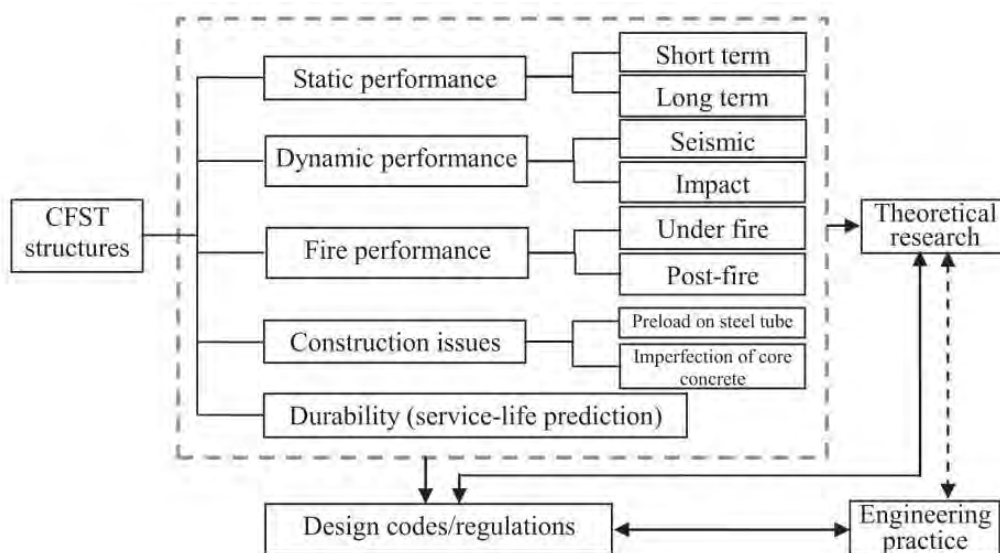
Figure 2.1   Framework of research on CFST structures

Various aspects are covered, including the static performance, the dynamic performance, the fire performance, and the construction and durability issues. The results should aim to provide design formulas and recommendations, to improve drafting of design codes or standards, and to promote the applications of these composite structures in real civil engineering projects.

In this chapter, a review of the research conducted on axially loaded CFST columns is presented with an emphasis on theoretical and experimental studies. A comparison of current design codes is also included. The review includes research work that has investigated the effect of concrete strength, plate slenderness ratio, column overall slenderness ratio and load eccentricity ratio on failure mode, load-strain response, ductility and confinement for both concentrically and eccentrically loaded CFST columns. Finally, the advantages, current developments and advanced application of CFST columns have been reviewed.

2.2 Advantages of Concrete Filled Steel Tubular (CFST) Columns

CFST columns possess many benefits over conventional steel concrete composite columns, such as (1) the steel tube acts as formwork for the concrete core and also supports a considerable amount of construction loads during construction, which results in quick and efficient construction; (2) the compressive capacity of infilled concrete is enhanced because of the confinement effect provided by steel tubes (under bi-axial or tri-axial restraint); (3) the infilled concrete delays or eliminates local buckling of the steel tube, while the steel tube confines the infilled concrete, which prevents concrete spalling and maintains tube's stiffness after concrete cracking, so that its compressive strength can be further increased; (4) composite columns have high stiffness due to the infilled concrete.

It is well known that the compressive strength of concrete is much higher than its tensile strength. Furthermore, the compressive strength is enhanced under bi-axial or tri-axial restraint. For the structural steel, the tensile strength is high while the shape may buckle locally under compression. In concrete filled steel tubular members, steel

and concrete are used such that their natural and most prominent characteristics are taken advantage of. The confinement of concrete is provided by the steel tube, and the local buckling of the steel tube is improved due to the support of the concrete core. Figure 2.2 shows schematic failure modes for the stub concrete filled steel tubular column and the corresponding steel tube and concrete. It can be seen that both inward and outward buckling is found in the steel tube, and shear failure is exhibited for the plain concrete stub column. For the concrete filled steel tube, only outward buckling is found in the tube, and the inner concrete fails in a more ductile fashion.
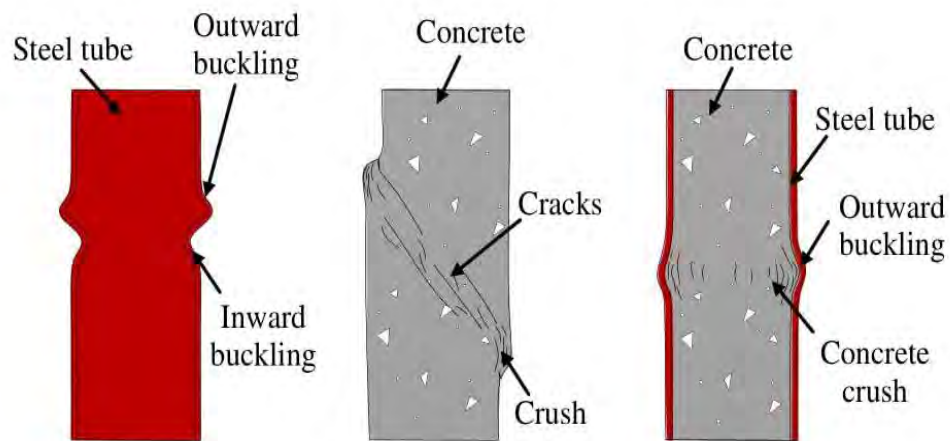
Figure 2.2   Schematic failure modes of hollow steel tube, concrete and CFST stub columns (Han et al., 2014)

Figure 2.3 shows a schematic view of the load versus deformation relationship of the hollow steel tube, the concrete stub column by itself and the concrete filled steel tube. It can be seen that the ductility of the concrete-filled steel tube is significantly enhanced, when compared to those of the steel tube and the concrete alone.
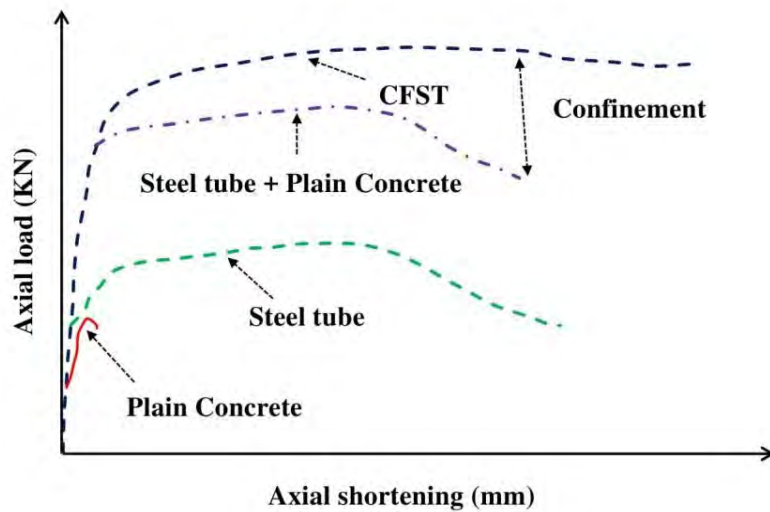
Figure 2.3 Schematic view of the axial load versus axial shortening relationship of the hollow steel tube, the concrete stub column by itself and the concrete filled steel tube (Han et al., 2014)

Extensive researches were carried out for studying the static properties of CFST over last several decades, the databases show that the CFST combine the benefits of steel and concrete, and the properties of CFST were favourable in terms of compression, tension, bending, shear and torsion. Han et al. (2014) provided the schematic failure modes for the CFST column under tension, bending and torsion, as shown in Figure 2.4. For the CFST member in tension (Figure 2.4 (a)), the steel tube is elongated under the tension, while there is a main crack through the whole cross-section in the concrete column. The tension performance of the CFST column is modified due to the interaction between steel tube and concrete, cracks are small and evenly distributed along the infilled concrete of CFST. Figure 2.4 (b) illustrates the failure mode of the steel tube, concrete and CFST subjected to bending moment. Cracks and crushes of the concrete are considerably altered as well as the buckling of the steel tube wall in the CFST column. Torsion is another significant external action. Figure 2.4 (c) shows the torsional failure deformation of each member, it is apparent that the torsional deformation of the CFST is obviously decreased compared with that of the hollow steel tube. This is because the infilled concrete resists the compressive force

and the steel tube resists the tensile force in the diagonal direction, a space "truss action" is formed and the local buckling is modified by the infilled concrete.
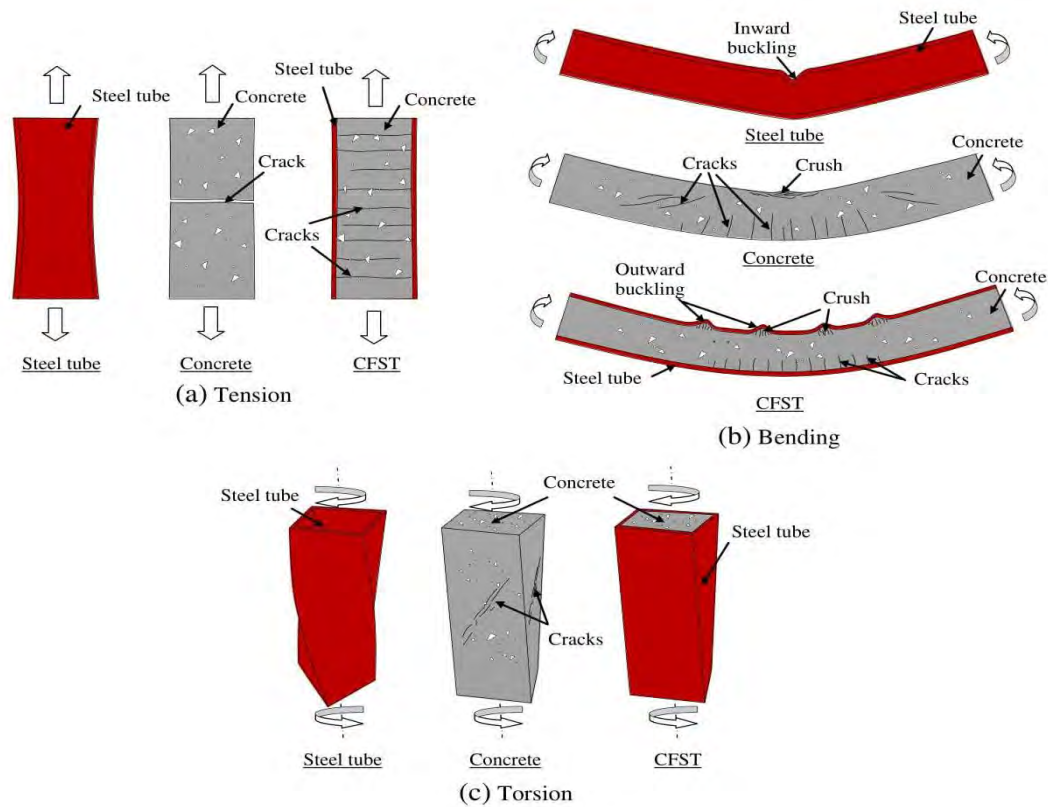
Figure 2.4 Schematic failure modes of steel tube, concrete and CFST under tension, bending and torsion (Ren et al., 2014)

2.3 Applications in Construction of Concrete Filled Steel Tubular (CFST) Columns

In recent decades, the pace of the concrete filled steel tube construction has increased rapidly. The concrete filled steel tubes are used as major compressive components or key members under various loading conditions in buildings, bridges and other structures. Some examples are presented here to provide some insight into how CFST column, currently, plays a significant role in civil engineering. In the 1980s, the concrete filled steel tube was used in buildings to avoid having a very large size column. In high-rise buildings or super high-rise buildings, the CFST composite frame structures are often combined with other lateral load resisting systems such as

11

RC core tubes or steel shear walls. The frame using concrete filled steel tubular columns integrates the high stiffness and the high ductility, and works well with the core tubes or shear walls in hybrid structural systems. Figure 2.5 shows the SEG Plaza in Shenzhen, which was one of the earliest applications of concrete filled steel tubular columns in super high-rise buildings. The main structure is 291.6 m, and CFST columns with circular cross section were used. The profile of the steel section is Φ 1600 mm $\times$ 28 mm, and Q345 steel and C60 concrete were used. When compared to the column using hollow steel section, the steel usage for the CFST column was only a half, and the use of very thick steel plate was prevented. The concrete filled steel tube with rectangular (including square) cross section also gained a popular usage in buildings, for the convenience when dealing with the connections (Han et al., 2014).

Figure 2.5 SEG plaza in Shenzhen (Han et al., 2014)
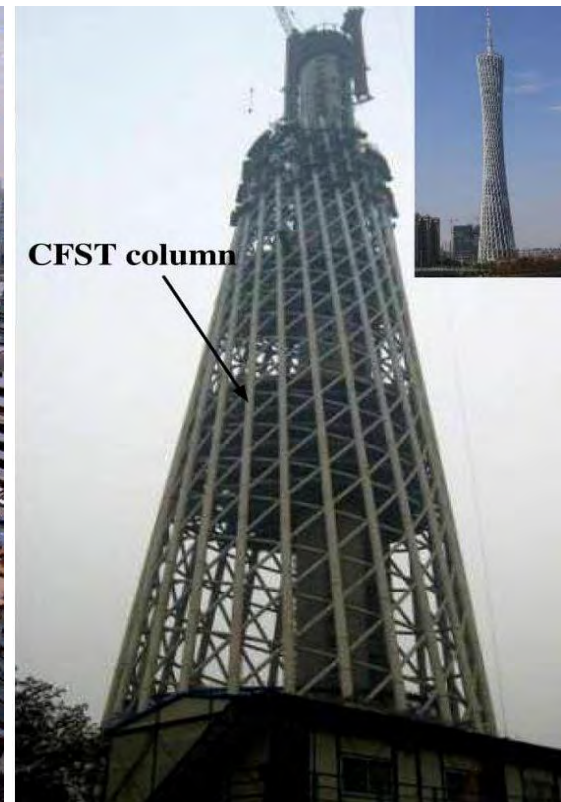
Figure 2.6 Canton Tower (Han et al., 2014)

Figure 2.6 shows the Canton Tower in Guangzhou, where the structure consists of a space lattice composite frame and a RC core. The height of the main body is 454 meters, and the pinnacle height is 600 meters. Twenty-four inclined concrete filled steel circular tubular members are utilized, with a maximum tube diameter of 2000 mm and a maximum wall thickness of 50 mm. Figure 2.7 shows Ruifeng International Commercial Building built in Hanzhou in 2001, where concrete filled steel tubular columns with square cross sections were used. The west and the east towers are 84.3 m (24 storeys) and 55.5 m (15 storeys) in height, respectively. The hybrid structural system consists of a CFST composite frame and RC shear walls. The maximum CFST column profile is 600 mm, and the maximum and minimum tube thicknesses are 28 mm and 16 mm, respectively.

Figure 2.7   Ruifeng building in Hangzhou (Yang and Han, 2011)

Concrete filled steel tubular members have been applied in many types of bridges, such as arch bridges, cable stayed bridges, suspension bridges, and truss bridges. CFST members can serve as piers, bridge towers and arches, and they can also be used in the bridge deck system. Figure 2.8 depicts the usage of CFST members in various bridge structures.
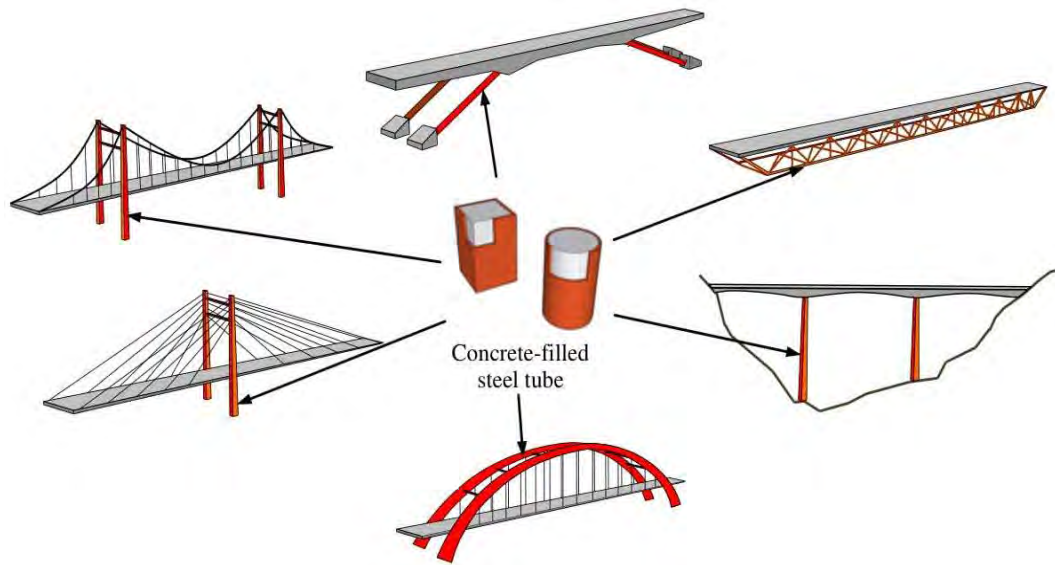
Figure 2.8 CFST used in bridges (Yang and Han, 2011)

Figure 2.9 shows one of the earliest CFST arch bridges in China, the Wangcang East River Bridge, which was built in 1992. The cross section of the main arch is in dumbbell shape, and the total depth is 2 meters. Steel tubes with a diameter of 800 mm and a thickness of 10 mm are used for upper and lower chords, and the hollow sections are filled with C30 concrete. The main span of this bridge is 115 meters. The use of concrete filled steel tube in arch bridges effectively exploits the advantages of this kind of construction. An important advantage of using CFST in an arch bridge is that, during the stage of erection, the hollow steel tubes can serve as the formwork for casting the concrete, which significantly reduces the construction cost (Ren et al., 2014). Furthermore, the composite arch can be erected without the aid of a temporary bridging due to the inherent stability of tubular structure. The hollow steel tubes can be filled with concrete to convert the system into a composite structure. Since the weight of the hollow steel tubes is comparatively small, relatively simple construction technology can be used for the erection. The most common methods include cantilever launching methods, and either horizontal or vertical "swing" methods, whereby each half arch can be rotated horizontally into position. The general CFST members such as concrete encased concrete filled steel tube are being used in bridges in China. Figure 2.10 shows the Zhaohua Jialing River Bridge in Sichuan province, China, which has a span length of 364 meters. The arch ring

14

consists of two parallel arch ribs, and each arch rib is 8 meters in width and 5.2 meters in height. The cross section of the arch rib is a double-cell concrete encased concrete filled steel tubular box one. The diameter of tubes is 451mmand filled with C80 concrete inside. A truss skeleton consisted of 6 hollow steel tubes and steel angles are established first to resist the construction load for each rib. The reinforced concrete is then attached outside the truss skeleton to form the complex composite cross section (Han et al., 2014).

Figure 2.9 Wangcang East River Bridge (Han et al., 2014)

Figure 2.10 Zhaohua Jialing River Bridge (Han et al., 2014)

Concrete filled steel tubular columns have also been used in various structures such as subway stations, workshops, electricity pylons and poles. It is well known that the columns in subway stations are usually subjected to large axial compressive loads. The concrete filled steel tubular member is suitable being used as the supporting column. Figure 2.11 (a) shows the Qianmen subway station in Beijing, which is one of the earliest applications of CFST columns. Figure 2.11 (b) shows the transportation center connecting subway line 2 and 9 in Tianjin, China, where CFST columns are connected with single or double reinforced concrete beams in the structure. The concrete filled steel tube has been used in industrial buildings in the north of China since 1970s. Single or build-up CFST members can be applied depending on the load resistance requirement (Yang and Han, 2011).
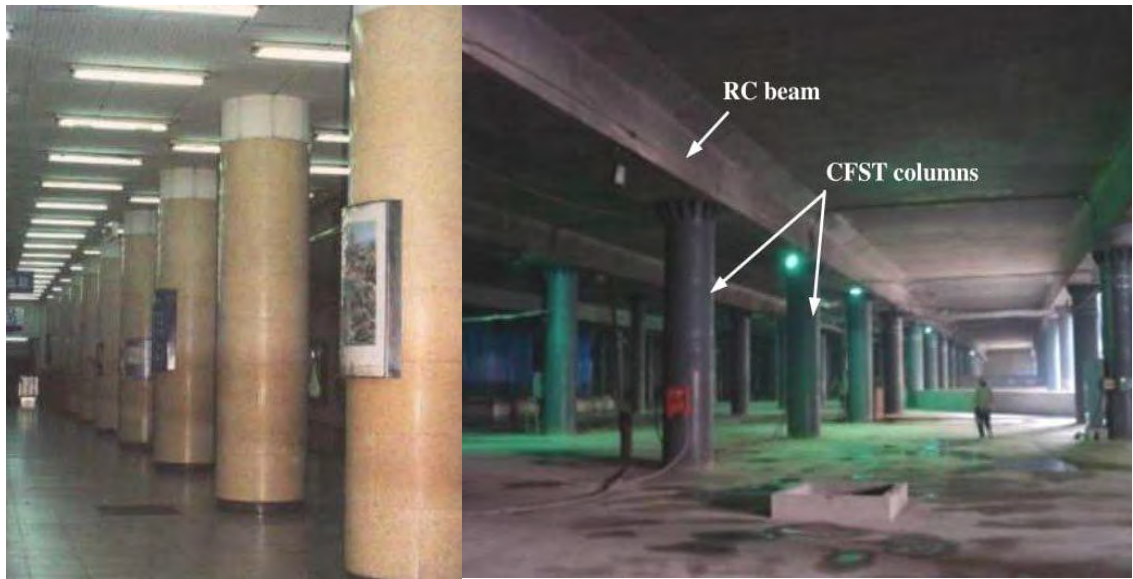
(a)　　　　　　　　　　　　　　　　　(b)

Figure 2.11　Subway stations using CFST columns (Tao and Han, 2006)

Figure 2.12 shows the concrete filled steel tubular columns used in a power plant workshop. The steel used in the CFST column is only 55% of that used in the hollow steel column for similar workshops. The concrete filled steel tubes can be used in the construction and the upgrade of poles and transmission towers as well (Han et al., 2014). Figure 2.13 shows a long-span transmission tower built in Zhoushan, China. The tower is the largest electricity pylons in the world with a height of 370 meters. This tower is a tubular lattice one with four concrete filled steel tubular columns. The diameter of the CFST column is 2000 mm, and the concrete is filled up to 210 meters height. Concrete filled double skin steel tubes are being used in electrical grid infrastructures in recent years. This composite section has high bending stiffness, and the self-weight is lighter when compared with the fully filled CFST section (Tao and Han, 2006). A photo of CFDST pole is shown in Figure 2.14. The bearing capacity of the pole is enhanced when compared to the traditional steel lattice tower, while the occupied land area is reduced and the total cost is not raised.
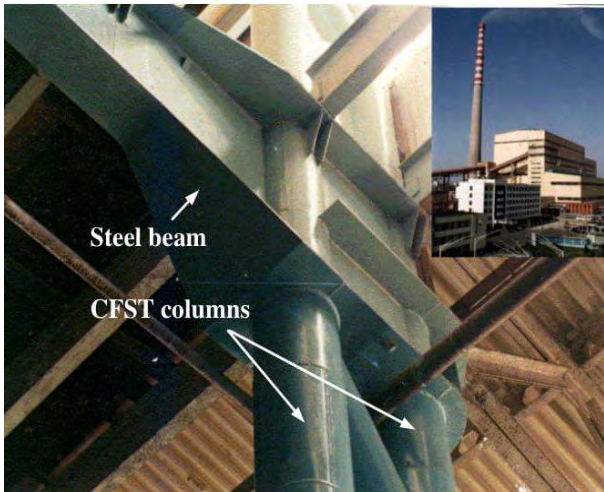
Figure 2.12 Power plant workshop using CFST columns (Ren et al., 2014)

Figure 2.13 Zhoushan electricity pylon (Ren et al., 2014)

Figure 2.14 CFDST pole (Ren et al., 2014)

2.4   Current Development of Concrete Filled Steel Tubular (CFST) Columns

Concrete filled steel tubular (CFST) columns have been widely used in engineering structures. In the past extensive experimental and numerical studies have been conducted in different parameters, namely: section type; section diameter; thickness of the steel tube; strengths of steel and core concrete; length of the column; load eccentricity, and so on (Schneider, 1998). It is commonly accepted that CFST columns have high load bearing capacity, ductility due to the confinement effect, convenience in fabrication and construction due to the steel tube acting as permanent formwork, when compared with steel and reinforced concrete columns (Han et al., 2014). Currently, several design guidelines have been developed for the design of CFST columns in different areas, such as Eurocode 4 (2004) in Europe, DBJ/T 13-51-2010 (2010) in China, AIJ (2008) in Japan, ANSI/AISC 360-10 (2010) in U.S.A. and AS 5100.6-2004 (2004) in Australia.

To further improve structural efficiency and meet different design requirements, some recent research has focused on the development of different types of novel CFST columns. One approach is aimed at using new alloys or at changing the configuration of conventional CFST columns to improve the structural performance of composite columns. The CFDST consists of inner and outer tubes, and the sandwiched concrete between two tubes. The concrete-steel-concrete sandwich cross-section has high bending stiffness that avoids instability under external pressure. Research results have shown that the inner tube provides effective support to the sandwich concrete, and the behavior of the composite member is similar to that of the concrete filled steel tube. The outward buckling of the outer tube and the inward buckling of the inner tube was observed after beam and column ultimate strength tests. The steel tubes and the concrete can work together well and the integrity of the steel-concrete interface is maintained. This composite column could also have higher fire resistance than the regular CFST columns, due to the inner tubes being protected by the sandwiched concrete during fire. The CFDST could be a good option when designing members with large cross-sections. The thickness of the steel tube wall can be reduced significantly when compared to the steel tube member

by itself, and the self-weight is less when compared to the concrete-filled steel tube. Another advantage of the CFDST is that both the outer and the inner steel tubes can act as primary reinforcement and permanent formwork, which is convenient for construction (Zhao and Grzebieta, 2002; Tao et al., 2004). In the same way, stiffened CFST columns were investigated for the feasibility of thin-walled steel tubes using in CFST columns for economical purposes, where welded stiffeners were used to reduce the effect of local buckling on the thin-wall steel tubes (Tao et al., 2005). Recently, Han et al. (2010) conducted a series of tests on inclined, tapered and straight-tapered-straight CFST columns, with the aim of potentially applying these structures which may meet the architectural requirements. Furthermore, investigations on the tapered CFDST columns have been reported by Li et al. (2012), showing that this kind of innovative composite column could be used as transmission towers.
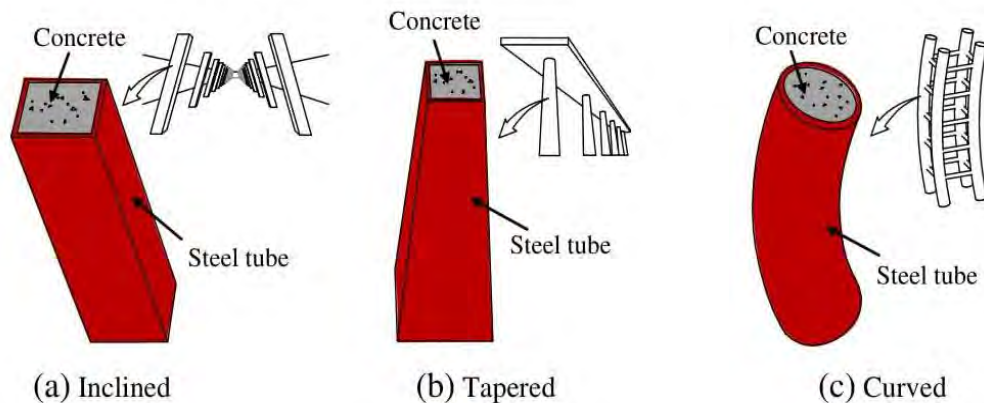
Figure 2.15   Inclined, tapered and curved CFST columns (Li et al., 2012)

Adopting high performance steel is another approach for new development of CFST columns. Therefore, high strength steel with yield strength up to 700 MPa was used in steel tubes of CFST columns and several experimental investigations were carried out in recent years (Uy, 2001; Mursi and Uy, 2004). Stainless steel was another high performance steel with high strength, as well as better corrosion resistance and hardness, which has been investigated as an outer material for CFST columns by researchers for nearly a decade (Young and Ellobody, 2006; Uy et al., 2011). On the

other hand, since concrete also plays an important role in CFST columns, various engineers and researchers have tried to use new types of concrete other than conventional concrete to construct composite columns. For example, high strength concrete (compressive strength higher than 100 MPa) or even ultra-high strength concrete (compressive strength close to 200 MPa) could significantly increase the load-carrying capacities of CFST columns (Varma et al., 2002; Yu et al., 2008; Xiong, 2012) CFST columns constructed with recycled aggregate concrete were developed to conserve natural resources and reduce landfill requirements (Yang and Han, 2006; Tam et al., 2014). The utilisation of lightweight aggregate concrete in CFST columns was proposed to reduce the structural weight significantly (Fu et al., 2011a; Fu et al., 2011b).

2.5 Experimental Investigation on Concentrically and Eccentrically Loaded CFST Columns

The behaviour of CFST columns has been the subject of numerous experimental and theoretical studies since Knowles and Park (1969). Tests have been performed on short and slender columns under a variety of axial and eccentric load conditions. Detailed experimental studies into the enhanced strength and ductility of short columns have been published. Accompanying such investigations a multitude of design models derived empirically or theoretically. Such research has lead to the implementation of CFST design provisions in several International design standards. Due to variations analytical procedures, design philosophy or empirical data-bases used, significant discrepancies exist with respect to quantifying the ultimate capacity of the composite section. This non-uniformity has emphasized the importance of further research required into the behavior of CFST columns. Table 2.1 shows the summary of past literatures on axially loaded concrete-filled steel tubular columns. Findings of these experimental studies are presented below:

Table 2.1 Experimental studies on CFST columns

Reference	Experimental Synopsis	Number of Tests	Main Parameters
Knowles and Park, 1969	Concentric and eccentric loading of columns	28 CFST (18 concentric, 10 eccentric) and 30 HST (20 concentric, 10 eccentric)	• Type of tubing • D/t • L/D • e/D
Masuo et al., 1991	Concentric testing of lightweight concrete CFST	26 CFST	• D/t • Slenderness ratio
Bergmann, 1994	Concentrically loaded circular and square CFST with different load introduction.	16 CFST	• Section shape and size • Load introduction • Length
Tsuda et al., 1996	Concentrically and eccentrically axially slender CFST	48 CFST (24 circular, 24 square) and 12 HST	• Eccentricity • Buckling length-section depth ratio (kL/D).
Shakir Khalil et al., 1997	Concentric & eccentric loading of full-scale rectangular CFST	11 CFST (concentric) and 11 CFST (eccentric)	• L/D • λ • e_x/D • e_y/D
Schneider, 1998	Monotonic axial loading of circular, square and rectangular CFST	14 CFST	• D/t • Shape
Zhang and Zou, 2000	Monotonic axial loading of CFST	36 CFST	• D/t • f_y
Han and Yan, 2001	Monotonic loading of square CFST	8 CFST (concentric) and 21 CFST (eccentric)	• f_c' • D/t • Magnitude of eccentricity • Slenderness

Fujimoto et al., 2004	CFST columns subjected to uniaxial eccentric compression	28 CFST	• e/D
Tao and Han, 2006	CFDST stub columns under axial compression and CFDST beams under four point bending test	18 CFDST stub columns and 8 CFDST beams	• Steel ratio • Slenderness ratio
Liu, 2006	Rectangular CFT columns subjected to eccentric loading	4 slender and 16 stub CFT columns	• f_y • f_c' • Slenderness ratio • e/H ratio
Uy, 2008	Concentric axial load on CFT Column.	8 CFST	
Uy, 2011	Eccentrically and concentrically loaded stainless steel CFST and HST.	33 HST (2 eccentric, 31 concentric) and 84 CFST (all concentric)	• D/t • f_c' • e
Yang and Han, 2011	CFST stub columns subjected to eccentric partial compression	28 CFST	• Section type • e/D ratio • Shape of the load bearing plate
Dundu, 2012	Concentrically loaded circular CFST columns	24 CFST	• L/D ratio • D/t ratio • f_y • f_c'
Li et al., 2013	Tapered CFDST columns under eccentric compression	12 CFDST	• e/D ratio
Kim et al., 2013	Eccentrically loaded CFT columns	6 CFT	• Sectional shape • e/D • f_y • f_c'
Qu et al., 2013	Rectangular CFST columns subjected to uniaxial and biaxial eccentric loading	17 CFST	• f_y • f_c' • B/t • e/B

Ren et al., 2014	Elliptical CFST beams and columns under bending and compression	8 CFST beams and 18 CFST columns	- Span to depth ratio - Slenderness ratio load - eccentricity ratio
Mahgub et al., 2016	Test on self compacting elliptical CFST column	8 CFST and 2 HST	$f_c^/$ - L/D
Lee et al., 2016	Thin walled CFT columns under eccentric axial loading	5 CFT	- D/t f_y - Use of stiffener
Petrus et al., 2016	Slender CFST columns subjected to uniaxial eccentric loading	26 CFST	- Load eccentricity ratio - Type of stiffener
Wang et al., 2016	TSRC columns under eccentric loading	12 short square TSRC columns	- Width-to-thickness ratio of the steel tube - Eccentricity of the axial load - Flange shear studs
Kim et al., 2017	CFT columns subjected to long term uniaxial eccentric compression	4 CFST	- Duration of load e/D f_y $f_c^/$
Kim et al., 2017	Concentric and eccentric loading of CFT columns	6 CFT	- Sectional shape f_y $f_c^/$ - Modes of stiffener

Knowles and Park (1969)

This paper investigated axially loaded CFTs and hollow tubes over a wide range of slenderness ratios, with particular attention paid to the effect of the slenderness ratio on the lateral pressure exerted by the tube on the concrete. The authors also looked at the effect of loading the materials together and individually (i.e., load the concrete and not the steel and vice versa). They examined concentrically loaded columns theoretically by the tangent modulus approach and they constructed a straight line interaction formula to estimate the behavior of eccentrically loaded CFTs.

All of the hollow tubes tested under axial loads failed by inelastic flexural buckling; no local buckling was observed before the ultimate load was reached. Since local buckling is often sudden and catastrophic, the authors suggested that the ratio of the wall thickness to the diameter of the tube should be limited, although no specific values were given. The concrete-filled tubes failed in the same manner as the hollow tubes, with the region of plasticity always located at mid height. It was noted that the square tube columns with small slenderness ratios did not gain additional strength due to confinement. Although it has been shown by other investigators that square tubes provide less confinement than circular tubes, square ties in reinforced concrete have produced good confinement results. The authors stated that the issue of square tube confinement has yet to be resolved.

Masuo et al. (1991)

The buckling behavior of CFT columns was studied both experimentally and analytically, using both lightweight and normal weight concrete subjected to concentric axial load. Ultimate loads were discussed with regard to three parameters: concrete weight, size of the steel tube, and effective column length.

The initial deflection at mid-height for columns in this range of slenderness ratios was computed as the deflection of the column before the test divided by the effective length. In the tests, an initial deflection of L/4000 or L/8000 was used, the higher number for more slender columns. The authors found that both weights of concrete with slenderness factors around 0.3 were definitely affected by confinement, the

normal weight concrete showing a somewhat larger effect. The load-deflection relations were also significantly affected by the confining effect in this range of slenderness factors. Several detailed graphs elucidate this point. Varying the D/t ratio from 30-40 and holding the other test parameters constant did not seem to affect the squash load. Finally, the ultimate loads of the CFTs for both weights at a slenderness factor of 0.6 were somewhat larger than the European column curve.

Bergmann (1994)

Sixteen tests were performed to investigate the behavior of CFT columns with high strength concrete under various methods of load introduction. The specimens that were loaded only on a small portion of the concrete experienced local failures at the point of load application and exhibited lower strength than the other specimen. The strength of three of the four specimens with the larger circular cross-section exceeded the capacity of the testing machine and only a lower bound of load was determined. The load deformation curves of the remaining specimens exhibited similar traits. Most notably, upon reaching ultimate load, the strength decreased suddenly, followed by a relatively constant strength.

Tsuda et al. (1996)

An experimental study conducted on circular and square CFT beam-columns was presented in two companion papers (see also Matsui et al. 1995). The behavior of CFT specimens was examined under axial loading and combined axial and flexural loading. Columns having a wide range of L/D ratios were tested. The experimental results were compared with AIJ (1987, 1990) and CIDECT (1994) design code provisions.

It was observed that the specimens having a higher magnitude of eccentricity exhibited lower axial strength and larger mid-height deflection. The effect of eccentricity decreased for high L/D ratios. The columns with L/D ratios less than 18 achieved the plastic moment capacity. The circular specimens in this range even exhibited larger capacities due to the confinement effect. For square specimens, the

confinement effect was not observed. The capacities of the columns having L/D ratios above 18 could not attain the plastic capacity due instability effects.

Shakir Khalil et al. (1997)

Stub columns of rectangular CFTs were first tested to determine the squash load of CFT members. Column CFT specimens were then tested monotically in a horizontal position. Pin-ended support conditions were simulated by the test setup. The L/D ratios were ranging from 21 to 49. For major and minor axis bending, the D/t ratio of the specimens was 30 and 20, respectively. The applied eccentricities did not exceed one half the diameter of the column. The yield strength of steel was varying from 47.0 ksi to 53.3 ksi. The compressive strength of concrete ranged between 5.3 ksi and 6.0 ksi. The stub columns exhibited 16 to 30% higher strength than their nominal axial load capacity calculated according to BS5400 (1979). Their strength was observed to decrease with an increase in length due to local buckling. The local buckling generally took place at the longer side of the tubes. The concrete was investigated after testing. It was crushed but kept its integrity, thus facilitating the achievement of the large strengths in the stub columns. In addition, the CFT columns were found to have an increase in strength of 25-37% over similar hollow tubes. Except for one case, the failure load decreased with an increase in end eccentricity. This was because that specimen experienced pure bending response about the major axis. The authors noted that the behavior of columns subjected to small eccentricities about the major axis was especially sensitive to any imperfections, most notably, out-of-straightness.

Zhang and Zou (2000)

An experimental and an analytical study on square CFT columns were presented. The steel tube response was isolated from the overall behavior of the specimens and the response of the concrete and steel were examined separately. Formulations were proposed for the confined concrete strength, the confined concrete strain, and the longitudinal stress in the steel tube.

Thirty-six CFT columns were tested under monotonically applied axial loading. The D/t ratio of the specimens ranged between 20 and 50. The measured compressive strength of concrete was 5.87 ksi and the yield strength of the steel ranged from 41.28 ksi to 58.51 ksi. The L/D ratio varied between 4 and 5. From the experimental results, it was found that the confinement effect increased the concrete strength and ductility. They also determined that the longitudinal stress in the steel tube was always less than the yield stress due to the biaxial stress condition. Confinement was found to be larger when the D/t ratio was smaller.

Han and Yan (2001)

A series of monotonic tests were conducted on square CFTs including stub-columns, columns, and beam-columns. In addition, the authors presented analytical models to estimate the capacity and load-deformation response of the specimens. The objective of the experiments was to investigate the strength and failure patterns of CFTs. Two sets of experiments were conducted. In the first set, twenty stub-columns were tested. Eight columns and twenty-one beam-columns were tested in the second set. The authors defined a confinement factor to account for the composite action between steel and concrete. This factor was used as a parameter in each set of experiments, with a range of values varying from 1.08 to 5.64. Other parameters included concrete strength, D/t ratio, eccentricity, and slenderness. The average measured yield strength of steel was 47.14 ksi and the measured cubic concrete strength ranged between 2.35 ksi and 7.15 ksi. The D/t ratio varied from 20.5 to 36.5.

Fujimoto et al. (2004)

Beam columns of concrete-filled steel tubular (CFT) columns are designed using a design formula established by the Architectural Institute of Japan (AIJ). However, the scope of the formula in the current AIJ standard is limited to ordinary material strengths, and a rational mathematical model which makes it possible to reproduce load-deformation behavior in CFT columns has not yet been established. The main objectives of this research were to investigate the effect of higher material strengths on the flexural behavior and to create mathematical models of the steel tube and filled concrete. Adequate study of the effects of the section shape, diameter (width)-

to-thickness ratio, and the combination of strengths of the steel tube and filled concrete was included in the scope of this investigation. Based on the experimental results of 65 eccentric compression tests, an analytical model for the restoring force characteristics of the flexural behavior of CFT columns is proposed, and is found to reproduce experimental results such as the synergistic interaction between the steel tube and filled concrete with good accuracy.

Tao and Han (2006)

Double skin composite columns are formed from two steel skins filled with concrete in between. This new form of hybrid column has the potential to be used in many domains such as high-rise bridge piers and large diameter columns in high-rise buildings, etc. This paper describes a series of tests carried out on concrete-filled double skin steel tubular (CFDST) stub columns, beams and beam–columns. Both outer and inner tubes are cold-formed rectangular hollow sections (RHS). The failure modes, and load–deformation behaviour of CFDST specimens are compared with those of conventional concrete-filled steel tubular members and empty double skin tubular members. A theoretical model is developed in this paper for the CFDST stub columns, beams and beam–columns. Reasonably good agreement is observed between the predicted and tested curves. Simplified models are derived to predict the load-carrying capacities of the composite members.

Liu (2006)

This paper presents an experimental and analytical study of the behaviour of high-strength rectangular concrete-filled steel tubular (CFT) columns subjected to eccentric loading. Four slender and 16 stub CFT columns were tested to investigate their structural behaviour. The test parameters were material strengths (f_y = 495 MPa, $f_c^{/}$ = 60 MPa), cross-sectional aspect ratio (1.0–2.0), slenderness ratio (10 and 60) and load eccentricity ratio (e/H = 0.10–0.42). Favourable ductility performance was observed for all specimens during the tests. Experimental failure loads are employed to calibrate the specifications in the design codes EC4, ACI and AISC. Results show that EC4 overestimates the failure loads of the specimens by 4%. ACI and AISC conservatively predict the failure loads by 14% and 24%, respectively. An analytical

model is developed to predict the behaviour of high-strength rectangular CFT columns subjected to eccentric loading. Calibration of the model against the test results shows that it closely estimates the ultimate capacities of the columns by 3%.

Uy (2008)

This paper aims to investigate the stability and ductility characteristics of concrete filled columns using high performance steel (HPS). Previous research in HPS and current applications of HPS are discussed at length. Eight columns were tested under compression as two hollow high strength steel and two hollow stainless steel box sections were compared to two concrete filled high strength and stainless steel box sections.

The high strength steel columns considered were constructed with a box section of 4.3 x 4.3 in. with a 0.197 in. nominal plate thickness. A nominal yield stress of 65 ksi was chosen. The hollow sections exhibited quite ductile behavior. The concrete filled sections reached a peak load and gradually experienced a load reduction; the author attributes this to internal concrete crushing. The paper suggests that confinement is less likely to take place for high strength steel sections because the strains at which yields are often achieved are often in the vicinity of the crushing strains of most normal strength concrete. The stainless steel columns had a nominal dimension of 3.94 x 3.94 in. cross section with 0.197 in. nominal wall thickness. The tensile coupon tests revealed a mean 0.2% proof stress of this material to be about 32 ksi and the mean ultimate stress to be about 61 ksi. The hollow section columns achieved a maximum load just larger than 180000 lbs., at which point loads began to stabilize. Results for the concrete filled steel sections revealed that the presence of the concrete infill allowed local buckling to be considerably delayed and a gradual increase in the steel allowed. Furthermore, the steel section appeared to significantly confine the concrete in these sections.

Uy et al. (2011)

This paper discusses axial compression tests performed on concrete filled steel tubes, as well as hollow steel sections. A combination of circular, square, and rectangular

columns were tested. The specimens were divided into four groups; group 1 was composed of 72 short columns under axial loading, group 2 was 9 short columns, group 3 was 12 short beams-columns under axial compression and bending, and group 4 was 24 columns under axial loading. Group 2 investigates how a different loading method may affect the results, and group 4 investigates slender columns. Group 3 which was under combined loading, displayed very ductile characteristics, and both the strength and stability were significantly increased. For the short columns, short knife edges were placed on the end plates, and grooves were added to the plates to apply moments. For group 4, two hinges were added to both ends of the column to simulate pin-ended supports. Two strain gauges were added to both sides of each short column for a total of six gauges per column. Deflection for the short specimens was measured at mid height due to limited space. Longitudinal and transverse strains were measured using strain gauges with a length of 3mm. Both circular and square CFST columns displayed local outward folding failure, and thicker sections displayed local buckling at mid-span height. With the square hollow sections, local buckling occurred in convex and concave surfaces. The columns with a larger D/t ratio displayed less ductile characteristic than a column with a smaller D/t ratio. The specimens using stainless steel over carbon steel displayed more ductile behavior and a greater residual strength. The specimens using high-strength concrete had a compressive strength of two times the normal strength of concrete.

Yang and Han (2011)

This paper investigates the behaviour of concrete filled steel tubular (CFST) stub columns subjected to eccentric partial compression. Twenty-eight specimens were tested and presented. The main parameters in test program include: (1) section type: circular, square and rectangular; (2) load eccentricity ratio (including uniaxial and biaxial loading): from 0 to 0.4; and (3) shape of the loading bearing plate (BP): circular, square, strip and rectangular. The test results indicated that, similar to the corresponding fully loaded CFST stub columns under eccentric loading, CFST stub columns under eccentric partial compression have generally reasonable bearing capacity and favorable ductility. A finite element analysis (FEA) model for CFST stub columns under eccentric partial compression is developed and the predicted

performances are validated through measured results. The FEA model is then used to investigate the mechanisms of such composite columns further.

Dundu (2012)

An experimental study was undertaken to investigate the behaviour of 24 concrete-filled steel tube (CFST) columns, loaded concentrically in compression to failure. Variables in the tests include the length, diameter, strength of the steel tubes and the strength of the concrete. The large slenderness ratio caused all composite columns in Series 1 to fail by overall flexural buckling. Although overall flexural buckling was also experienced in the composite columns of Series 2 tests, the stockier columns failed by crushing of the concrete and yielding of the steel tube. A comparison of the experimental results with the loads predicted by the South African code (SANS 10162-1) and Eurocode 4 (EC4) shows that the codes are conservative by 8.4% and 13.6%, respectively, for Series 1 tests, and 10.5 and 20.2%, respectively, for Series 2 tests. A plot of the compressive load versus the vertical deflection shows the composite columns to be fairly ductile.

Li et al. (2013)

The tapered concrete-filled double skin steel tubular (CFDST) columns have been used in transmission towers with potential for other types of composite frame structures. However, the behavior of the tapered CFDST column under eccentric compression has not yet been studied, which will hinder the employment of such members. This paper reports an investigation on eccentrically loaded tapered CFDST columns with different load eccentricities. The numerical investigation was also carried out by using the finite element model to predict the behavior of the tapered member. Comparisons were made between the tapered and straight members on the strength and stress distribution. The stability of the tapered column was studied through numerical calculation. Finally, the load carrying capacity of the tapered CFDST column under eccentric compression was predicted using the concept of "equivalent column".

Kim et al. (2013)

Two concrete-filled steel tube columns and four concrete-encased steel columns using high-strength steel (yield strength f_{ys} = 913, 806, and 812 MPa) and high-strength concrete (compressive strength $f_c^/$ = 94, 113, 104, and 184 MPa) were tested to investigate the effect of various sectional shapes and configurations on the eccentric axial load carrying capacity. This study focused on maximizing the contribution of the high-strength steel, preventing early crushing of the concrete (1) by using steel tubes or closely spaced ties for lateral confinement, (2) by using ultra high-strength (200 MPa) concrete with a high-crushing strain, and (3) by placing L-shaped steel sections at the corners of the cross section. The test results showed that the steel tube successfully restrained early concrete crushing and developed its full plastic stress; unlike expectation, early crushing occurred in the ultra high-strength concrete column; and the concrete-encased L-section column had higher peak strength and flexural stiffness than the conventional concrete-encased H-section columns. For the design of the concrete-filled columns, the conventional plastic design method is applicable, whereas the strain-compatibility method should be used for the design of the concrete-encased columns with limited lateral confinement.

Qu et al. (2013)

To study the behavior of rectangular CFST columns subjected to eccentric loading, a total of 17 rectangular CFST columns uniaxial and biaxial bending tests were carried out. Concrete compressive strength, steel strength, cross-sectional proportion and eccentricity were selected as the variables to be investigated. The relationship between the load and the lateral displacement at the mid-height of the columns in the directions of both the strong and weak axes and the relationships of load versus end shortening for each specimen were duly recorded. The influences of the constraining factor and eccentric ratio in relation to the strength and ductility indexes of the specimens were investigated. Moreover, in order to achieve the ultimate bearing capacity of the relative rectangular hollow sections with a load of the same eccentricity, the rectangular hollow section models were established by means of the FEM. The concrete contribution ratio necessary for the rectangular CFST columns to

be able to resist the eccentric loading was obtained also through comparison of the simulated results and the test data.

Ren et al. (2014)

This paper presents a series of test results of elliptical concrete filled steel tubular (CFST) beams and columns to explore their performance under bending and compression. A total of twenty-six specimens were tested, including eight beams under pure bending and eighteen columns under the combination of bending and compression. The main parameters were the shear span to depth ratio for beams, the slenderness ratio and the load eccentricity for columns. The test results showed that the CFST beams and columns with elliptical sections behaved in ductile manners and were similar to the CFST members with circular sections. Finally, simplified models for predicting the bending strength, the initial and serviceability-level section bending stiffness of the elliptical CFST beams, as well as the axial and eccentric compressive strength of the composite columns were discussed.

Mahgub et al. (2016)

This paper presents an experimental study into the axial compressive behaviour of self compacting concrete filled elliptical steel tube columns. In total, ten specimens, including two empty columns, with various lengths, section sizes and concrete strengths were tested to failure. The experimental results indicated that the failure modes of the self-compacting concrete filled elliptical steel tube columns with large slenderness ratio were dominated by global buckling. Furthermore, the composite columns possessed higher critical axial compressive capacities compared with their hollow section companions due to the composite interaction. However, due to the large slenderness ratio of the test specimens, the change of compressive strength of concrete core did not show significant effect on the critical axial compressive capacity of concrete filled columns although the axial compressive capacity increased with the concrete grade increase. The comparison between the axial compressive load capacities obtained from experimental study and prediction using simple methods provided in Eurocode 4 for concrete filled steel circular tube columns showed a reasonable agreement. The experimental results, analysis and

comparison presented in this paper clearly support the application of self-compacting concrete filled elliptical steel tube columns in construction engineering practice.

Lee et al. (2016)

An experimental study was performed to investigate the structural behavior of thin-walled rectangular concrete-filled tubular (RCFT) columns. This study mainly focused on the effects of a high-strength steel slender section on the overall eccentric compression capacity. The test parameters included the width-to-thickness ratio of steel plates, yield strength of steel plates, and use of stiffeners. Five specimens were tested under eccentric axial loading. In the slender-section specimens, despite early local buckling, significant post buckling reserve strength developed. Consequently, the predictions of a current specification significantly underestimated the load-carrying capacity of the slender-section specimens. The specimens strengthened with vertical stiffeners exhibited enhanced strength and ductility, attaining the plastic capacity of the composite section. Furthermore, a design method of vertical stiffener was developed for high-strength steel RCFT columns.

Petrus et al. (2016)

This paper presents an experimental investigation into the structural behaviour of eccentrically loaded concrete filled, thin walled, steel tubular slender column with tab stiffeners (CFST). The primary parameters studied through the experimental work are load eccentricity and type of stiffeners. Three different types of stiffeners used in this study are longitudinal stiffeners of 10mm height, longitudinal and tab stiffeners of 25mm height and longitudinal and extended tab stiffeners at 40mm. The effects of the stiffeners on the structural behavior were investigated experimentally using 26 specimens of slender CFST, loaded with eccentricity ranging from 0 mm to 60 mm. It was observed that all specimens failed mainly by overall buckling and, the compressive strength and bending strength of the specimens decreases as the applied load eccentricity increases.

Wang et al. (2016)

The tubed-steel-reinforced-concrete (TSRC) column is a kind of special concrete-encased steel composite columns using the thin-walled steel tube instead of a reinforcement cage to confine the concrete core. The steel tube discontinues at the beam-column joints and thus does not carry any direct axial load. In this study, twelve short square TSRC columns were tested to investigate their load-carrying and deformation capacities under eccentric compression. The studied parameters are width-to-thickness ratio of the steel tube, eccentricity of the axial load, and the flange shear studs. The test results indicate that the encased steel shape works with the concrete compatibly due to the confinement from the steel tube, and the flange shear studs are not effective in enhancing the flexural stiffness and the axial resistance. To account for the inelastic behaviour of structural steel and concrete materials, a numerical model based on the fibre sectional analysis was developed, which predicts the results in general agreement with the test results. Parametric analysis is carried out based on the numerical model.Moreover, a new simplified method to estimate the capacity interaction diagram of a square TSRC section is proposed.

Kim et al. (2017)

To investigate the effect of sustained loads on the ultimate strength of high-strength composite columns using grade 800-MPa steel and 100-MPa concrete, ultimate load tests were performed after long-term loading. Two concrete-encased steel (CES) columns were tested under concentric loading, and a CES column and a concrete-filled steel tube (CFT) column were tested under eccentric loading. The test results showed that stress-relaxation in the concrete and gradual stress-transfer to the steel and longitudinal bars occurred, and the ultimate shrinkage strain and ultimate creep coefficient of the high-strength concrete were estimated as 553 $\mu\varepsilon$ and 1.44, which are lower than those of normal-strength concrete but belong to the ranges specified in concrete standards. To confirm the tests, a numerical parametric study was performed, considering the age-adjusted effective modulus and relaxation. The results of the experimental and numerical studies showed that, in the case of the high-strength composite columns, the sustained load increased deformation (axial strain and curvature) at service load conditions, but the detrimental effect on the

ultimate strength was not significant. The factors for the long-term effect specified in current design codes gave good predictions for the long-term effective flexural stiffness.

Kim et al. (2017)

Composite columns of various sectional configurations are studied to maximize the contribution of high-strength steel under compression-flexural loading. For concrete-encased steel (CES) columns, steel angles were placed at four corners of the cross-section and connected by various types of transverse reinforcements. In the case of a concrete-filled steel tube (CFT) column, a slender steel tube was stiffened by welding longitudinal bars. To verify structural capacities, eccentric axial load tests were performed for three concrete-encased steel angle (CES-A) columns and a stiffened concrete-filled slender steel tube (S-CFT) column, using Grade 800 MPa steel and 100 MPa concrete. The CES-A columns showed good structural performance in strength, flexural stiffness, and ductility due to the high contribution and good confinement effect of the corner steel angles and transverse reinforcement. In the S-CFT column the welded longitudinal bars successfully restrained local buckling of the slender steel tube so that the full plastic strength of the composite section developed.

2.6   Summary

Considerable progress over the last 40 years has been made in the investigation of CFST columns. Fundamental knowledge on composite construction systems has already been obtained by the researcher. However, intensive research is required, on the applicability of the design provisions in the construction environment of Bangladesh. While much of the current available research draws similar conclusions on the behaviour of CFST columns, there are a number of conflicting views being documented. In investigating CFST columns under uniaxial eccentric compression, previous studies have mainly focused on their compressive strength. Very little attention has been paid to their compressive stiffness and deformation capacity. For structural analysis, compressive stiffness of a member affects the internal force distribution; therefore accurate values should be provided. Meanwhile, designers

nowadays are paying more attention to extreme loading, such as seismicity, impact and fire; and other abnormal events. Accordingly, the issue of ductility or deformation capacity is of considerable interests to the designers. Therefore, this experimental study mainly focuses on the failure mode, load-strain response and ductility of the square CFST column under uniaxial eccentric loading.

Chapter 3
EXPERIMENTAL PROGRAM

3.1 General

An experimental investigation, to determine the complete load-deflection behavior and failure modes of eccentrically loaded CFST columns is presented in this study. The main variables considered in the test program were concrete compressive strength, cross-sectional dimensions, column overall length and load eccentricity. The loads were applied eccentrically through both end knife edges on top of the plate of CFST columns. The failure modes, peak load, peak strain and experimental load-deflection behaviour of the specimens were examined for eccentric loading. The composite column specimens were tested in the Structure and Materials Laboratory of Bangladesh University of Engineering and Technology (BUET), Dhaka, Bangladesh during the month of June in 2018. The description of the test specimens, test setup, loading conditions are presented in the following sections.

3.2 Description of Test Specimens

Total eleven CFST columns with square cross section were tested under eccentric loading. Figure 3.2 shows the cross-section and elevation of a typical square CFST column. The geometric parameters illustrated in the plan view Figure 3.2 (b) are the width (B) and tube thickness (t) of CFST column. The column length, L is illustrated in the elevation view in Figure 3.2 (a). The tested columns had a cross sectional width (B): 100, 125 and 150 mm; length (L): 1000, 500 and 300 mm; tube thickness (t): 3, 4 and 5 mm; concrete compressive strength ($f_c^{/}$): 27, 35 and 44 MPa. The geometric properties of the test specimens are given in Tables 3.1.

(b) Square cross-section of hollow built-up
steel tube
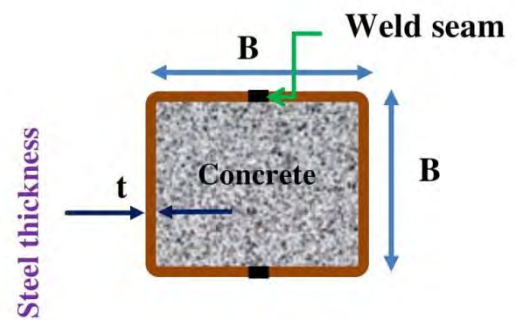
(c) Square cross-section of column

(a) Elevation of composite column E1

Figure 3.1   Geometry of CFST columns

Table 3.1 Geometric properties of test specimens

Specimen design	Cross-sectional size	Concrete compressive strength	Yield stress	Width to thickness ratio	Length to width ratio	Load eccentricity ratio
	B x t x L	f_c'	f_y	B/t	L/B	e/B
	(mm x mm x mm)	(MPa)	(MPa)			
E1	100 x 4 x 1000	27	350	25	10	0.30
E2	100 x 4 x 1000	35	350	25	10	0.30
E3	100 x 4 x 1000	44	350	25	10	0.30
E4	125 x 3 x 1000	35	350	42	8	0.30
E5	125 x 4 x 1000	35	350	31	8	0.30
E6	125 x 5 x 1000	35	350	25	8	0.30
E7	100 x 4 x 500	44	350	25	5	0.30
E8	100 x 4 x 300	44	350	25	3	0.30
E9	150 x 5 x 1000	44	350	30	7	0
E10	150 x 5 x 1000	44	350	30	7	0.30
E11	150 x 5 x 1000	44	350	30	7	0.45

3.3   Explanation of Test Parameters

The parameters considered in the test were: concrete compressive strength (f_c'): 27 MPa to 44 MPa; width to thickness ratio (B/t): 25 to 42; length to width ratio (L/B): 3 to 10 and load eccentricity ratio (e/B): 0 to 0.45. Specimens E1, E2 and E3 were constructed with concrete compressive strength (f_c'):   27, 35 and 44 MPa respectively. The parameters varied between these columns were concrete compressive strength. The columns E4, E5 and E6 were designed to have width to thickness ratio (B/t): 42, 31 and 25 respectively. These three specimens were designed to examine the cross-sectional effect on the behavior of eccentrically loaded CFST column. Effect of Column overall slenderness was examined with the specimen of E2, E7 and E8 which had length to width ratio (L/B): 10, 5 and 3 respectively. And the columns E9, E10 and E11 were subjected to load eccentricity ratio (e/B): 0, 0.30 and 0.45 respectively.

3.4   Test Column Fabrication

There are mainly two parts in CFST columns, i.e. steel and concrete. The steel part consists of steel tube, top and bottom plates. The structural steel tubes were

fabricated by McDonalds Steel Building Products Ltd, Dhaka, Bangladesh. And concrete was poured into the steel tube for the construction of CFST columns.

3.4.1 Steel section fabrication

All the steel tubes were fabricated by joining two channels through continuous welding. The thickness of the tube was measured by a screw-gauge at four places and the mean value was taken. Using a vernier caliper, the width of the tube was measured. All the steel tubes were machined and welded to 25 mm thick steel bottom and top plate. End plate was welded to each of the specimens for uniform distribution of the applied load.

3.4.2 Mixing, placing and curing of concrete

Cement, fine aggregate and coarse aggregate were weighed and batched as per the required quantity. An electrically operated concrete mixer was used for mixing the concrete. The materials are mixed in a mechanical mixer of revolving drum type. The main purpose of mixing is to produce an intimate mixture of cement, water, fine and coarse aggregate of uniform consistency throughout each batch. To cast all the CFST columns, three types of concrete mixes were used: M20, M30 and M40. The mix designs are presented in Table 3.2.

Table 3.2 Mix designs for plain concrete

Mix design	Cement (OPC)	Coarse aggregate		Fine aggregate	Water
		¾ inch black stone	½ inch black stone chips		
	(Kg/m^3)	(Kg/m^3)	(Kg/m^3)	(Kg/m^3)	(Kg/m^3)
M20	355	711	305	799	185
M30	385	719	308	732.5	181
M40	435	699	299	712	183

For composite columns the empty steel tube was kept ready for placing of concrete. The tubes were filled in a vertical position. Concrete was poured into the steel tube from top. The tube was placed on a smooth surface before concreting. The concrete

was compacted by means of a needle vibrator. The compaction by tamping rod is used for adopting the high water cement ratio to enable the concrete to flow readily around the tube. The compaction by needle vibrator was used for all mixes. Such compaction prevents honeycombing, ensures more impermeable and dense concrete, better bond between concrete and steel tube. After filling the tube the concrete was finished smooth at the top. The specimens were cured with water after the day of casting for 28 days. To avoid surface water evaporation jute and polyethylene sheets were used. Figure 3.3 shows the mixing, placing and compaction of concrete.

(a) Mechanical mixture

(b) Fresh Concrete

(c) Hollow steel tube

(d) Concrete placement

42

<div style="text-align:center">

(e) Compaction   (d) Constructed CFST columns

Figure 3.2 Mixing, placing and compacting of concrete

</div>

3.5 Material Properties

The CFST columns consist of steel tube and concrete. To determine the stress-strain characteristics of the steel plate in tension, tensile coupons were conducted on steel plates. Concrete cylinders were cast and tested to ascertain the characteristic compressive strength of the concrete. In total eighteen cylinders were tested for the three types of concrete strength used in this study.

3.5.1 Steel

The mechanical properties of steel materials were measured by tensile coupon test according to ASTM D638-02a (2003). Three steel plate samples were tested to determine the material properties of steel. Typical stress-strain diagram and the dimensions of each coupon are shown in Figure 3.4. The tension tests on the plates were conducted in the universal testing machine (UTM), with a tensile capacity of 2000 kN, in the Structure and Materials Laboratory of BUET. Load measurements were taken using the internal load cell of the UTM. The results of the steel-plate tension tests are given in Table 3.3.

Table 3.3 Tensile properties of structural steel tube plate

Specimen no.	Yield Stress (f_y)	Ave. (f_y)	Ultimate Stress (f_u)	Ave. (f_u)	Elastic modulus (E_s)	Yield strain (ε_y)	Ave. (ε_y)	Ultimate strain (ε_u)
	(MPa)	(MPa)	(MPa)	(MPa)	(GPa)	(με)	(με)	(με)
1	352		423		200	2150		27167
2	350	350	428	428	200	2148	2148	25167
3	348		433		200	2146		33159
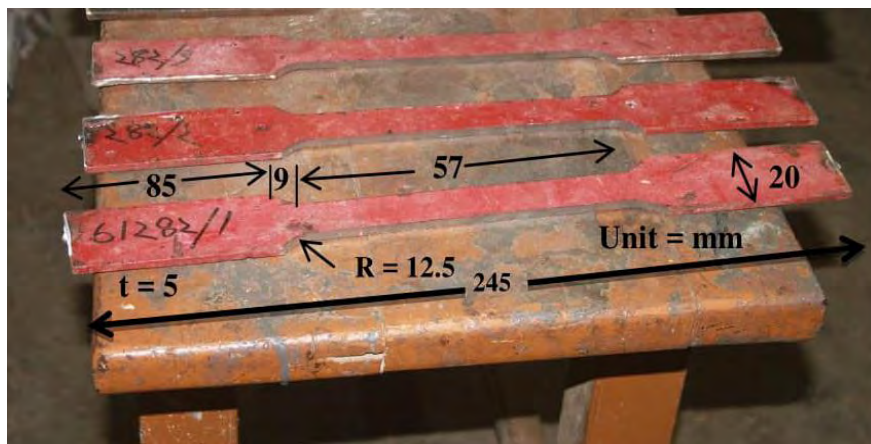
(a) The dimensions of coupon

(b) Tensile coupon test
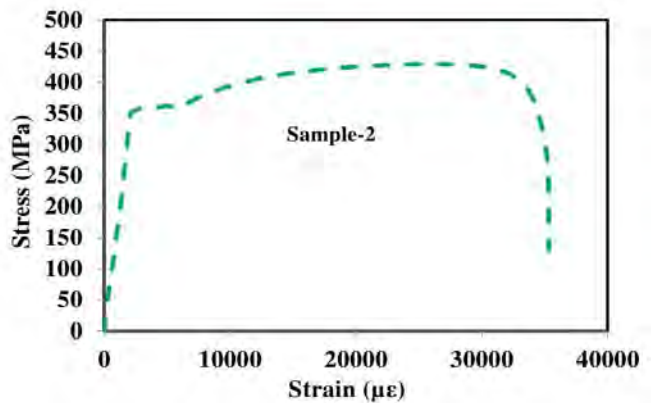
(c) Typical stress-strain diagram of tensile coupon test

Figure 3.3 Tensile coupon test of steel tube

44

3.5.2 Concrete

A total of three mixes were required to batch the eleven CFST columns. Three different strengths of concrete (20, 30 and 40 MPa) were cast for constructing these columns. In order to determine the material properties, six concrete cylinders with (4inch*8inch) were cast from each mix. The designation of the individual cylinder for three different strengths of concrete is shown in Table 3.4. Twenty four hours after casting, cylinders were removed from the molds and kept in the lime water. Nine concrete cylinders (three from each mix) were brought out of the lime water after 28 days to determine the compressive strength of concrete and the other nine cylinders were tested during the day of column testing.

Table 3.4 Designation of concrete cylinder for different strength

Concrete strength	Cylinder designation
20 MPa Column E1	20CY1, 20CY2, 20CY3, 20CY4, 20CY5, 20CY6
30 MPa Column (E2, E4, E5 & E6)	30CY1, 30CY2, 30CY3, 30CY4, 30CY5, 30CY6
40 MPa Column (E3, E7, E8, E9, E10 & E11)	40CY1, 40CY2, 40CY3, 40CY4, 40CY5, 40CY6

All cylinders were capped with a high strength capping compound prior to testing to ensure uniform bearing in the testing machine. Cylinders were tested in the concrete Materials Laboratory at BUET. The compressive strength of all twelve cylinders is given in Table 3.5. Average compressive strength of these cylinders (M20, M30 and M40) after 28 days were found to be 26, 33 and 42 MPa. Remaining cylinders were tested at the same day of the testing of CFST columns. Average compressive strength of those cylinders were slightly greater than 28 days compressive strength. This variation was due to the reason that concrete gains strength with time.

Table 3.5 Concrete cylinder strength

Concrete strength	Column symbol	Designation of cylinders		Strength		Strength increase (28 day to test day)	
		28 day	Test day (40 day)	28 day (MPa)	Test day (MPa)	(MPa)	(%)
20 MPa	E1	20CY1	20CY4	26.5	27.4	+0.9	3.4
		20CY2	20CY5	25.9	26.7	+0.8	3.0
		20CY3	20CY6	25.6	26.9	+1.3	5.0
Mean				26	27	1.0	3.8
30 MPa	E2 E4 E5 E6	30CY1	30CY4	33.6	35.8	+2.2	6.1
		30CY2	30CY5	32.5	34.6	+2.1	6.0
		30CY3	30CY6	32.9	34.6	+1.7	4.9
Mean				33	35	2.0	5.6
40 MPa	E3 E7 E8 E9 E10 E11	40CY4	40CY4	41.9	44.4	+2.5	5.9
		40CY5	40CY5	42.5	43.7	+1.2	2.8
		40CY6	40CY6	41.6	43.9	+2.3	5.5
Mean				42	44	2.0	4.7

3.6   Test Setup and Data Acquisition System

All specimens were tested under eccentric loading about the major axis in a 2000 kN capacity universal testing machine. Since the standard accessories of the testing machine were unable to produce eccentric loading, knife edges were constructed which allow the load from the testing machine to be applied at designed eccentricities to the specimens similar to end assemblage used by Liu (2006), with slight modification. The knife edges were employed at both the bottom and the top of the specimens to simulate pin-pin boundary conditions and subjected to single curvature bending. The knife edges consisted of an outer edge and inner edge counterpart. The outer edge consisted of a 310 mm x 310 mm x 20 mm thick hardened steel block with 50 mm width x 60 mm long V-shaped outer edge. It was bolted to the top and bottom platen of the testing machine. The inner edge consisted of 310 mm x 210 mm x 20 mm thick hardened steel block with inner V-shaped grooves of 30 mm depth. It was positioned to the top and bottom end plates of the

specimen with four numbers of bolts in order to align and to prevent the slippage between the inner edges and the specimens. Axial loading was applied through the V-shaped inner edges at each specimen so that the load eccentricity (e) could be precisely controlled. The experimental setup of the tested specimens is shown in Figure 3.5. Four strain gauges were used on four faces of steel tube to measure the longitudinal and transverse strains of the tube, where linear variable differential transducers were used to measure out of plane deflection in vertical and lateral direction. Displacement control loading at a rate of 0.5 mm/min was used throughout the loading of the test specimens. The data acquisition system used two PC running Horizon data acquisition software and Labview software. The digital readings of UTM machine were collected from Horizon data acquisition software and the readings of LVDT and strain gauges were collected from Labview software.

(a) Installation of strain gauge

(b) Installation of vertical LVDT

(c) Installation of lateral LVDT
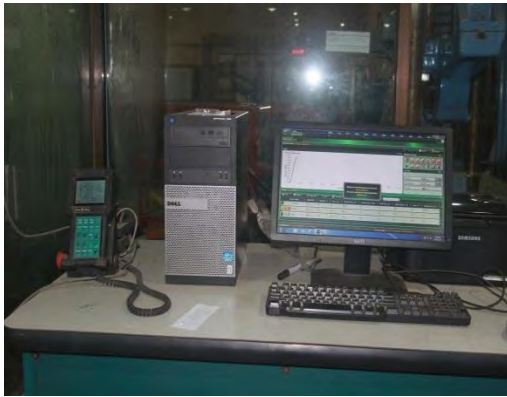
(d) Vertical LVDTs data analysis

(e) Strain gauges and LVDTs data analysis
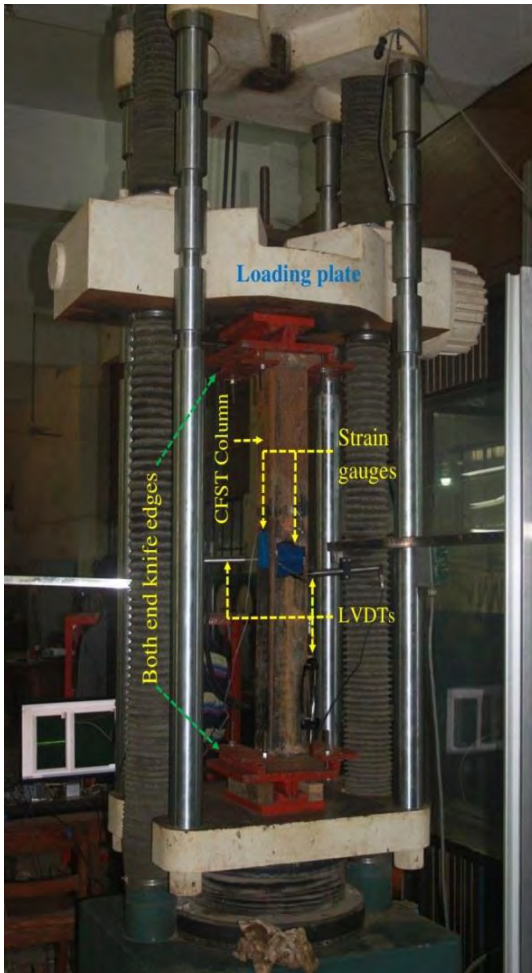
(f) Column before the test
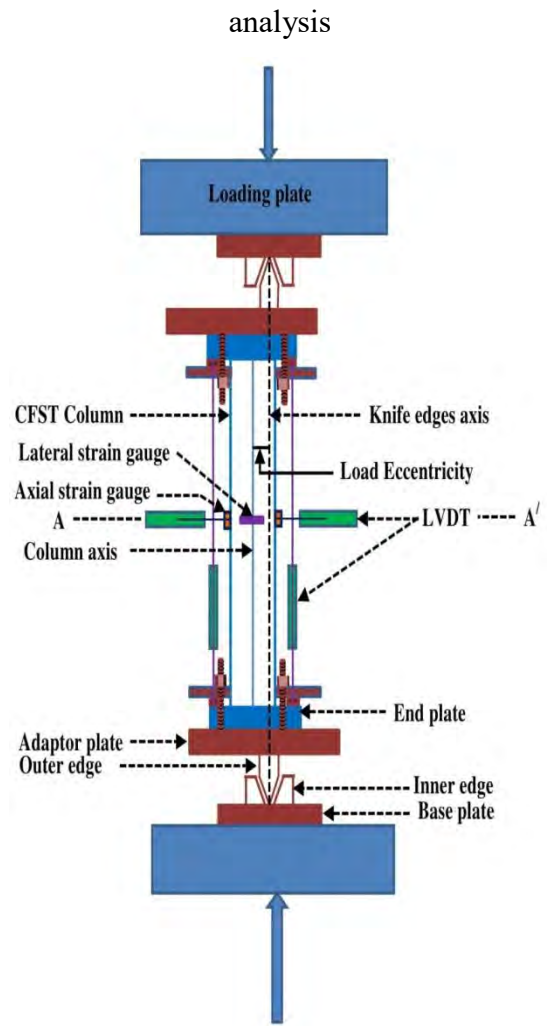
(g) Assemblage arrangement of test columns
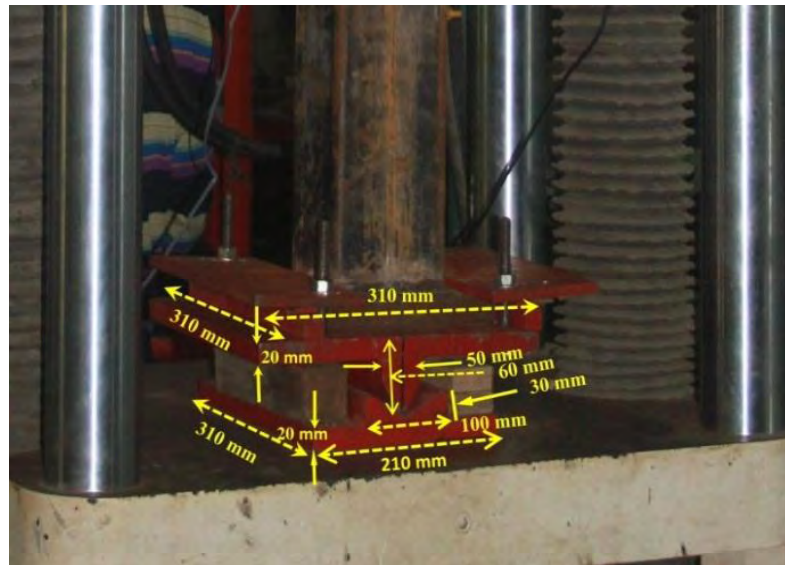
(h) Knife edge details
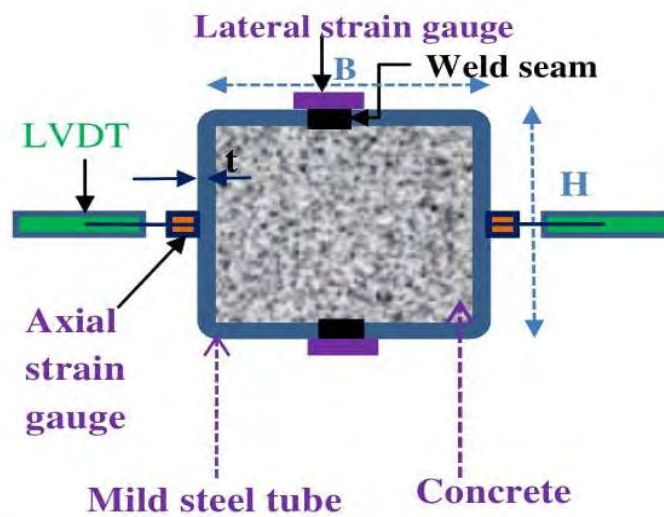
(i) Cross-section

Figure 3.4 Test setup for CFST columns

Chapter 4
RESULTS AND DISCUSSIONS

4.1   General

In this study, an experimental program has been designed to investigate the behavior and failure mode of concrete filled steel tubular column under uniaxial eccentric compression. Total eleven CFST columns with square cross section were tested under eccentric loading. The parameters considered in the test were: concrete compressive strength, plate slenderness ratio, global slenderness ratio and load eccentricity ratio. Axial load, axial strain, mid-height deflection, ultimate moment and failure modes of the columns were obtained from the experimental test. The performance indexes such as ductility index and concrete contribution ratio were also determined to observe the performance and cost-effective design of CFST column. All the results obtained from the experimental investigation were organized and presented to highlight the individual effect of each parameter. In the following sections, the significant observations from the experimental study have been reported along with the relevant tables and figures.

4.2   Failure Modes

Generally global slenderness ratio (L/B), plate slenderness ratio (B/t), load eccentricity ratio (e/B) and concrete infill have a significant effect on the failure mode of the CFST column subjected to eccentric loading. Figure 4.1 demonstrates the typical failure modes of the eccentrically loaded CFST column.

During the experiment, Both end knife edges were used which allow the load from the testing machine to be applied at designed eccentricities to the specimens in order to simulate pin-pin boundary conditions of the specimens. During the loading process, there was no obvious deformation at the beginning of the loading for all the columns. When the load was applied near the ultimate load, cracking sounds were audible and then buckling of the columns appeared. The configurations of the

columns after the testing are shown in Table 4.1 and Figure 4.2. Close observations of the tested columns lead to the following:

i. The eccentrically loaded columns developed a somewhat lateral deflection due to the generation of secondary moment. For columns (E1, E2 and E3) with higher global slenderness ratio (L/B = 10), failure was observed to occur by global buckling. Actually failure was initiated by steel yielding which was followed by global buckling of the steel tube. Finally, cracking of concrete was noticed at the tension side of the eccentrically loaded specimen. Test columns with higher slenderness ratio had greater flexibility which resulted in larger mid-height lateral displacement. No local buckling was observed around the specimens" cross-section at failure. This is due to the fact that specimens were constructed with compact section. Similar failure behaviour was observed in columns E4, E5 and E6 where the value of global slenderness ratio (L/B) was 8.

ii. Columns (E9, E10 and E11) having (L/B ratio = 7) and variations of e/B ratio (e/B = 0, 0.30 and 0.45) showed overall flexural buckling due to the generation of excess second order moment.

iii. Failure was initiated by steel yielding which was followed cracking of concrete in the stockier columns (E7 and E8) with lower L/B ratio (L/B = 5 and 3). This is attributed to the fact that columns with lower L/B ratio showed greater rigidity and compactness which resulted in smaller mid-height lateral deflection.

Table 4.1   Failure modes of test columns

Specimen design	Cross-sectional size	Concrete compressive strength	Yield stress	Cross-sectional slenderness	Overall slenderness	Load eccentricity ratio	Failure pattern
	B x t x L	$f_c^/$	f_y	B/t	L/B	e/B	
	(mm x mm x mm)	(MPa)	(MPa)				
E1	100 x 4 x 1000	27	350	25	10	0.30	Steel yielding + Global buckling
E2	100 x 4 x 1000	35	350	25	10	0.30	Steel yielding + Global buckling
E3	100 x 4 x 1000	44	350	25	10	0.30	Steel yielding + Global buckling
E4	125 x 3 x 1000	35	350	42	8	0.30	Steel yielding + Global buckling
E5	125 x 4 x 1000	35	350	31	8	0.30	Steel yielding + Global buckling
E6	125 x 5 x 1000	35	350	25	8	0.30	Steel yielding + Global buckling
E7	100 x 4 x 500	44	350	25	5	0.30	Steel yielding
E8	100 x 4 x 300	44	350	25	3	0.30	Steel yielding
E9	150 x 5 x 1000	44	350	30	7	0	Steel yielding + Global buckling
E10	150 x 5 x 1000	44	350	30	7	0.30	Steel yielding + Global buckling
E11	150 x 5 x 1000	44	350	30	7	0.45	Steel yielding + Global buckling
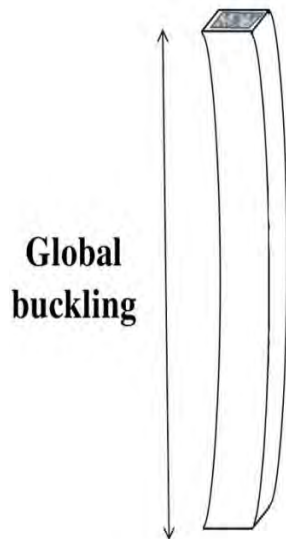
(a) Due to higher slenderness ratio   (a) Due to lower slenderness ratio
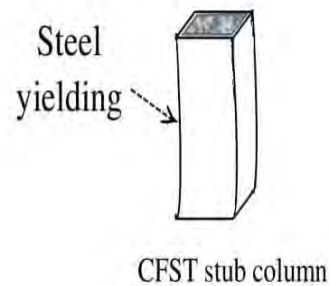
Figure 4.1   Typical failure modes of eccentrically loaded CFST column

(a) E1 (L/B = 10)

(b) E2 (L/B =10)
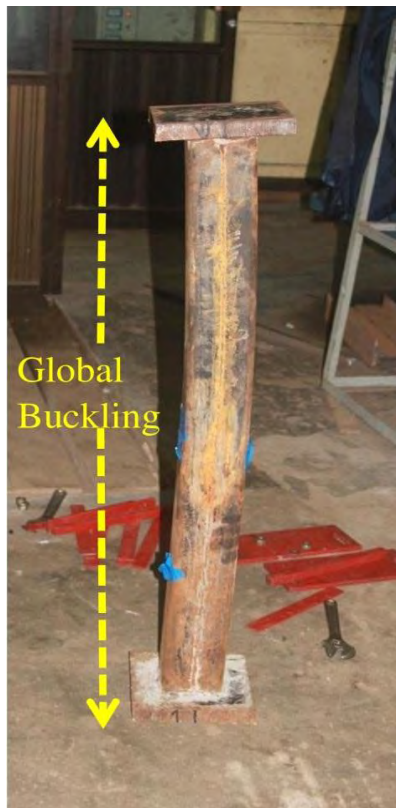
(c) E3 (L/B = 10)

(d) E4 (L/B = 8)

(e) E5 (L/B = 8)

(f) E6 (L/B = 8)

(g) E7 (L/B = 5)

(h) E8 (L/B = 3)

54
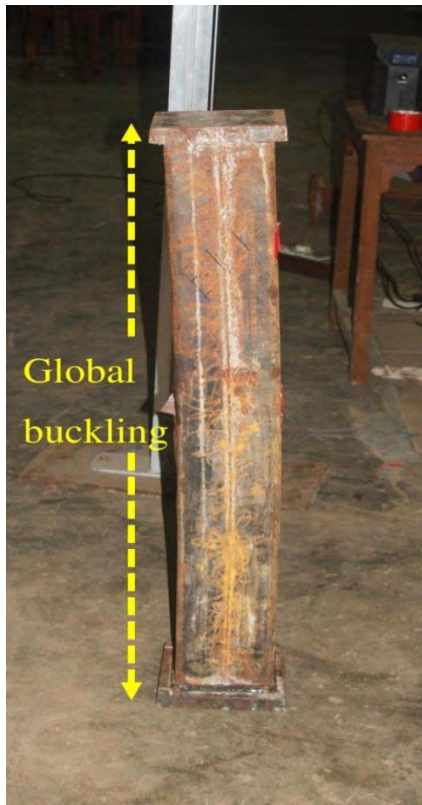
(i) E9 (L/B = 8)

(j) E10 (L/B = 8)

(k) E11 (L/B = 8)

Figure 4.2 Failure modes of tested CFST columns

4.3 Load-Strain Responses

In general, three types of load-strain curves can be observed: strain softening, linear elastic and strain hardening as shown in Figure 4.3. The classification of these curves mainly depends on the confinement of the materials. As the confinement increases, the curves move from softening to linear elastic and then to hardening response.

A typical load strain curve can be divided into four stages as follows:

Stage I (points O-A: Elastic stage): The load is shared by the steel tube and concrete core based on their stiffness. The outer steel tube will yield at point A, and the total yield load is approximately 0.80 to 0.90 times the ultimate strength. After the yielding, the specimen enters the elasto-plastic stage.
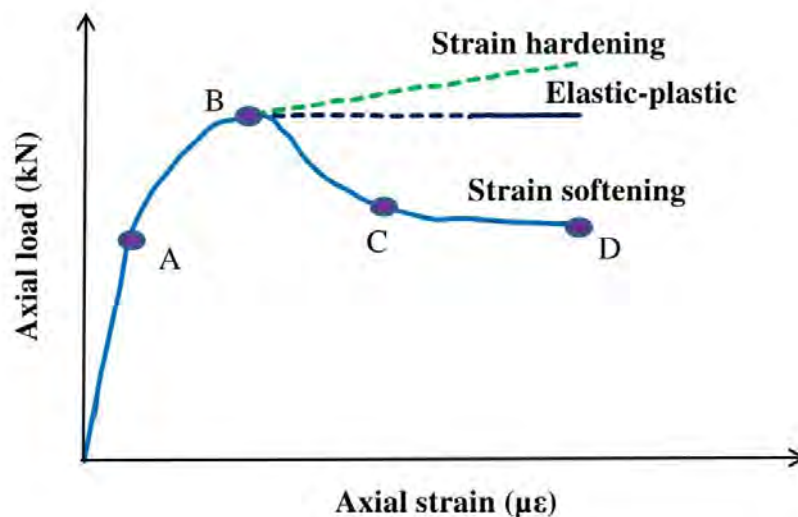
Figure 4.3 Typical axial load versus axial strain curves

Stage II (points A-B: Elasto-plastic stage): As the load increases, the concrete becomes plasticize. Therefore, the steel tube confines the concrete and reaches the ultimate capacity of the specimen except in case of strain hardening response. In case of strain hardening, the ultimate strength of the specimen gains at a later stage because of the higher confinement.

Stage III (points B-C: Softening stage): Considering tested specimens, points B-C represent descending curve. In this stage, the composite action decreased because of

the propagation of micro-cracks in the concrete core and the outward buckling of the tube. The load at point C is approximately 85% of the peak load.

Stage IV (points C-D: Residual stage): The unloading operation was done and the test was ended when the axial load dropped down 65% of the peak load at point D.

The effects of concrete compressive strength ($f_c^/$), plate slenderness ratio (B/t), global slenderness ratio (L/B) and a load eccentricity ratio of the measured axial load (N) versus axial strain (ε) curves are shown in Figures 4.4, 4.5, 4.6 and 4.7 respectively. In the figures, the axial loads were calculated from the testing machine and axial strains were calculated from the average value of strain gauges and LVDTs. To measure the strains: strain gauges were used before tube buckling and after that, displacement readings of the LVDTs (linear variable displacement transducers) were divided by the length of the specimens (Yu et al. 2016). The steel yield strains obtained from the steel coupon tests are also indicated in the figures. Additionally, the moment when the initial steel yielding was observed is marked by a solid circle on the load-strain curve shown in Figures 4.4, 4.5, 4.6 and 4.7 for each specimen under uniaxial eccentric compression. Columns developed steel yielding at a load level of about 90% of the peak loads. This indicates that the steel tubes buckled after yielding of steel.

4.3.1 Effect of concrete compressive strength ($f_c^/$)

It can be observed from Figure 4.4 that, the ascending curves of the specimens become steeper with the increase of concrete strength. It indicates that as the concrete strength increased, the stiffness and peak load of the specimen also increased. This is owing to the formation of less micro cracks in high strength concrete. Such kind of formation is occurred due to the smooth nature of the fracture surface which situates between the interfacial transition zone and aggregate in high strength concrete. The descending branch represents the gradual decrease of the peak load for normal strength concrete, whilst specimens with higher strength concrete showed a sudden drop from the peak load. Therefore, as the concrete strength increases the axial strength of the column increases sacrificing its ductility.
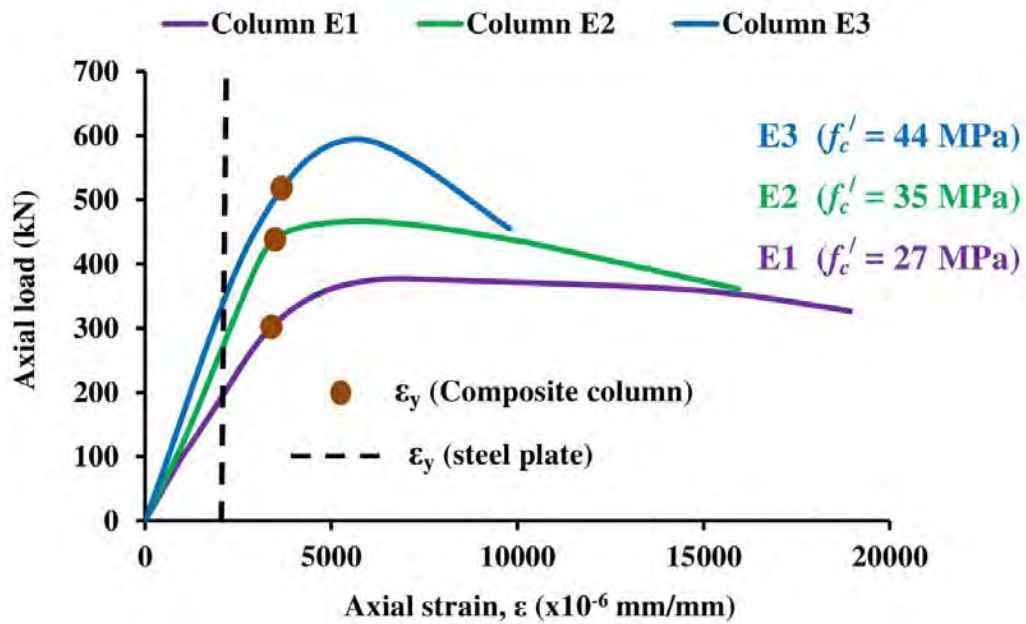
Figure 4.4 Effect of Concrete compressive strength on axial load versus axial strain

4.3.2 Effect of cross-sectional slenderness ratio (B/t)

The effect of B/t ratio on the load-strain curves are demonstrated in Figure 4.5. The Figure 4.5 indicates that decreasing the B/t ratio increased their initial stiffness.
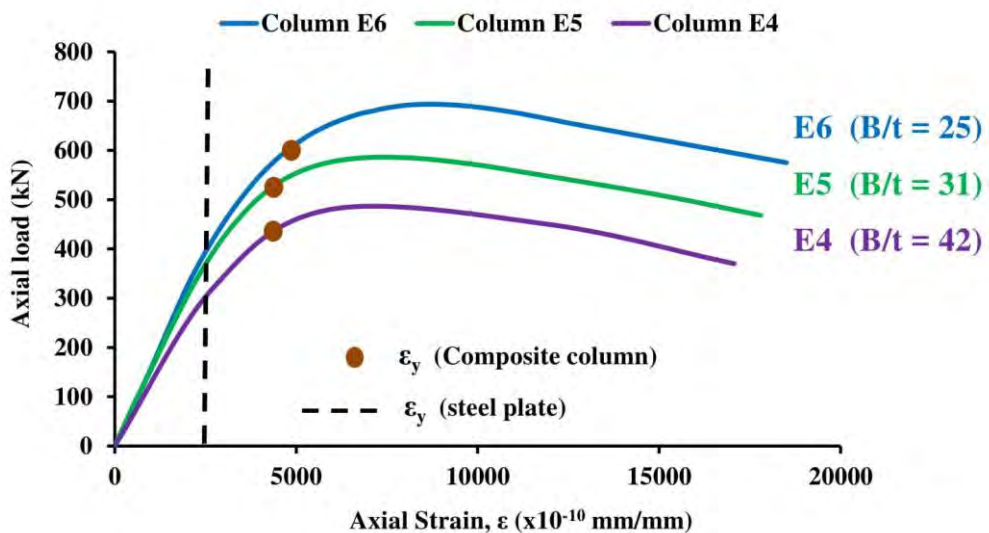
Figure 4.5 Effect of cross-sectional slenderness ratio on axial load versus axial strain

This is owing to the fact that a column with a smaller B/t ratio had a larger steel area. Since the specimens with higher B/t ratio also experienced earlier steel yielding than the specimens having lower B/t ratio. Specimen with lower B/t ratio exhibited better deformation capacity as well as ductility due to its greater lateral support to the concrete core.

4.3.3 Effect of global slenderness ratio (L/B)

Figure 4.6 demonstrates the effect of global slenderness ratio with considering different length of the specimens. It can be observed from Figure 4.6 that, column with lower slenderness ratio had a higher stiffness and load carrying capacity. Generally, the stiffness decreases with the increase in length of all columns. This is attributed to the fact that column with higher L/B ratio shows greater flexibility compared to column with lower L/B ratio.
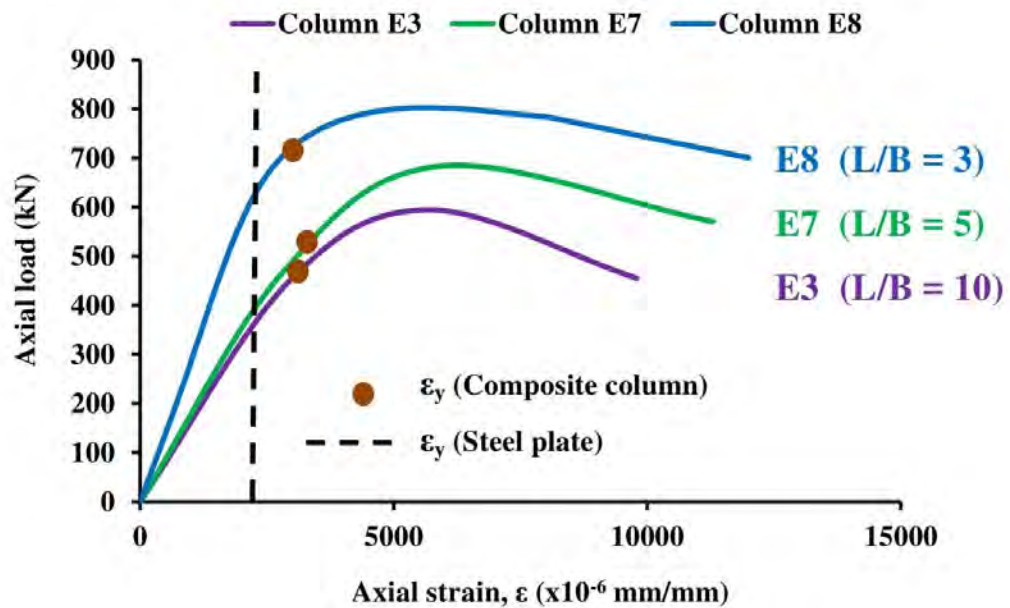
Figure 4.6 Effect of global slenderness ratio on axial load versus axial strain

4.3.4 Effect of load eccentricity ratio (e/B)

The effect of load eccentricity ratio on the load-strain curves are illustrated in Figure 4.7. The Figure 4.7 shows that increasing e/B ratio reduced their initial stiffness and

ultimate axial strength. This is attributed to the fact that the axial forces do not directly apply on the center position of the specimen. Since the specimen with larger e/B ratio also experienced earlier steel yielding than the specimens having lower e/B ratio. This is due to the fact that load is quickly transferred to the adjacent steel tube wall by the specimens with higher e/B ratio.
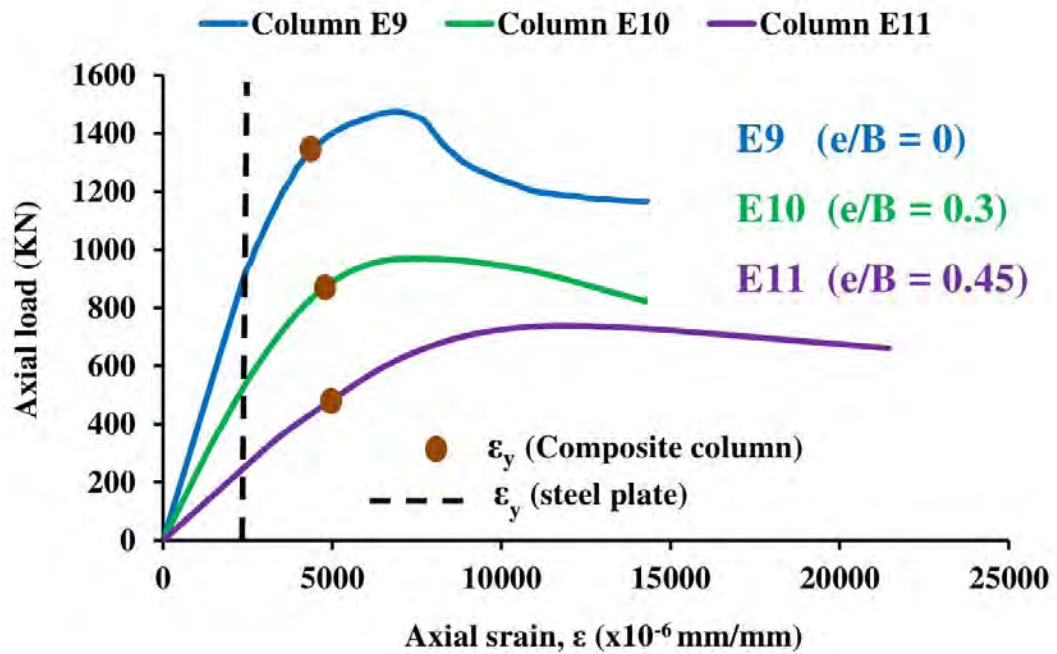
Figure 4.7   Effect of load eccentricity ratio on axial load versus axial strain

4.4   Ultimate Load

The maximum load during loading is defined as the ultimate load. The ultimate load of the specimens is shown in Table 4.2.

Table 4.2 Ultimate load of test columns

Specimen design	Cross-sectional size	Concrete compressive strength	Yield stress	Cross-sectional slenderness	Overall slenderness	Load eccentricity ratio	Ultimate load	% of variation
	B x t x L	$f_c^/$	f_y	B/t	L/B	e/B	P_u	$\% \Delta P_u$
	(mm x mm x mm)	(MPa)	(MPa)				(kN)	
E1	100 x 4 x 1000	27	350	25	10	0.30	377	–
E2	100 x 4 x 1000	35	350	25	10	0.30	466	+ 24%
E3	100 x 4 x 1000	44	350	25	10	0.30	595	+ 58%
E6	125 x 5 x 1000	35	350	25	8	0.30	693	–
E5	125 x 4 x 1000	35	350	31	8	0.30	586	– 16%
E4	125 x 3 x 1000	35	350	42	8	0.30	480	– 31%
E8	100 x 4 x 300	44	350	25	3	0.30	801	–
E7	100 x 4 x 500	44	350	25	5	0.30	688	– 14%
E3	100 x 4 x 1000	44	350	25	10	0.30	595	– 26%
E9	150 x 5 x 1000	44	350	30	7	0	1474	–
E10	150 x 5 x 1000	44	350	30	7	0.30	968	– 35%
E11	150 x 5 x 1000	44	350	30	7	0.45	738	– 50%

4.4.1 Effect of concrete compressive strength ($f_c^/$)

The effect of concrete compressive strength ranging from 27 MPa to 44 MPa on the ultimate axial strength of eccentrically loaded CFST columns is indicated in Figure 4.8. This figure demonstrates that increasing the concrete compressive strength remarkably increases the ultimate load of CFST columns.
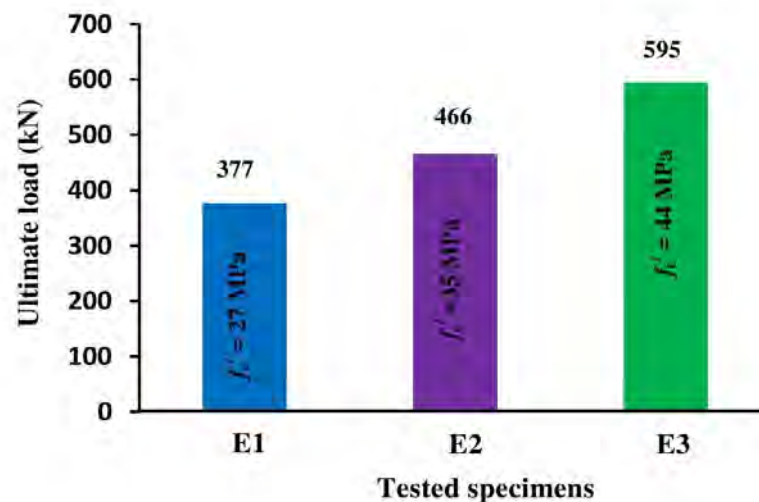
Figure 4.8 Effect on concrete compressive strength on ultimate load

This is owing to the fact that the high strength concrete with higher elastic modulus and better internal bond strength are helpful for a column to gain higher strength. When the concrete compressive strength was increased from 27 MPa to 35 MPa and 44 MPa, the ultimate axial load of column was found to increase by 24% and 58% respectively.

4.4.2 Effect of cross-sectional slenderness ratio (B/t)

The effect of B/t ratio ranging from 25 to 42 on the ultimate axial load of eccentrically loaded CFST columns is illustrated in Figure 4.9. It can be found from Figure 4.9 that, the ultimate strength increases with the decrease of B/t ratio for CFST columns. It is because the specimens with a thicker steel tube could provide more support on the concrete core. When the B/t ratio was increased from 25 to 31 and 42, the ultimate axial strength of the tested column was noticed to decrease by 16% and 31% respectively.
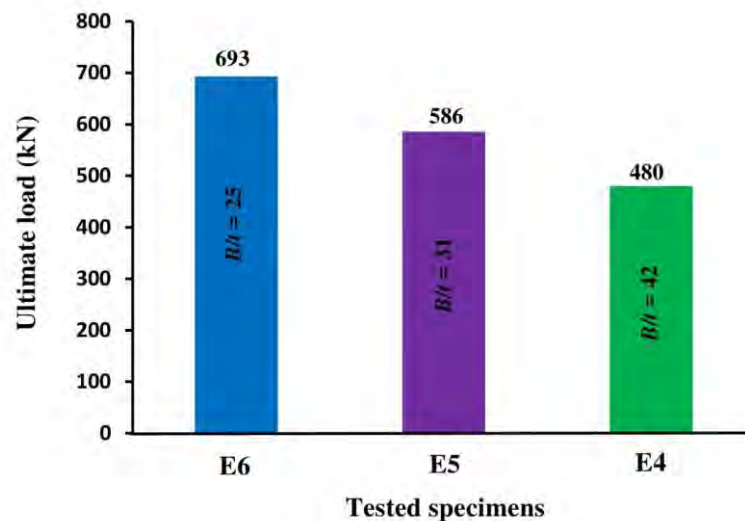
Figure 4.9 Effect of cross-sectional slenderness ratio on ultimate load

4.4.3 Effect of global slenderness ratio (L/B)

Figure 4.10 illustrates the influence of L/B ratio ranging from 3 to 10 on the ultimate axial strength of the tested columns. It would appear from Figure 4.10 that increasing L/B ratio causes a significant reduction of ultimate axial strength. When L/B ratio

was increased from 3 to 5 and 10, the ultimate load of CFST column was found to decrease by 14% and 26% respectively. It is not surprising since the materials of specimens with higher L/B ratio had not been fully utilized.
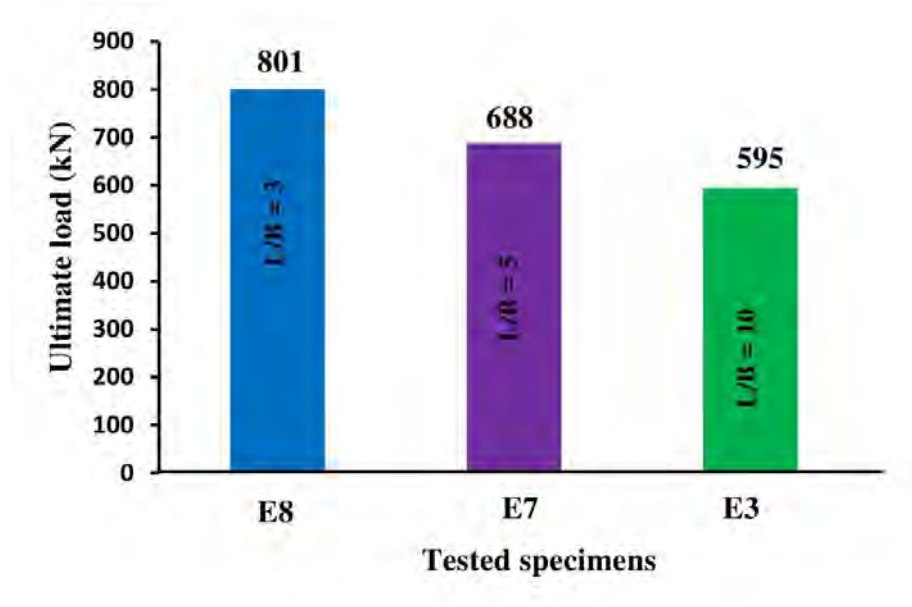
Figure 4.10 Effect of global slenderness ratio on ultimate load

4.4.4 Effect of load eccentricity ratio (e/B)

The relationship between the ultimate axial strength and the load eccentricity ratio ranging from 0 to 0.45 is illustrated in Figure 4.11.
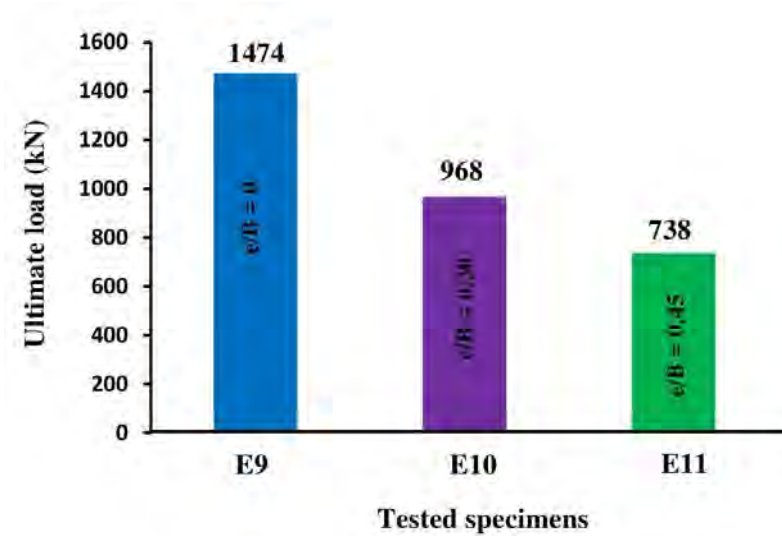
Figure 4.11 Effect of load eccentricity ratio on ultimate load

63

It can be observed from figure 4.11 that, ultimate axial strength decreases by 35% and 50% when e/B ratio increases from 0 to 0.30 and 0.45. When load eccentricity is applied, the ultimate load decreases rapidly due to the generation of secondary moment.

4.5 Axial strain at peak load

Axial strain at peak load is a great indicator of confinement and deformability as well as ductility of the specimen which is very interesting parameter in design consideration. The effect of concrete compressive strength (f_c'), plate slenderness ratio (B/t), global slenderness ratio (L/B) and load eccentricity ratio (e/B) on the peak axial strain is shown in Table 4.3.

Table 4.3 Axial strain at ultimate load of test columns

Specimen design	Cross-sectional size	Concrete compressive strength	Yield stress	Cross-sectional slenderness	Overall slenderness	Load eccentricity ratio	Strain at peak load	% of variation
	B x t x L	f_c'	f_y	B/t	L/B	e/B	ε_u	% $\Delta\varepsilon_u$
	(mm x mm x mm)	(MPa)	(MPa)				($\mu\varepsilon$)	
E1	100 x 4 x 1000	27	350	25	10	0.30	6773	–
E2	100 x 4 x 1000	35	350	25	10	0.30	5884	– 13%
E3	100 x 4 x 1000	44	350	25	10	0.30	5698	– 16%
E6	125 x 5 x 1000	35	350	25	8	0.30	8821	–
E5	125 x 4 x 1000	35	350	31	8	0.30	7509	– 15%
E4	125 x 3 x 1000	35	350	42	8	0.30	5900	– 33%
E8	100 x 4 x 300	44	350	25	3	0.30	5908	–
E7	100 x 4 x 500	44	350	25	5	0.30	5864	– 2%
E3	100 x 4 x 1000	44	350	25	10	0.30	5698	– 4%
E9	150 x 5 x 1000	44	350	30	7	0	6928	–
E10	150 x 5 x 1000	44	350	30	7	0.30	7796	+ 13%
E11	150 x 5 x 1000	44	350	30	7	0.45	11824	+ 71%

4.5.1 Effect of concrete compressive strength (f_c')

Figure 4.12 shows the effect of concrete compressive strength ranging from 27 to 44 MPa on the axial strain at ultimate load of eccentrically loaded CFST columns. It can be seen from Figure 4.12 that, a specimen comprised of high strength concrete generally has a smaller strain at peak load compared with the corresponding

specimen infilled with normal strength concrete. This is attributed to the fact that high strength concrete dilates much slower than normal strength concrete, thus the confinement effect from steel tube is more pronounced for the normal strength concrete. When increasing the concrete compressive strength from 27 MPa to 35 MPa and 44 MPa, the peak strain was found to decrease by 13% and 16% respectively.
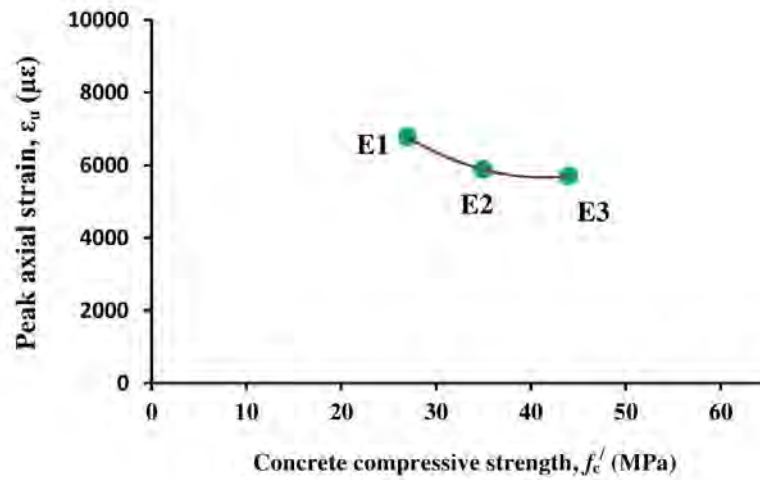
Figure 4.12 Effect of concrete compressive strength on peak axial strain

4.5.2 Effect of cross-sectional slenderness ratio (B/t)

The effect of B/t ratio ranging from 25 to 42 on the peak axial strain of eccentrically loaded CFST columns is indicated in Figure 4.13. This figure illustrates that the values of peak strains increase with the decrease of B/t ratio. It is not surprising since thicker steel tube could delay the steel yielding of the corresponding specimen and thus increase the strain. When the B/t ratio increased from 25 to 31 and 42, the strain at peak load of CFST column was observed to decrease by 15% and 33% respectively.
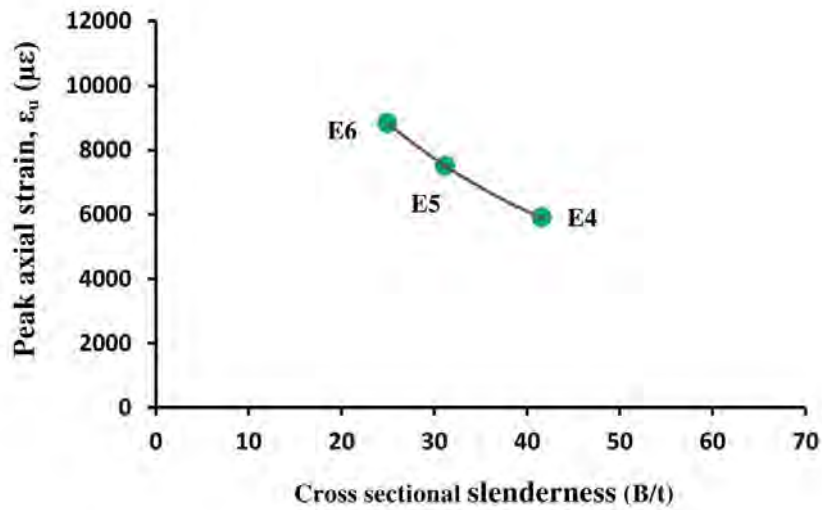
Figure 4.13 Effect of cross-sectional slenderness ratio on peak axial strain

4.5.3 Effect of global slenderness ratio (L/B)

The effect of L/B ratio ranging from 3 to 10 on the peak axial strain of eccentrically loaded column is demonstrated in figure 4.14. The peak axial strain was found to slightly decrease with the increase of L/B ratio for the CFST columns. This is owing to the fact that tube confinement is reduced with the increase of the L/B ratio of the tested columns.
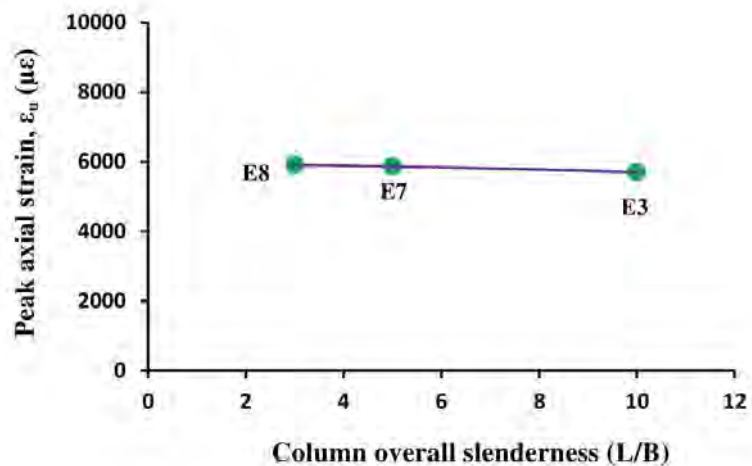
Figure 4.14 Effect of global slenderness ratio on peak axial strain

66

4.5.4 Effect of load eccentricity ratio (e/B)

The effect of load eccentricity ratio on the ultimate axial strain is shown in Figure 4.15. The value of peak strain increased with the increase of e/B ratio of the CFST columns. This is due to the fact that non-directly loaded concrete could provide extra support to the partially loaded concrete. When the e/B ratio was increased from 0 to 0.30 and 0.45, the peak axial strains of the tested columns were found to increase by 13% and 71% respectively with respect to the peak axial strain of concentrically loaded column.
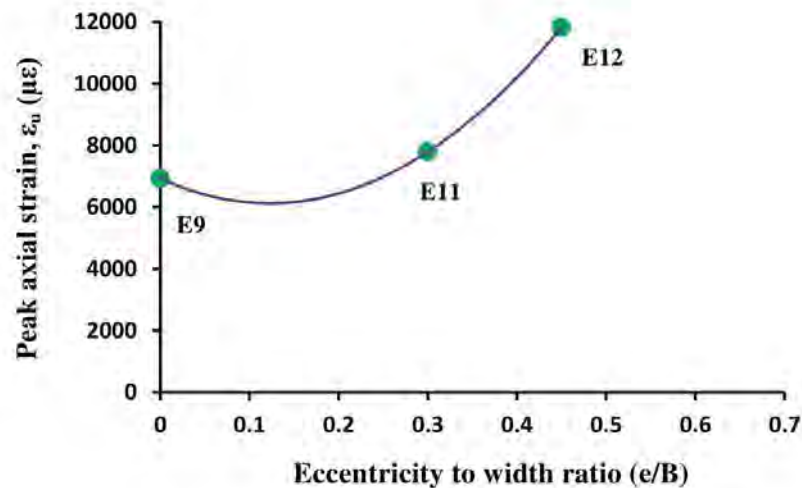
Figure 4.15 Effect of load eccentricity ratio on peak axial strain

4.6 Axial Load versus Mid-Height Deflection Relation

The eccentrically loaded columns developed a somewhat lateral deflection due to the generation of secondary moment. When the load was small, the lateral deflection of the specimen at mid-height was small and approximately proportional to the applied load. When the load reached about 60% to 70% of the maximum load, the lateral deflection at mid-height started to increase significantly. Two transverse strain gauges and two midory LVDTs (linear variable displacement transducers) at mid-height were used to measure the later deflection. The effects of concrete compressive strength ($f_c^/$), plate slenderness ratio (B/t) and global slenderness ratio (L/B) and load

eccentricity ratio (e/B) on the measured axial load (*N*) versus mid-height deflection (δ_m) curves are shown in Figures 4.17, 4.18, 4.19 and 4.20 respectively. In the figures, the axial loads were calculated from the testing machine and transverse strains were calculated from the average value of strain gauges. To measure mid-height deflection: the values of transverse strain gauges were used before tube buckling and after that, displacement readings of the midory LVDTs were taken (Tao and Han 2016). The values of the mid-height deflection of the specimens are shown in Table 4.4.
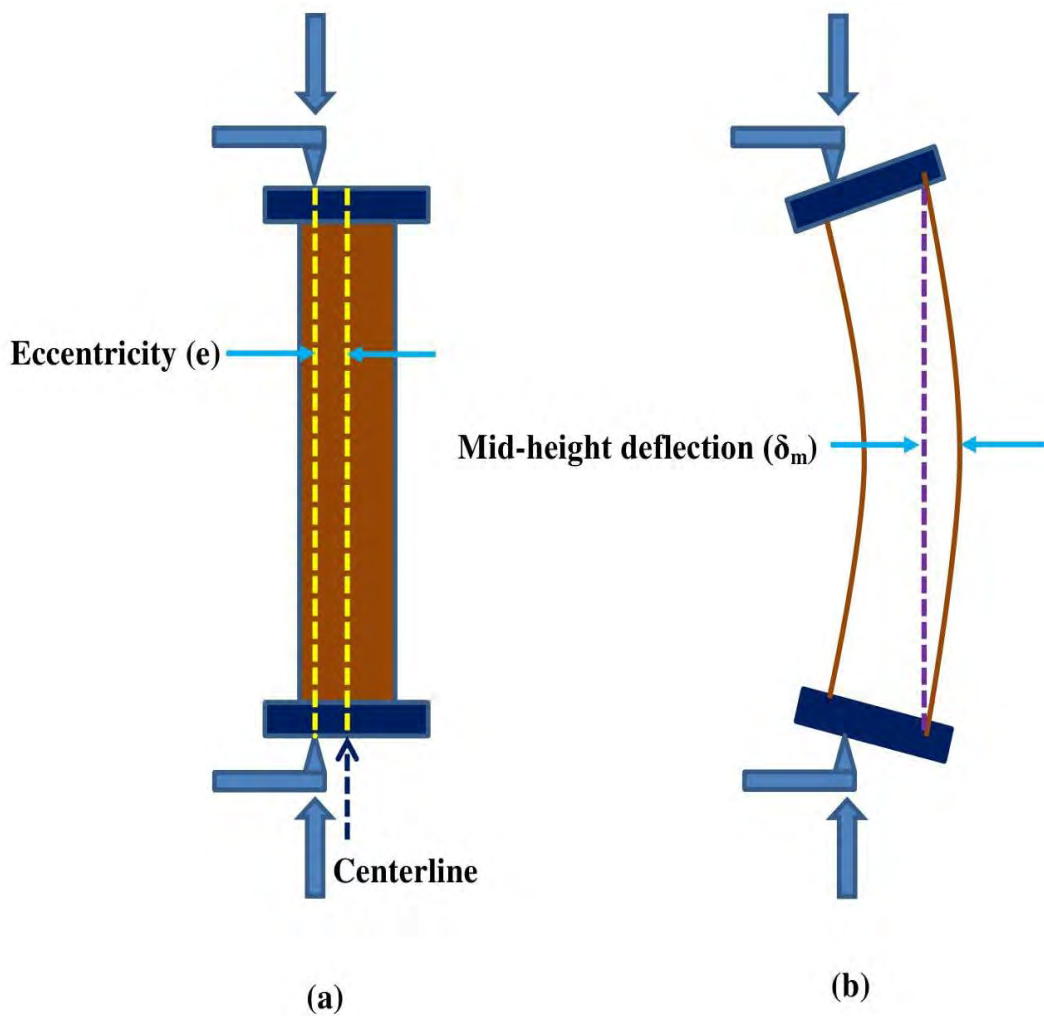
Figure 4.16 Mid-height deflection of test columns

Table 4.4 Mid-height deflection at peak load of test columns

Specimen design	Cross-sectional size	Concrete compressive strength	Yield stress	Cross-sectional slenderness	Overall slenderness	Load eccentricity ratio	Mid-height deflection at peak load	% of variation
	B x t x L	$f_c^/$	f_y	B/t	L/B	e/B	δ_m	$\Delta\%\delta_m$
	(mm x mm x mm)	(MPa)	(MPa)				(mm)	
E1	100 x 4 x 1000	27	350	25	10	0.30	4.80	–
E2	100 x 4 x 1000	35	350	25	10	0.30	2.21	– 54%
E3	100 x 4 x 1000	44	350	25	10	0.30	2.04	– 58%
E6	125 x 5 x 1000	35	350	25	8	0.30	2.72	–
E5	125 x 4 x 1000	35	350	31	8	0.30	3.26	+ 20%
E4	125 x 3 x 1000	35	350	42	8	0.30	3.95	+ 46%
E8	100 x 4 x 300	44	350	25	3	0.30	1.71	–
E7	100 x 4 x 500	44	350	25	5	0.30	1.83	+ 7%
E3	100 x 4 x 1000	44	350	25	10	0.30	2.04	+ 19%
E9	150 x 5 x 1000	44	350	30	7	0	3.11	–
E10	150 x 5 x 1000	44	350	30	7	0.30	3.34	+ 8%
E11	150 x 5 x 1000	44	350	30	7	0.45	5.31	+ 70%

4.6.1 Effect of concrete compressive strength ($f_c^/$)

The actual effect of concrete compressive strength which varies from 27 MPa to 44 MPa on the mid-height deflection of eccentrically loaded CFST columns is pointed out in Figure 4.17. It should be noted from figure 4.17 that, the mid-height deflection of CFST columns increases with the decrease of concrete compressive strength. It is not surprising since low strength concrete shows much quicker volumetric expansion than high strength concrete. Mid-height deflections of specimens were found to 4.80, 2.21 and 2.04 with increasing the corresponding concrete compressive strengths of 27 MPa, 35 MPa and 44 MPa.
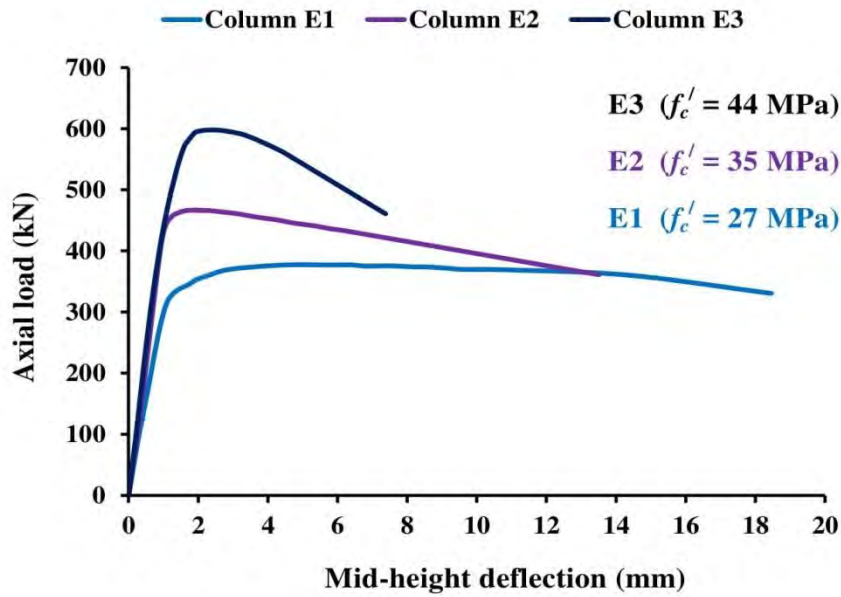
Figure 4.17 Effect of concrete compressive strength on mid-height deflection

4.6.2   Effect of cross-sectional slenderness ratio (B/t)

The relationship between mid-height deflection and B/t ratio ranging from 25 to 42 is demonstrated in Figure 4.18. It can be seen from Figure 4.18 that, mid-height deflection increases by 20% and 46% when B/t ratio increases from 25 to 31 and 42. This is due to the fact that thicker steel tube could restrict the lateral deformation of concrete.
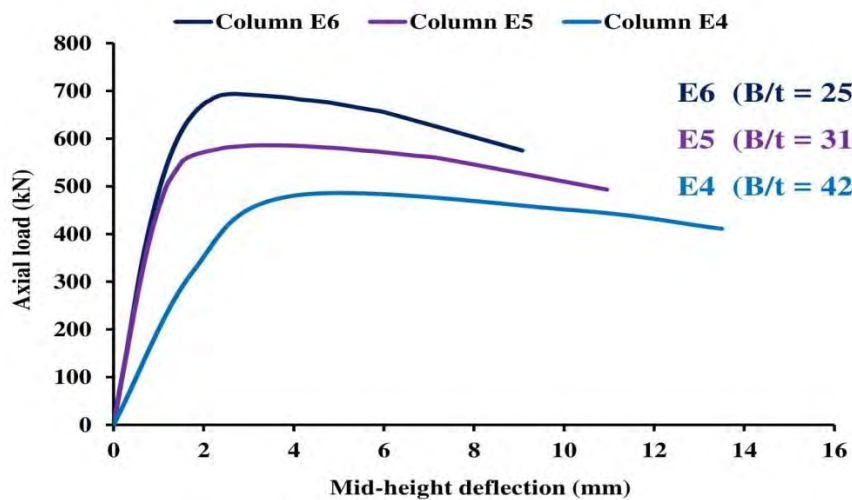
Figure 4.18 Effect of cross-sectional slenderness ratio on mid-height deflection

70

4.6.3 Effect of global slenderness ratio (L/B)

The relationship between mid-height deflection and L/B ratio ranging from 3 to 10 is demonstrated in Figure 4.19.
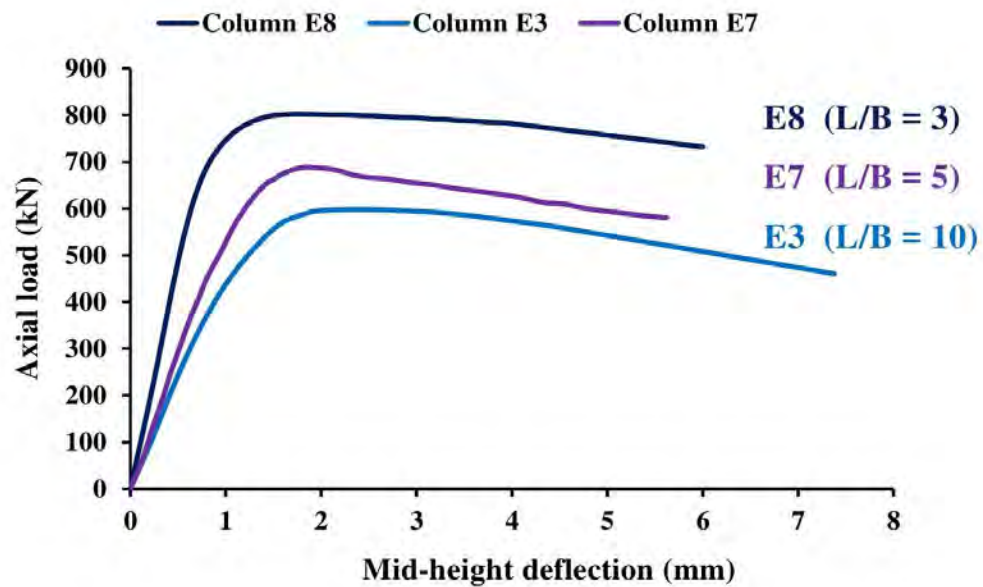
Figure 4.19 Effect of global slenderness ratio on mid-height deflection

It can be seen from Figure 4.19 that, mid-height deflection increases by 7% and 19% when L/B ratio increases from 3 to 5 and 10. This is owing to the fact that columns with higher L/B ratio generally undergo elastic buckling. This is because of the columns having higher overall slenderness ratio, buckle much earlier before gaining its full capacity.

4.6.4 Effect of load eccentricity ratio (e/B)

The effect of load eccentricity ratio ranging from 0 to 0.45 on the mid-height deflection of CFST columns are demonstrated in Figure 4.20. The Figure 4.20 illustrates that increasing e/B ratio remarkably increases the mid-height deflection of the tested columns. This is due to the generation of excess second order moment of specimen with higher e/B ratio. When the e/B ratio was increased from 0 to 0.30 and 0.45, the mid-height deflection of the columns was found to increase by 8% and 70% respectively.

71
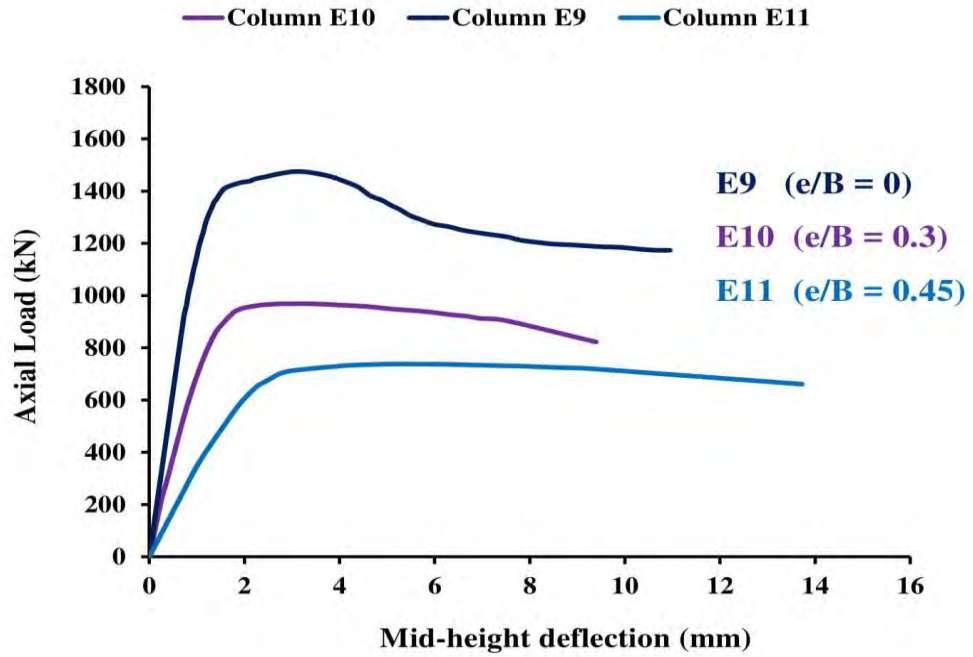
Figure 4.20 Effect of load eccentricity ratio on mid-height deflection

4.7   Ultimate Moment

Moment at peak load is defined as ultimate moment. Ultimate moment was determined considering the second-order effect of the columns using Equation 4.1. The maximum flexural moment occurred at the mid-height of the eccentrically loaded CFST columns.

$$M_{um} = P_u (e + \delta_m) \tag{4.1}$$

Where,

P_u is the peak load

e is the eccentricity

δ_m is the second order mid-height displacement at peak load

The ultimate moment of the specimens is shown in Table 4.5.

Table 4.5 Ultimate moment of test columns

Specimen design	Cross-sectional size	Concrete compressive strength	Yield stress	Cross-sectional slenderness	Overall slenderness	Load eccentricity ratio	Ultimate moment	% of variation
	B x t x L	$f_c^{/}$	f_y	B/t	L/B	e/B	M_{um}	$\Delta\%M_{um}$
	(mm x mm x mm)	(MPa)	(MPa)				(kN-m)	
E1	100 x 4 x 1000	27	350	25	10	0.30	13.11	–
E2	100 x 4 x 1000	35	350	25	10	0.30	15.00	+ 15%
E3	100 x 4 x 1000	44	350	25	10	0.30	19.06	+ 46%
E6	125 x 5 x 1000	35	350	25	8	0.30	27.90	–
E5	125 x 4 x 1000	35	350	31	8	0.30	23.88	– 15%
E4	125 x 3 x 1000	35	350	42	8	0.30	19.87	– 29%
E8	100 x 4 x 300	44	350	25	3	0.30	25.48	–
E7	100 x 4 x 500	44	350	25	5	0.30	21.92	– 14%
E3	100 x 4 x 1000	44	350	25	10	0.30	19.06	– 25%
E9	150 x 5 x 1000	44	350	30	7	0	0.00	–
E10	150 x 5 x 1000	44	350	30	7	0.30	46.83	+ 47%
E11	150 x 5 x 1000	44	350	30	7	0.45	53.73	+ 54%

4.7.1 Effect of concrete compressive strength ($f_c^{/}$)

The relationship between ultimate moment and concrete compressive strength ranging from 27 MPa to 44 MPa is demonstrated in Figure 4.21. It can be found from Figure 4.21 that, ultimate moment increases by 15% and 46% when concrete compressive strength increases from 27 MPa to 35 MPa and 44 MPa. This is due to the fact that the load resisting capability of high strength concrete is much higher than low strength concrete.
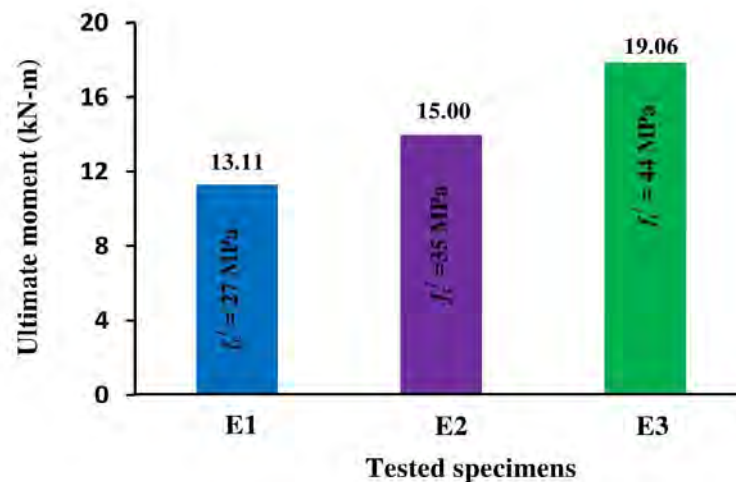
Figure 4.21 Effect of concrete compressive strength on ultimate moment

4.7.2 Effect of cross-sectional slenderness ratio (B/t)

Figure 4.22 illustrates the influence of B/t ratio ranging from 25 to 42 on the ultimate bending moment of the tested columns.
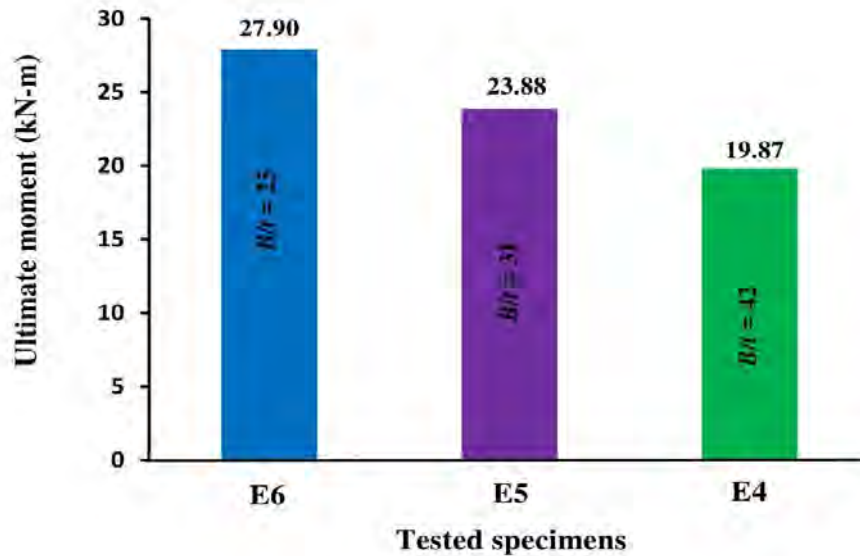
Figure 4.22 Effect of cross-sectional slenderness ratio on ultimate moment

It would appear from figure 4.22 that increasing the B/t ratio causes a significant reduction of ultimate moment. When B/t ratio was increased from 25 to 31 and 42, the ultimate moment of CFST columns was observed to decrease by 15% and 29%. This may be attributed due to the higher rigidity and better load carrying capability of the specimen with thicker steel tube.

4.7.3 Effect of global slenderness ratio (L/B)

The relationship between ultimate moment and L/B ratio ranging from 3 to 10 is pointed out in Figure 4.23. It can be found from figure 4.23 that, ultimate moment decreases by 14% and 25% when L/B ratio increases from 3 to 5 and 10. This is owing to the fact that column with lower L/B ratio shows much higher rigidity and stiffness than the specimen with higher L/B ratio.
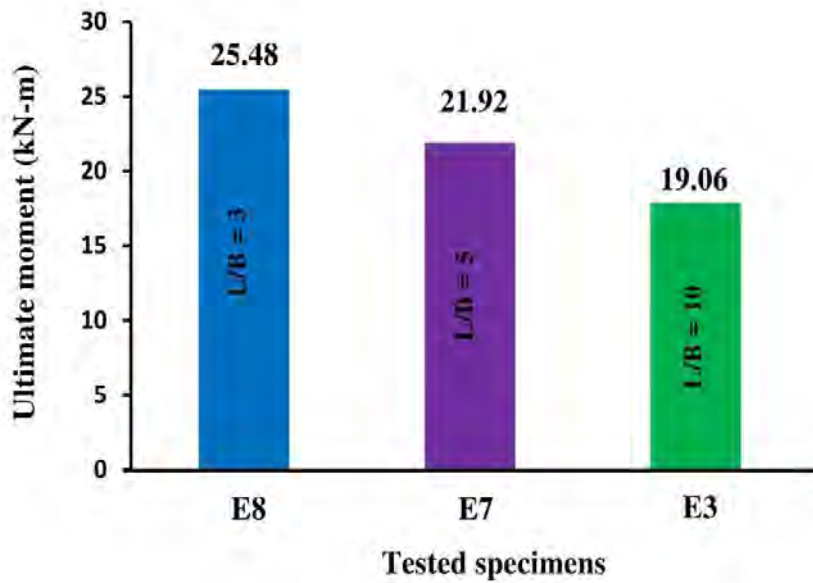
Figure 4.23 Effect of global slenderness ratio on ultimate moment

4.7.4 Effect of load eccentricity ratio (e/B)

The relationship between ultimate moment and e/B ratio ranging from 0 to 0.45 is illustrated in Figure 4.24. It can be observed from Figure 4.24 that, ultimate moment increases by 47% and 54% when e/B ratio increases from 0 to 0.30 and 0.45. This is owing to the fact that the rate of secondary moment generation is increased with the increase of e/B ratio.
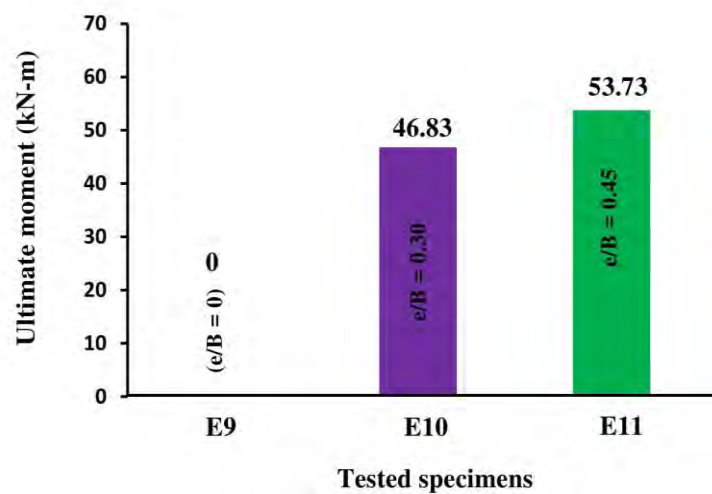
Figure 4.24 Effect of global slenderness ratio on ultimate moment

4.8 Performance Indicies

Performance indices are used to evaluate the contributions of the concrete and steel components to the ultimate strengths of CFST columns and to quantify the strength reduction caused by the section, column slenderness and initial geometric imperfections. These performance indices can be used to investigate the cost-effective designs of CFST under uniaxial eccentric loads. The performance indexes such as ductility index and concrete contribution ratio were determined to observe the performance and cost-effective design of CFST column.

4.8.1 Ductility index

"Ductility" often refers to the ability of a structure to sustain deformation beyond the elastic limit while maintaining a reasonable load carrying capacity until total failure. In modern seismic codes of practice, like EC8 (Eurocode 8, 2005), it is very common to design ductile structures to drastically reduce the design seismic force, leading to a more economical design. The influence of other extreme events, like blast, impact, cyclone and fire, on structures can also be mitigated if the structures are ductile. Currently, the design of ductile structures is to a large extent based on prescriptive detailing provisions. According to Ren et al. (2018), Ductility indexing is defined as the ratio of axial shortening at ultimate strength and post peak shortening corresponding to 85% of the ultimate strength as shown in Figure 4.25. The ductility index of the test specimens is shown in Table 4.6.
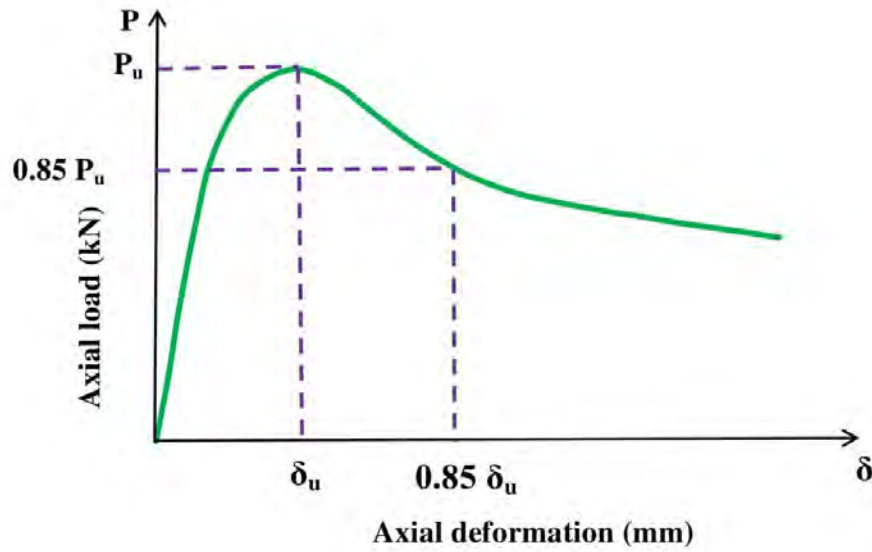
Figure 4.25 Definition of ductility index (DI)

Table 4.6 Ductility index of test columns

Specimen design	Cross-sectional size	Concrete compressive strength	Yield stress	Cross-sectional slenderness	Overall slenderness	Load eccentricity ratio	Ductility index	% of variation
	B x t x L	$f_c^/$	f_y	B/t	L/B	e/B	D.I.	% ΔD.I.
	(mm x mm x mm)	(MPa)	(MPa)					
E1	100 x 4 x 1000	27	350	25	10	0.30	2.84	–
E2	100 x 4 x 1000	35	350	25	10	0.30	2.31	– 19%
E3	100 x 4 x 1000	44	350	25	10	0.30	1.70	– 40%
E6	125 x 5 x 1000	35	350	25	8	0.30	2.39	–
E5	125 x 4 x 1000	35	350	31	8	0.30	2.24	– 7%
E4	125 x 3 x 1000	35	350	42	8	0.30	2.15	– 10%
E8	100 x 4 x 300	44	350	25	3	0.30	2.20	–
E7	100 x 4 x 500	44	350	25	5	0.30	1.92	– 13%
E3	100 x 4 x 1000	44	350	25	10	0.30	1.70	– 23%
E9	150 x 5 x 1000	44	350	30	7	0	1.41	–
E10	150 x 5 x 1000	44	350	30	7	0.30	1.82	+ 29%
E11	150 x 5 x 1000	44	350	30	7	0.45	1.95	+ 38%

a) Effect of concrete compressive strength ($f_c^/$)

Figure 4.26 illustrates the influence of concrete compressive strength ranging from 27 MPa to 44 MPa on the DI of the tested columns. It would appear from Figure 4.26 that increasing the concrete compressive strength causes a significant reduction of DI. This is due to the brittleness nature of high strength concrete. When the concrete

77

compressive strength was increased from 27 MPa to 35 MPa and 44 MPa, the DI of CFST columns was noticed to decrease by 19% and 40%.
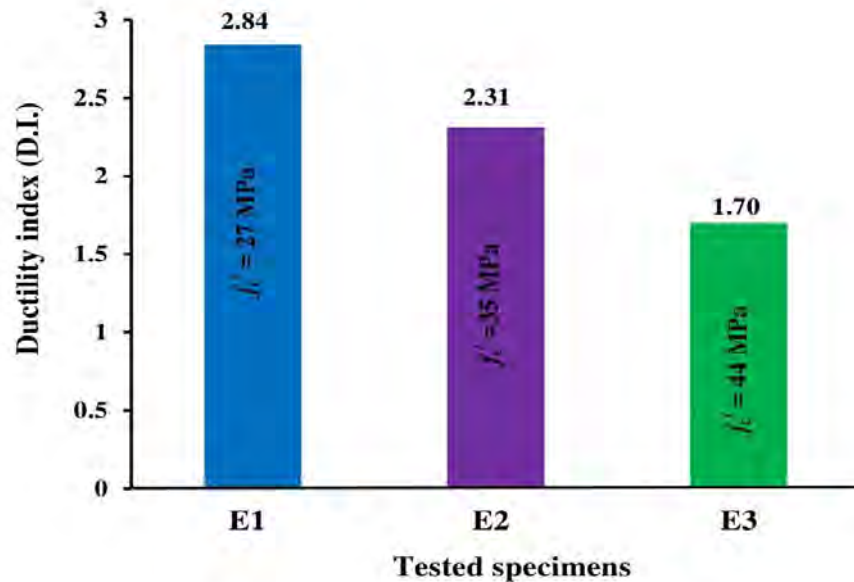
Figure 4.26 Effect of concrete compressive strength on ductility index

b) Effect of cross-sectional slenderness ratio (B/t)

The actual effect of B/t ratio which varies from 25 to 42 on the DI of the eccentrically loaded CFST columns is pointed out in Figure 4.27. It should be noted from Figure 4.27 that, the CFST columns with larger B/t ratio are generally less ductile. This is not surprising since a steel tube with a smaller B/t ratio is more effective to exert extra support on concrete. Ductility indices of specimens were found to 2.39, 2.24 and 2.15 with increasing the corresponding B/t ratios of 25, 31 and 42.
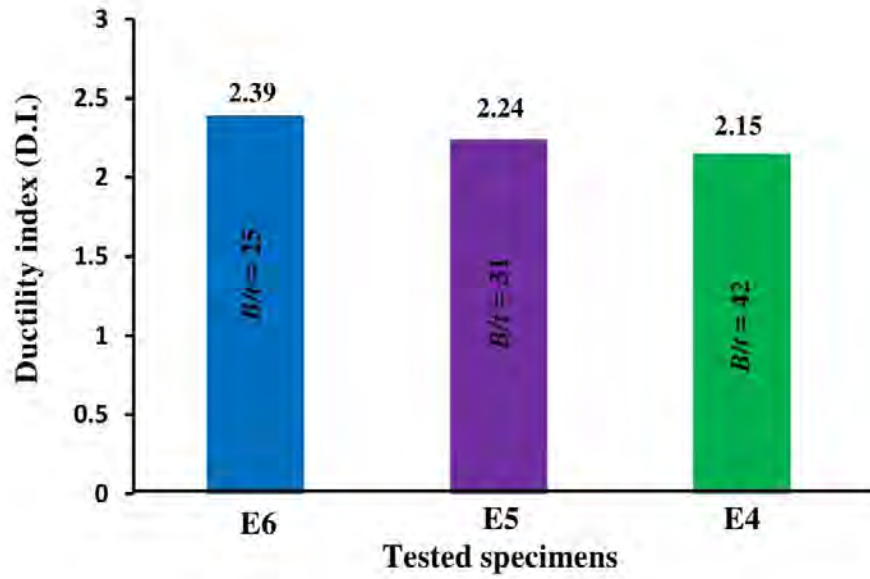
Figure 4.27 Effect of cross-sectional slenderness ratio on ductility index

c) Effect of global slenderness ratio (L/B)

In Figure 4.28, specimens with higher L/B ratio showed lower DI due to plasticity and confinement of a specimen decrease with the increase of the length of a specimen.
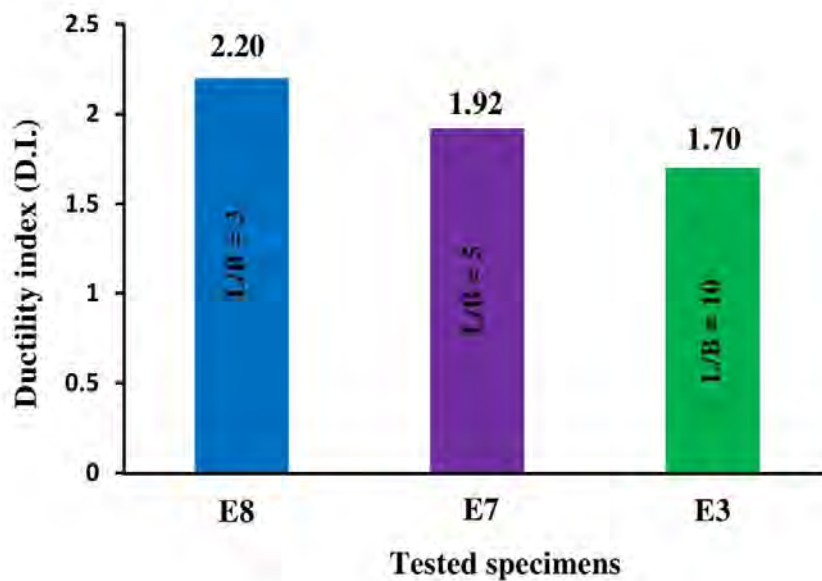
Figure 4.28 Effect of global slenderness ratio on ductility index

It seems that the composite action between the steel tube and the concrete core decreases with increasing global slenderness ratio. When slenderness ratio was increased from 3 to 5 and 10, the DI of CFST columns was found decreased by 13% and 23%.

d) Effect of load eccentricity ratio (e/B)

As shown in Figure 4.29, DI increases by 29% and 38% when load eccentricity ratio increases from 0 to 0.30 and 0.45. It is explained that the non-directly concrete can be considered as a continuous level arm to the steel tube, whilst non-directly loaded concrete and adjacent steel tube could provide extra support to the partially loaded concrete in specimens with higher e/B ratio.
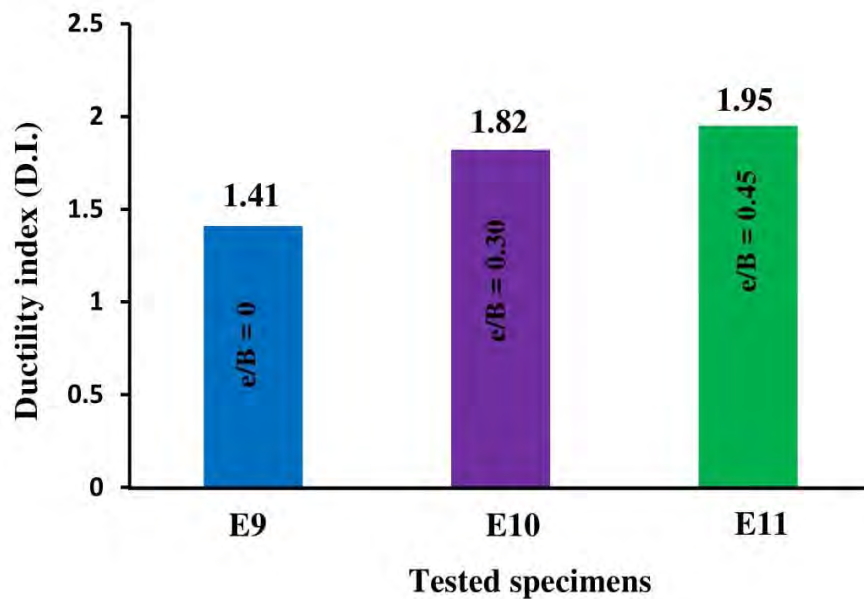
Figure 4.29 Effect of load eccentricity ratio on ductility index

4.8.2 Concrete contribution ratio

The concrete contribution ratio quantifies the contribution of the concrete component to the ultimate axial strength of a CFST column. The concrete core column without reinforcement carries very low loading and does not represents the concrete core in a CFST column. Portolés et al. (2011) used the capacity of the hollow steel tubular

column to define the concrete contribution concrete contribution ratio (CCR), which is given by, concrete contribution ratio $(\xi_c) = P_u\,/\,A_s f_y$ (4.2)

Where,

P_u = Ultimate load of the tested column

$A_s f_y$ = load of corresponding hollow steel with same eccentricity ratio

Table 4.7 presents concrete contribution ratio of test columns subjected to eccentric loading. This table also shows the effects of concrete compressive strength (f_c'), cross-sectional slenderness ratio (B/t), global slenderness ratio (L/B) and load eccentricity ratio (e/B) on the concrete contribution of the CFST columns.

Table 4.7   Concrete contribution ratio of test columns

Specimen design	Cross-sectional size	Concrete compressive strength	Yield stress	Cross-sectional slenderness	Overall slenderness	Load eccentricity ratio	Concrete contribution ratio	% of variation
	B x t x L	f_c'	f_y	B/t	L/B	e/B	ξ_C	$\%\,\Delta\xi_C$
	(mm x mm x mm)	(MPa)	(MPa)					
E1	100 x 4 x 1000	27	350	25	10	0.30	1.31	–
E2	100 x 4 x 1000	35	350	25	10	0.30	1.61	+ 30%
E3	100 x 4 x 1000	44	350	25	10	0.30	2.07	+ 58%
E6	125 x 5 x 1000	35	350	25	8	0.30	0.81	–
E5	125 x 4 x 1000	35	350	31	8	0.30	0.87	+ 8%
E4	125 x 3 x 1000	35	350	42	8	0.30	0.95	+ 17%
E8	100 x 4 x 300	44	350	25	3	0.30	1.83	–
E7	100 x 4 x 500	44	350	25	5	0.30	1.88	+ 4%
E3	100 x 4 x 1000	44	350	25	10	0.30	2.07	+ 14%
E9	150 x 5 x 1000	44	350	30	7	0	1.48	–
E10	150 x 5 x 1000	44	350	30	7	0.30	1.36	– 8%
E11	150 x 5 x 1000	44	350	30	7	0.45	1.17	– 21%

a)   Effect of concrete compressive strength (f_c')

As shown in Figure 4.30, concrete contribution ratio increases by 30% and 58% when concrete compressive strength increases from 27 MPa to 35 MPa and 44 MPa. The main reason for this commensurately increased concrete contribution ratio with the increase of concrete compressive strength is the higher axial strength performance of high strength concrete. The calculated concrete contribution ratios for the corresponding concrete compressive strengths of 27 MPa, 35 MPa and 44 MPa were 1.31, 1.61 and 2.07.
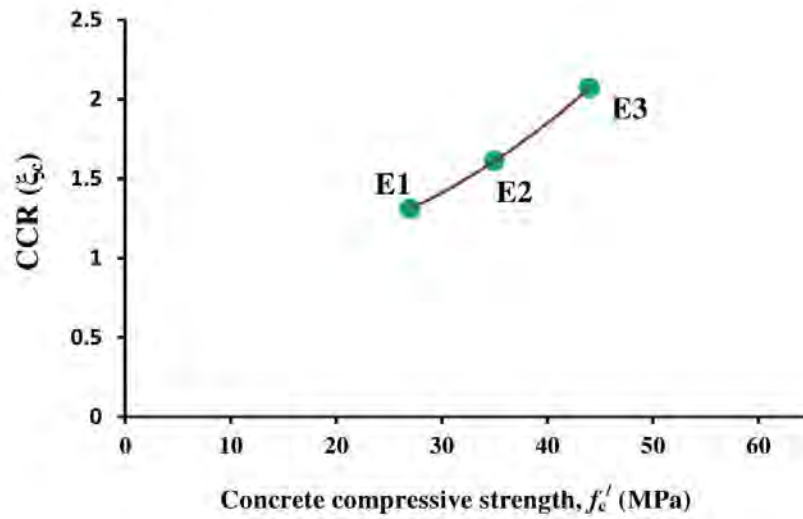
Figure 4.30 Effect of concrete compressive strength on concrete contribution ratio

b) Effect of cross-sectional slenderness ratio (B/t)

The effect of B/t ratio ranging from 25 to 42 on the concrete contribution ratio of eccentrically loaded CFST columns is shown in Figure 4.31.
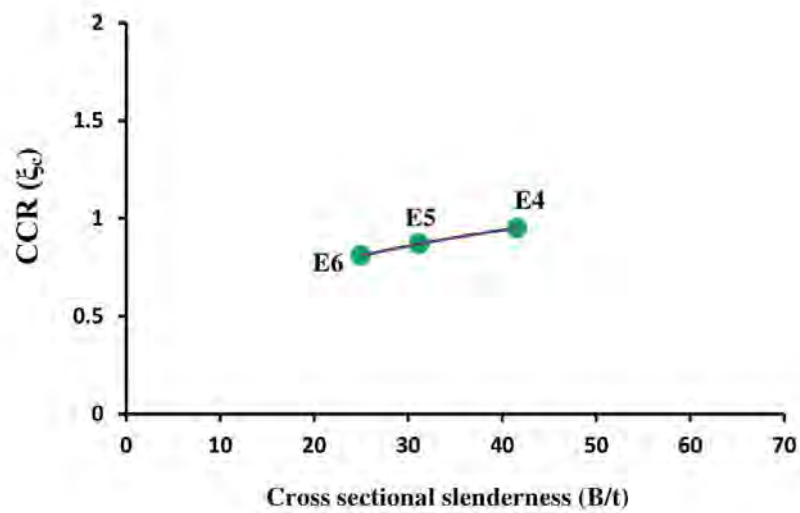
Figure 4.31 Effect of cross-sectional slenderness ratio on concrete contribution ratio

The concrete contribution ratio was found to increase significantly with an increase of the B/t ratio. This may be explained by the fact that increasing the B/t ratio reduces the axial load capacity of the steel tube and also increases the cross-sectional

area of the concrete core, thereby increasing the contribution of the concrete component. The calculated CCR for the B/t ratios of 25, 31 and 42 were 0.81, 0.87 and 0.95.

c) Effect of global slenderness ratio (L/B)

Figure 4.32 presents the results of the concrete contribution ratios calculated by varying slenderness ratios ranging from 3 to 10. It appears from Figure 4.32 that the concrete contribution ratio of CFST columns increases with the increase of the column slenderness ratio. This is due to the presence of larger concrete volume in specimens with higher global slenderness ratio.
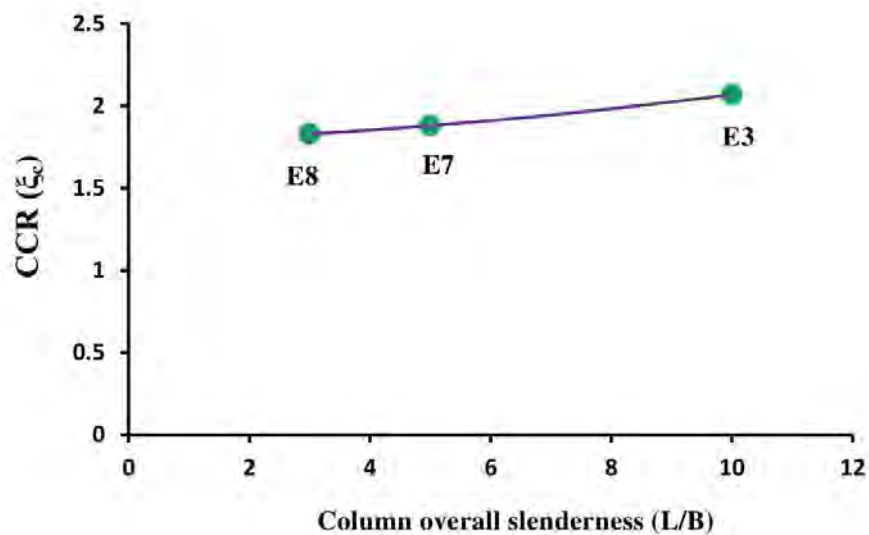
Figure 4.32 Effect of global slenderness ratio on concrete contribution ratio

d) Effect of load eccentricity ratio (e/B)

It can be seen from Figure 4.33 that the concrete contribution ratio decreases with the increase of load eccentricity ratio for tested columns. This may be attributed to the unequal distribution of load to the concrete core for the specimens with higher e/B ratio.
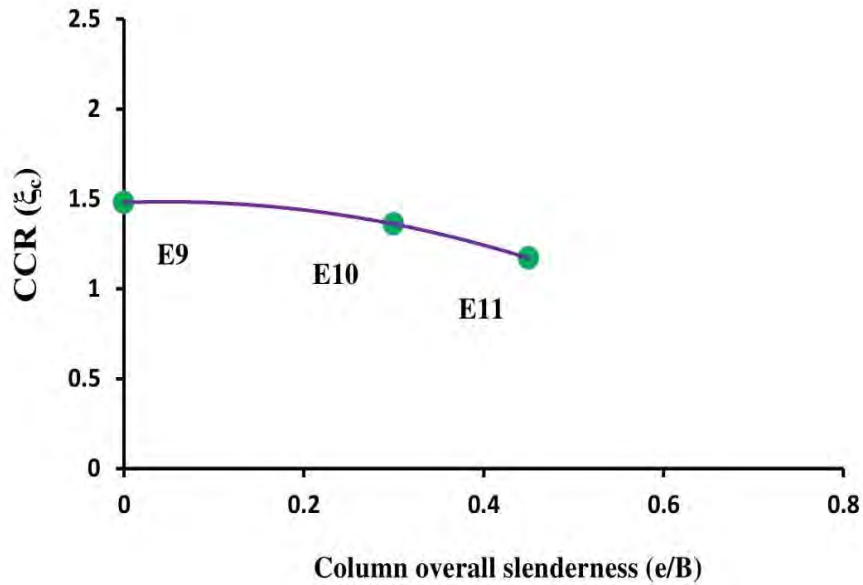
Figure 4.33 Effect of load eccentricity ratio on concrete contribution ratio

4.9   Summary

A detailed experimental investigation was performed to study the behavior of CFST columns under uniaxial eccentric compression. The geometric and material properties were varied and their influence was observed with respect to failure modes, ultimate load, mid-height deflection, load strain responses and performance indexes. Based on the results, it was determined that concrete compressive strength, cross-sectional slenderness ratio, global slenderness ratio and load eccentricity ratio have significant effect on the fundamental behavior of CFST column. Increasing the concrete compressive strength improved the ultimate capacity of the column but decreased the overall column performance because of its less ductile behavior. On the other hand, columns with higher global slenderness ratio showed lower ultimate capacity and less ductile behavior with global buckling failure. Column with lower cross-sectional slenderness ratio exhibited better column performance for its higher steel contribution of the specimens but columns with higher load eccentricity ratio showed lower ultimate capacity and stiffness due to the generation of excess second order moment.

84

Chapter 5
DESIGN CODES AND COMPARISIONS

5.1 General

Different formulae were proposed over the years to calculate the axial capacity and bending moment of the CFST columns. For instance, some of them accounted for the increase in the infilled concrete strength while other just ignored it. The American Institute of Steel Construction AISC (2010) formula is based on the structural steel. While the exclusively used for composite elements design, Eurocode 4 (2005) considers the full confining effect of CFST columns for the prediction of ultimate axial load and bending moment. In this chapter, the design approaches adopted in (Eurocode 4 and AISC-LRFD 2010) are reviewed and applied to calculate the ultimate strength and maximum bending moment of the tests columns. Subsequently, the predicted values are compared with the experimental results obtained from the experiments.

5.2 AISC-LRFD (2010) Formulae

The AISC-LRFD (2010) defines a composite column as a steel column fabricated from rolled or built-up steel shapes and encased in structural concrete or fabricated from steel pipe or tubing and filled with structural concrete. In this specification, the design method for composite columns is based on the ultimate strength of the materials part of the cross-section and takes into account the inelastic material properties with the required design loads as factored service loads. It contains the latest design approach of structural steel based on the ultimate strength concept. The nominal strength of a composite cross section is calculated from the ultimate resistance to load and reduction capacity factors related to material properties and characteristics of member failure are applied to the nominal strength of the cross-section.

For the plastic stress distribution method, the nominal strength shall be computed assuming steel components have reached a stress of f_y in either tension or

compression and concrete components in compression due to axial force and/or flexure have reached a stress of $0.85f_c^{\prime}$. For round HSS filled with concrete, a stress of $0.95f_c^{\prime}$ is permitted to be used for concrete components in compression due to axial force and/or flexure to account for the effects of concrete confinement.

Local buckling of the CFST should be accounted for through classification of these composite members into compact, non-compact or slender. The element is considered to be compact if its b/t ratio is less than λ_p and to be non-compact if its b/t ratio is more than λ_p but less than λ_r. Moreover, if the section"s ratio exceeds, then it is classified as slender. The maximum allowed ratio specified in the Table 5.1 should not be exceeded in order for the AISC"s formulae to be applicable. Table 5.2 shows the limits of b/t ratios for CFST members subject to axial compression and their calculation for local buckling classification. Based on these limits, all the tested sections in this study are compact.

Table 5.1 The condition for compact, noncompact and slender composite member subjected to axial compression (AISC-2010)

Description of Element	Width to thickness Ratio	λ_p Compact/Noncompact	λ_r Noncompact/Slender	Maximum Permitted
Walls of Rectangular HSS and Boxes of uniform Thickness	b/t	$2.26\sqrt{\dfrac{E}{F_y}}$	$3.00\sqrt{\dfrac{E}{F_y}}$	$5.00\sqrt{\dfrac{E}{F_y}}$
Round HSS	D/t	$\dfrac{0.15\,E}{F_y}$	$\dfrac{0.19\,E}{F_y}$	$\dfrac{0.31\,E}{F_y}$

Table 5.2 Compactness check of test columns

Specimen design.	Cross-sectional size	Width to thickness Ratio	λ_p	λ_r	Maximum Permitted	Type of cross-sectional slenderness
	B x t x L	b/t				
	(mm x mm x mm)					
E1	100 x 4 x 1000	23	54	72	119	Compact
E2	100 x 4 x 1000	23	54	72	119	Compact
E3	100 x 4 x 1000	23	54	72	119	Compact
E4	125 x 3 x 1000	40	54	72	119	Compact
E5	125 x 4 x 1000	29	54	72	119	Compact
E6	125 x 5 x 1000	23	54	72	119	Compact
E7	100 x 4 x 500	23	54	72	119	Compact
E8	100 x 4 x 300	23	54	72	119	Compact
E9	150 x 5 x 1000	30	54	72	119	Compact
E10	150 x 5 x 1000	30	54	72	119	Compact
E11	150 x 5 x 1000	30	54	72	119	Compact

5.2.1 Axial compressive strength

In AISC-LRFD (2010) the design of composite column is based on the design equations for steel columns. The compressive capacity of axially loaded circular concrete filled steel tubes can be determined for the limit state of flexural buckling with the following equations for compact sections:

$$P_u = f_y A_s + C_2 f_c' A_c \tag{3.1}$$

Where,

$C_2 = 0.85$ for rectangular section and 0.95 for circular section.

The effective stiffness of the composite section, EI_{eff}, for all section shall be:

$$EI_{eff} = E_s I_s + E_s I_{sr} + C_3 E_c I_c \tag{3.2}$$

Where, C_3 = Coefficient for calculation of effective rigidity of filled composite compression member.

$$C_3 = 0.6 + 2\left[\frac{A_s}{A_s + A_c}\right] \leq 0.9 \tag{3.3}$$

The available compressive strength need not be less than specified for the bare steel member

$$P_e = \frac{\pi^2 EI_{eff}}{(KL)^2} \tag{3.4}$$

$A_c =$ Area of concrete, in^2 (mm^2)

$A_s =$ Area of the steel section, in^2 (mm^2)

$E_c =$ Elasticity modulus of concrete $= W_c^{1.5}\sqrt{f_c'}$, Ksi $/ \left(0.043 W_c^{1.5}\sqrt{f_c'}\right)$, Mpa

$EI_{eff} =$ Effective stiffness of composite section, kip-in^2 (N-mm^2)

$E_s =$ Modulus of elasticity of steel $= 29,000$ ksi (200,000 MPa)

$f_y =$ Specified minimum yield stress of steel section, ksi (MPa)

$f_{ysr} =$ Specified minimum yield stress of reinforcing bars, ksi (MPa)

$I_c =$ Moment of inertia of the concrete section about the elastic neutral axis of the composite section, in^4 (mm^4).

$I_s =$ Moment of inertia of steel shape about the elastic neutral axis of the composite section, in^4 (mm^4)

$I_{sr} =$ Moment of inertia of reinforcing bars about the elastic neutral axis of the composite section, in^4 (mm^4)

$K =$ effective length factor

$L =$ laterally unbraced length of the member, in (mm)

$f_c' =$ specified compressive strength of concrete, ksi (MPa)

$W_c =$ weight of concrete per unit volume ($90 \leq W_c \leq 155$ lbs/ft3 or $1500 \leq W_c \leq 2500$ kg/m^3)

The design compressive strength, $\phi_c P_n$ of doubly symmetric axially loaded concrete filled composite members shall be determined for the limit state of flexural buckling based on member slenderness as follows:

When $P_{no}/P_e \leq 2.25$

$$P_n = P_{no}\,[0.658]^{P_{no}/P_e} \tag{3.5}$$

When $P_{no}/P_e > 2.2$

$$P_n = 0.877[P_e] \tag{3.6}$$

$P_{no} = P_u =$ Nominal compressive strength of axially loaded composite member (kN)

$P_e =$ Elastic critical buckling load (kN)

$$\lambda = (P_n/P_{no}) \tag{3.7}$$

$\lambda =$ Slenderness reduction factor

5.2.2   Axial loads and flexure (P-M)

Design for combined axial force and flexure may be accomplished using either the strain compatibility method or the plastic-distribution method. The strain compatibility method is a generalized approach that allows for the construction of an interaction diagram based upon the same concepts used for reinforced concrete design. Application of the strain compatibility method is required for irregular/nonsymmetrical sections, and its general application may be found in reinforced concrete design texts and will not be applied further here. Plastic stress distribution method provides three acceptable procedures for filled members. The first procedure, Method 1 invokes the interaction equations of CFST specimen. This is the only method applicable to sections with noncompact or slender elements. The second procedure, Method 2 involves the construction of a piecewise-linear interaction curve using the plastic strength equations. The third procedure, Method 2 – Simplified is a reduction of the piecewise-linear interaction curve that allows for the use of less conservative interaction equations. Among these procedures, Method 2 is used for adopting P-M diagrams of corresponding CFST specimens with considering the length effect.

To assist in developing the interaction curves illustrated within the design examples, a series of equations are provided in AISC-LRFD (2010). These equations define selected points on the interaction curve, without consideration of slenderness effects. For considering the overall length effect of the specimen, slenderness reduction factor is multiplied by the selected points on the interaction curve. Table 5.3 defines the plastic capacities for composite filled HSS bent about its principal axis. The interaction diagram AECBD shown in Figure 5.1 is approximated by the polygon ACDB. Point A and Point B are the pure axial strength and flexural strength of the section, respectively. Point C corresponds to a plastic neutral axis location that results in the same flexural strength as Point B, but including axial compression. Point D corresponds to an axial compressive strength of one half of that determined for Point C. An additional arbitrary Point E is included (between points A and C) for filled rectangular or square HSS bent about its principal axis (AISC-LRFD 2010).
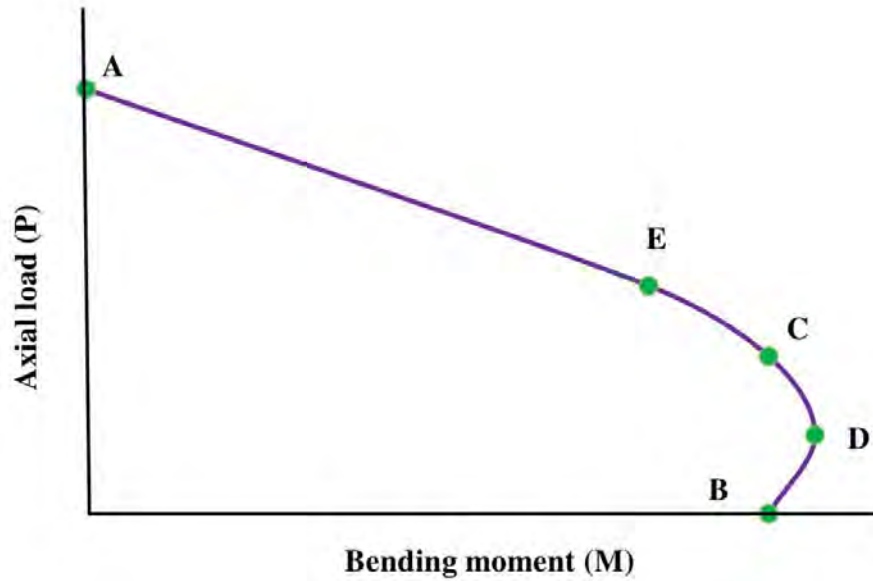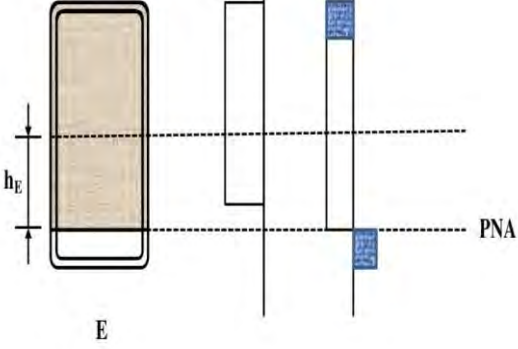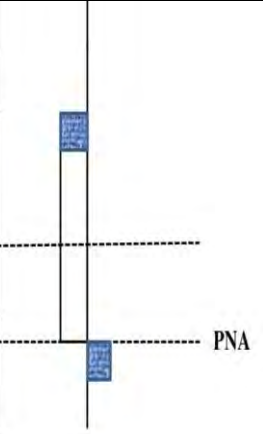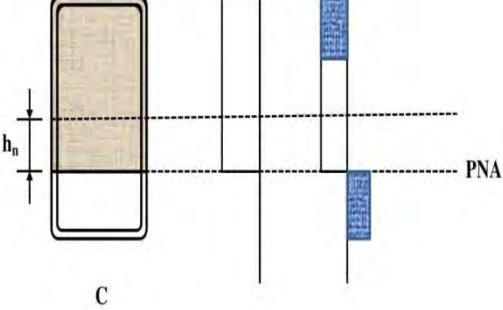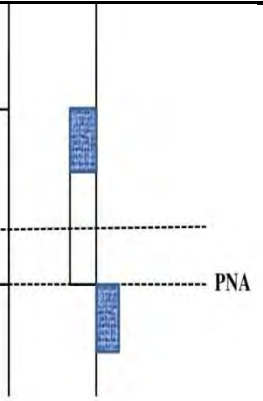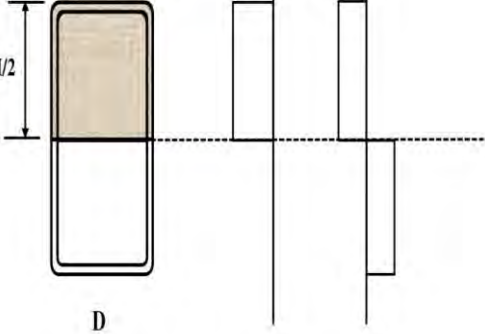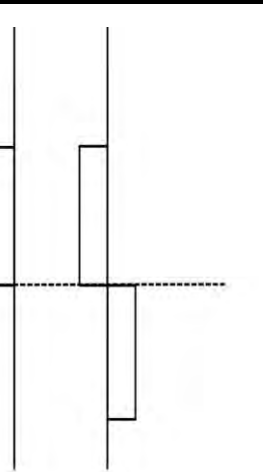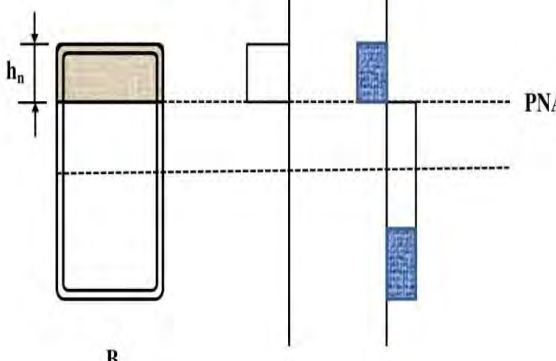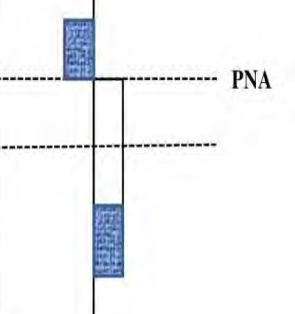
Figure 5.1 Interaction diagram (P-M) for composite columns according to AISC-LRFD (2010)

Table 5.3 Plastic capacities for rectangular CFST column major axis bending (AISC 2010)

Section	Stress Distribution	Point	Defining Equations
		A	$P_A = F_y A_s + 0.85 f_c' A_c$ $M_A = 0$ A_s = Area of steel shape $A_c = b_i h_i - 0.858 r_i^2$ $b_i = B - 2t$ $h_i = H - 2t$ $r_i = t$

Section	Stress Distribution	Point	Defining Equations
E		E	$P_E = \dfrac{0.85f_c'A_c}{2} + 0.85f_c'b_ih_E + 4F_yth_E$ $M_E = M_D - F_yZ_{sE} - \dfrac{0.85f_c'Z_{cE}}{2}$ $Z_{cE} = b_ih_E^2$ $Z_{sE} = 2th_E^2$ $h_E = (h_n/2) + (H/4)$
C		C	$P_C = 0.85f_c'A_c$ $M_C = M_D$
D		D	$P_D = \dfrac{0.85f_c'A_c}{2}$ $M_D = F_yZ_s + \dfrac{0.85f_c'Z_c}{2}$ $Z_s =$ Full x-axis plastic section modulus of HSS $Z_c = (b_ih_i^2/4) - 0.192r_i^3$

Section	Stress Distribution	Point	Defining Equations
		B	$P_B = 0$ $M_B = M_D - F_y Z_{sn} - \dfrac{0.85 f_c' Z_{cn}}{2}$ $Z_{sn} = 2 t h_n^2$ $Z_{cn} = b_i h_n^2$ $h_n = \dfrac{0.85 f_c' A_c}{2[0.85 f_c' b_i + 4 t F_y]} \leq \dfrac{h_i}{2}$

Note: Equations in this table are equally applicable to bending about the shape‶s X-X axis (when H ≥ B) and to bending about the shape‶s Y-Y axis (when B > H).

5.3 Eurocode 4 (2005) Formulae

There are two approaches adopted by the Eurocode 4 (2005) for calculating the axial capacity and bending moment of concrete filled steel tube columns, the general method and the simplified method. In the general method, the second order effects and imperfections of the compression members are taken into consideration explicitly. This method may be used for members with symmetrical sections, but they are also applicable to non-prismatic axial members. Consequently, appropriate software for numerical computation is essential for the application of the general method. In the simplified method, the European buckling curves for steel columns are utilized. The element‶s imperfections are implicitly taken into account. Unlike the general method, the simplified one is limited to prismatic composite axial members with symmetrical sections. Both methods are based on the following assumptions:

a) Flat sections stay flat while the column is deforming due to loading,

b) Till failure, the existence of full interaction between the concrete and steel surfaces is maintained.

In this research, only the simplified method is applied due to its applicability to the tested specimens and the calculation simplicity.

5.3.1 Resistance of cross sections

The Euro Code 4 column design assumes that concrete and steel interact fully with each other until failure. Design by the Euro Code method uses the full plastic axial and moment capacity of the cross-section. Reduction factors are applied to these values based on the column slenderness and other considerations. The Euro Code composite design considers all material properties of the cross-section, including partial safety factors for the different materials.

The plastic resistance to compression $N_{pl,Rd}$ of a composite cross-section should be calculated by adding the plastic resistance of its components:

$$N_{pl,Rd} = A_a f_{yd} + A_c f_{cd} \qquad (3.8)$$

For members in axial compression, the design value of the normal force N_{Ed} should satisfy:

$$\frac{N_{Ed}}{\chi \, N_{pl,Rd}} \leq 1.0 \qquad (3.9)$$

Where: $N_{pl,Rd}$ is the plastic resistance of the composite section.

χ is the reduction factor for the relevant buckling mode.

$$\chi = \frac{1}{\Phi \sqrt{\Phi^2 - \bar{\lambda}^2}}$$

$$\Phi = 0.5(1 + \alpha \, (\lambda - 0.2) + \lambda_2) \qquad (3.10)$$

For concrete filled tubes of circular cross-section, account is taken of increase in strength of concrete caused by confinement provided that the relative slenderness λ does not exceed 0.5 and $e/d < 0.1$, where e is the eccentricity of loading given by M_{Ed}/ N_{Ed} and d is the external diameter of the column.

The plastic resistance to compression is calculated from the following expression:

$$N_{pl,Rd} = \eta_a A_a f_{yd} + A_c f_c d \left(1 + \eta_c \frac{t}{d} \frac{f_y}{f_{ck}}\right) \qquad (3.11)$$

Where: t is the wall thickness of the steel tube, for members with e = 0 the values η_a = η_{ao} and η_c= η_{co} are given by the following expressions:

$$\eta_{ao} = 0.25 \, (3 + 2\lambda) \text{ (but } 1.0) \qquad (3.12)$$

$\eta_{co} = 4.9 - 18.5\lambda_2 + 17\lambda_2$ (but 0) (3.13)

For high strength concrete with $f_{ck} > 50$ MPa, the effective compressive strength of concrete accordance with EC2 (EN 1992-1-1, 2004) is determined by multiplying the characteristic strength by a reduction factor η as given below.

$\eta = 1.0 - (f_{ck} - 50)/200$ (3.14)

The relative slenderness λ for the plane of bending being considered is given by:

$$\lambda = \sqrt{\frac{N_{p1,RK}}{N_{cr}}}$$ (3.15)

N_{cr} is the elastic critical normal force for the relevant buckling mode, calculated with the effective flexural stiffness $(EI)_{eff}$

Where, K_e is a correction factor that should be taken as 0.6.

I_a, and I_c are the second moments of area of the structural steel section, the un-cracked concrete section for the bending plane being considered.

5.3.2 Axial load and bending moment

The resistance of the cross-section subjected to axial load and bending moment can be calculated by utilizing a full plastic stress distribution assumption. In the steel beam-column interaction curve, the moment resistance reduces with increasing axial load. However, in the composite beam-column interaction curve, the moment resistance increases up to the "balance point" due to the presence of axial load because of the pre-stressing effect of the compressive forces. The interaction curve can be drawn by determining the stress block at numerous levels of axial load. This calculation is easily performed by computer routines. An approximation of the full interaction curve can be determined by calculating several points on the curve and connecting those points with straight lines. These points may be calculated by assuming rectangular stress blocks (Euro code 4, 2005). As a simplification, the interaction curve is a polygonal diagram as shown in Figure 5.2. The plastic stress distributions of a CFST cross section for the points A, B, C and D are also shown in Table 5.4. The design formulae for the section analysis of rectangular CFST columns can be determined from Table 5.4.
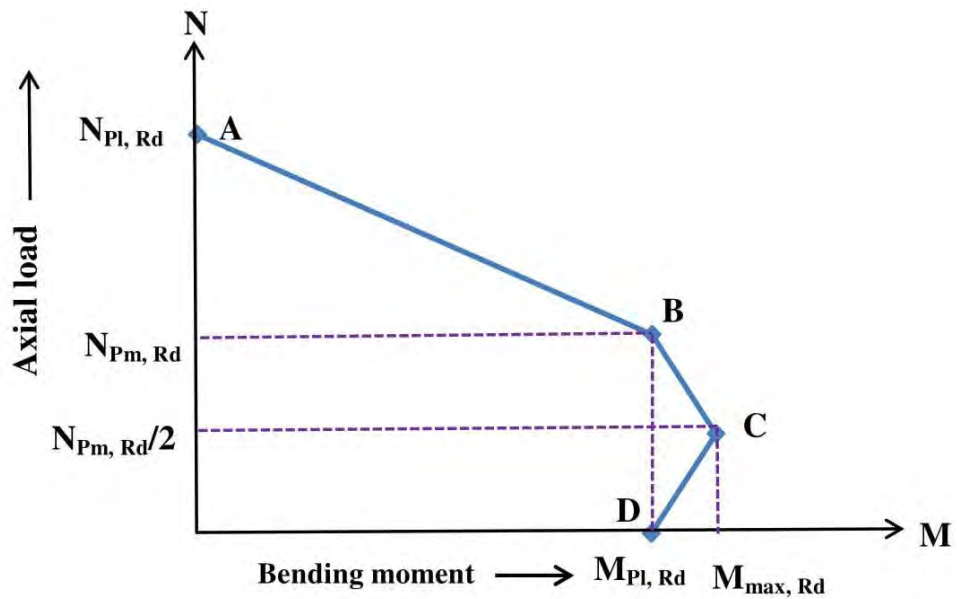
Figure 5.2 Simplified interaction curve composite columns according to Eurocode 4 (2005)

Table 5.4 Section analysis of rectangular CFST column

Section	Stress Distribution	Point	Defining Equations
		A	$N_{pl,Rd} = A_a f_{yd} + A_c f_{cd}$

	B	$$h_n = \frac{A_c f_{cd}}{2bf_{cd} + 4t(2f_{yd} - f_{cd})}$$ $$W_{pc} = \frac{(b-2t)(h-2t)^2}{4} - (2/3)r^3 - r^2(4-\pi)\left(\frac{h}{2} - t - r\right)$$ $$W_{pc,n} = (b-2t)h_n^2$$ $$W_{pa} = (bh^2/4) - (2/3)(r+3)^3 - (r+t)^2(4-\pi)\left(\frac{h}{2} - t - r\right) - W_{pc}$$ $$W_{pa,n} = bh_n^2 - W_{pc,n}$$ $$M_{pl,Rd} = (W_{pa} - W_{pa,n})f_{yd} + 0.5(W_{pc} - W_{pc,n})f_{cd}$$
	C	$$N_{pm,Rd} = A_c f_{cd}$$
	D	$$M_{pl,Rd} = W_{pa}f_{yd} + 0.5\,W_{pc}f_{cd}$$

Note: For bending about the weak axis, the dimensions **b** and **h** are to be exchanged.

5.4 Limitations of Design Standards

For design purposes, both codes have provided some limitations on material strengths and section slenderness, as summarized in Table 5.5. Beyond those limitations, the existing codes might give less accurate strength predictions. Even within the limitations, the strength and moment predictions from the existing codes show considerable deviation from the experimental results and the prediction accuracy could be further improved.

Table 5.5 Predicted guidelines and limitations

Corresponding guidelines	Cross sectional shape	Prediction of ultimate strength	$f_c^{/}$ (MPa)	f_y (MPa)	H/t (H = Cross-sectional height)
AISC	Rectangular	$P_{AISC} = A_s f_y + 0.85 A_c f_c^{/}$ $P_n = P_{no} [\, 0.659^{\frac{P_{no}}{P_e}} \,]$ $P_e = \pi^2 (EI_{eff}) / (KL)^2$ $EI_{eff} = E_s I_{sy} + E_s I_{sr} + C_3 E_c I_{cy}$ K=1.00	$21 \le f_c^{/}$ ≤ 70 Mpa	$f_y \le 525$ Mpa	$H/t \le 2.26 \sqrt{E_s/f_y}$
EC4	Rectangular	$P_{EC} = A_s f_y + A_c f_c^{/}$	$20 \le f_c^{/}$ ≤ 60 Mpa	$235 \le f_y$ ≤ 460 Mpa	$H/t \le 52 \sqrt{235/f_y}$

5.5 Comparison of Results with Code Predictions

Nowadays, there are several well-known national standards or recommendations to address the design of cold-formed carbon steel CFST columns, such as Eurocode 4, AISC-LRFD 2010, ACI 2014, British standard BS 5400 and Canadian standard association CSA. Based on the compressive experimental program undertaken in this investigation, the design codes (AISC-LRFD 2010 and Eurocode 4) were compared with the test results to evaluate their applicability under uniaxial loading combined with bending. In design calculations, reduction factors or material safety factors are set to unit. In order to determine the error of the predicted capacity and ultimate bending moment which was found from the axial loads (N) versus moment (M)

interaction curves of corresponding guidelines of the tested specimens, the experimental results were divided by the predicted results.

5.5.1 Eurocode 4 (2005)

a) Compared with ultimate axial loads of tested specimens

The experimental ultimate loads were compared to the maximum loads calculated according to the design method proposed by EC4 (2005) for composite members. EC4 (2005) uses a different model in function of the cross-sectional shape. For rectangular sections, the capacity of the column is obtained as the sum of the contributions of each material. The results obtained by this method are summarized in Table 5.6 together with the error calculated with respect to the experimental values. It can be observed from Table 5.6 and Figure 5.3 that, the mean and standard deviation of P_{EC4}/P_{exp} are 1.06 and 0.20. It indicates that EC4 produces in general unsafe predictions and overestimates columns" strength by about 6% on average. This is attributed to the fact that EC4 considers the full confining effect of square CFST columns for the prediction of ultimate axial load.

Table 5.6 Comparisons of ultimate axial strengths between test results and design codes (EC4 2005)

Symbol	B x t x L	$f_c^{/}$	f_y	B/t	L/B	e/B	P_{exp}	P_{EC4}	P_{EC4} / P_{exp}
	(mm x mm x mm)	(Mpa)	(MPa)				(kN)	(kN)	
E1	100 x 4 x 1000	27	350	25	10	0.30	377	440	1.17
E2	100 x 4 x 1000	35	350	25	10	0.30	466	470	1.01
E3	100 x 4 x 1000	44	350	25	10	0.30	595	530	0.89
E4	125 x 3 x 1000	35	350	42	8	0.30	480	631	1.31
E5	125 x 4 x 1000	35	350	31	8	0.30	586	710	1.21
E6	125 x 5 x 1000	35	350	25	8	0.30	693	791	1.14
E7	100 x 4 x 500	44	350	25	5	0.30	688	530	0.77
E8	100 x 4 x 300	44	350	25	3	0.30	801	530	0.66
E9	150 x 5 x 1000	44	350	30	7	0	1474	1859	1.26
E10	150 x 5 x 1000	44	350	30	7	0.30	968	1078	1.11
E11	150 x 5 x 1000	44	350	30	7	0.45	738	888	1.20
								Mean	1.06
								Standard deviation	0.20
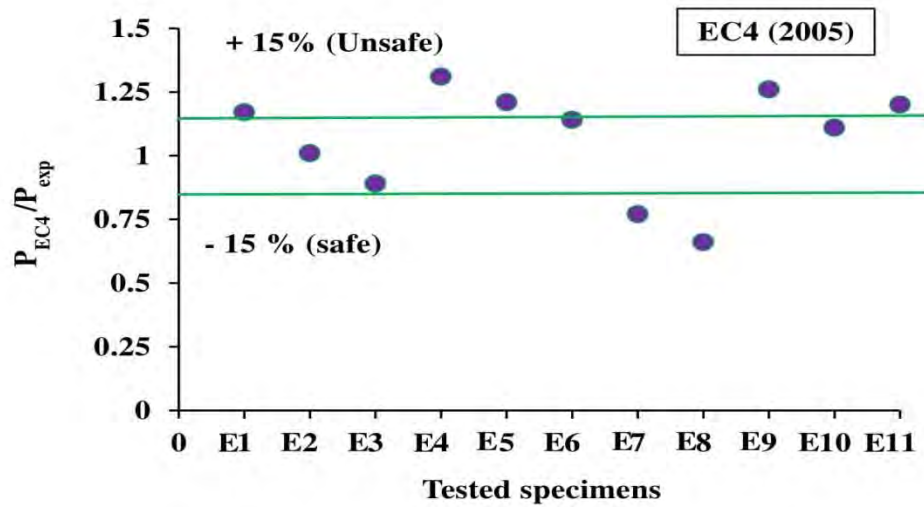
Figure 5.3 Comparison between the predicted (EC4) and measured strength

b) Compared with ultimate moments of tested specimens

The experimental ultimate bending moments were compared to the maximum moments calculated from the axial load (N) versus moment (M) interaction curves proposed by EC4 (2005). It can be seen from Figure 5.4 and Table 5.7 that, EC4 underestimates the columns" ultimate bending moment with a mean and standard deviation of 0.88 and 0.33.

Table 5.7 Comparisons of ultimate bending moments between test results and design codes (EC4 2005)

Symbol	B x t x L	$f_c^{/}$	f_y	B/t	L/B	e/B	M_{exp}	M_{EC4}	M_{EC4} / M_{exp}
	(mm x mm x mm)	(Mpa)	(MPa)				(kN-m)	(kN-m)	
E1	100 x 4 x 1000	27	350	25	10	0.30	13.11	13.19	1.01
E2	100 x 4 x 1000	35	350	25	10	0.30	15.00	14.50	0.97
E3	100 x 4 x 1000	44	350	25	10	0.30	19.06	16.00	0.84
E4	125 x 3 x 1000	35	350	42	8	0.30	19.87	23.71	1.19
E5	125 x 4 x 1000	35	350	31	8	0.30	23.88	26.87	1.13
E6	125 x 5 x 1000	35	350	25	8	0.30	27.90	29.35	1.05
E7	100 x 4 x 500	44	350	25	5	0.30	21.92	16.00	0.73
E8	100 x 4 x 300	44	350	25	3	0.30	25.48	16.00	0.63
E9	150 x 5 x 1000	44	350	30	7	0	0.00	0.00	0.00
E10	150 x 5 x 1000	44	350	30	7	0.30	46.83	48.54	1.04
E11	150 x 5 x 1000	44	350	30	7	0.45	53.73	59.83	1.11
								Mean	0.88
								Standard deviation	0.33

99
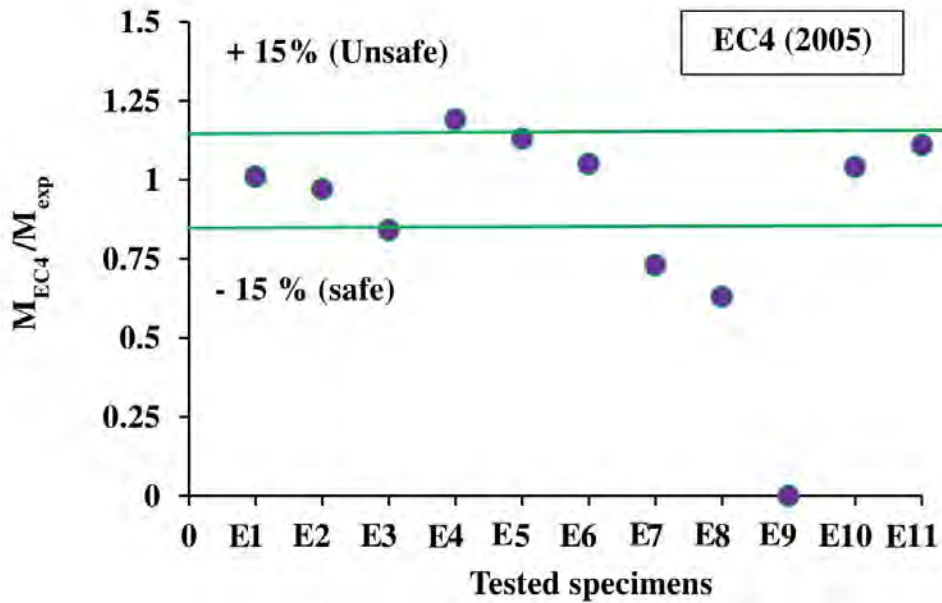
Figure 5.4 Comparison between the predicted (EC4) and measured moment

5.5.2 American Institute of Steel Construction (AISC)

a) Compared with ultimate axial loads of tested specimens

AISC (2010) composite column design presents different equations for the cross-sectional strength depending on the shape of the column and the ratio maximum dimension to thickness. Besides, the expression for the nominal axial capacity of stub columns incorporates the effect of slenderness. AISC (2010) presented the best and safe prediction of the ultimate axial strengths of specimens with a mean of 0.98 and standard deviation of 0.17. The predicted axial strength for each specimen is given in Table 5.8 and the graphical representation of this data is displayed in Figure 5.5.

Table 5.8 Comparisons of ultimate axial strengths between test results and design codes (AISC 2010)

| Symbol	B x t x L	$f_c^/$	f_y	B/t	L/B	e/B	P_{exp}	P_{AISC}	P_{AISC} / P_{exp}
	(mm x mm x mm)	(Mpa)	(MPa)				(kN)	(kN)	
E1	100 x 4 x 1000	27	350	25	10	0.30	377	418	1.11
E2	100 x 4 x 1000	35	350	25	10	0.30	466	444	0.95
E3	100 x 4 x 1000	44	350	25	10	0.30	595	488	0.82
E4	125 x 3 x 1000	35	350	42	8	0.30	480	555	1.16
E5	125 x 4 x 1000	35	350	31	8	0.30	586	621	1.06
E6	125 x 5 x 1000	35	350	25	8	0.30	693	710	1.02
E7	100 x 4 x 500	44	350	25	5	0.30	688	500	0.73
E8	100 x 4 x 300	44	350	25	3	0.30	801	515	0.64
E9	150 x 5 x 1000	44	350	30	7	0	1474	1687	1.14
E10	150 x 5 x 1000	44	350	30	7	0.30	968	1021	1.05
E11	150 x 5 x 1000	44	350	30	7	0.45	738	844	1.14
								Mean	0.98
								Standard deviation	0.17
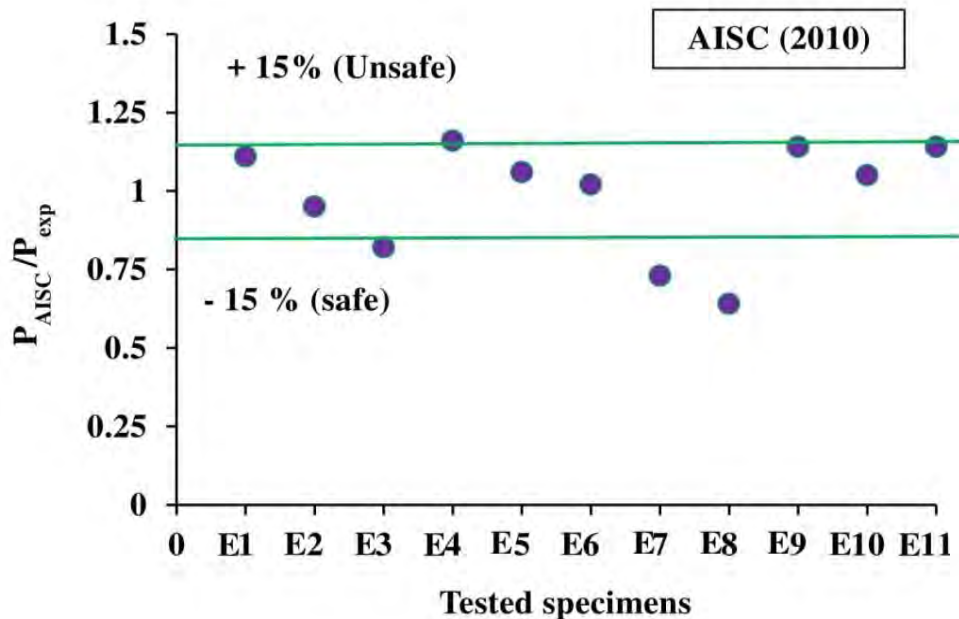
Figure 5.5 Comparison between the predicted (AISC) and measured strength

b) Compared with ultimate moments of tested specimens

It can also be seen from Figure 5.6 and Table 5.9 that, AISC-LFRD (2010) underestimates the ultimate bending moment of the tested specimens where the

average M_{AISC}/M_{exp} ratio is 0.81 with a standard deviation of 0.16. In addition, the predicted accuracy of AISC is more accurate than that of EC4, where the average M_{EC4}/M_{exp} ratio was 0.88.

Table 5.9   Comparisons of ultimate bending moments between test results and design codes (AISC 2010)

Symbol	B x t x L	$f_c^/$	f_y	B/t	L/B	e/B	M_{exp}	M_{AISC}	M_{AISC} / M_{exp}
	(mm x mm x mm)	(Mpa)	(MPa)				(kN-m)	(kN-m)	
E1	100 x 4 x 1000	27	350	25	10	0.3	13.11	12.75	0.97
E2	100 x 4 x 1000	35	350	25	10	0.3	15.00	13.54	0.90
E3	100 x 4 x 1000	44	350	25	10	0.3	19.06	14.67	0.77
E4	125 x 3 x 1000	35	350	42	8	0.3	19.87	21.00	1.06
E5	125 x 4 x 1000	35	350	31	8	0.3	23.88	23.71	0.99
E6	125 x 5 x 1000	35	350	25	8	0.3	27.90	26.64	0.95
E7	100 x 4 x 500	44	350	25	5	0.3	21.92	15.00	0.68
E8	100 x 4 x 300	44	350	25	3	0.3	25.48	15.35	0.60
E9	150 x 5 x 1000	44	350	30	7	0	0.00	0.00	0.00
E10	150 x 5 x 1000	44	350	30	7	0.3	46.83	45.72	0.98
E11	150 x 5 x 1000	44	350	30	7	0.45	53.73	56.45	1.05
								Mean	0.81
								Standard deviation	0.30
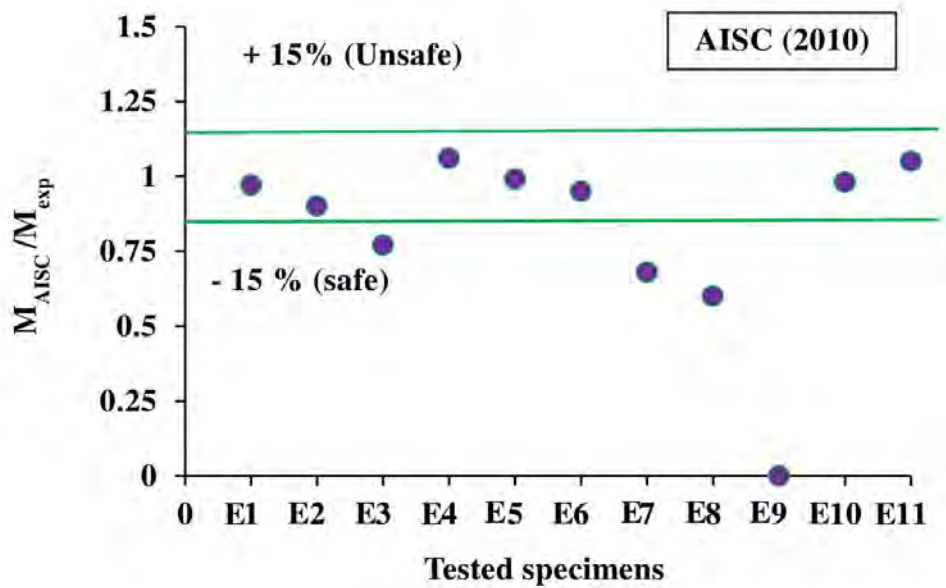
Figure 5.6   Comparison between the predicted (AISC) and measured moment

5.6 Comparison of Results with Axial Load-Bending Moment (P-M) Interaction Curves

To evaluate the applicability of current design codes to the composite sections, the test results were compared with the P-M interaction curves predicted by current design codes: AISC-LFRD (2010) and Eurocode 4 (2005) under the variation of concrete compressive strength (f_c'), cross-sectional slenderness ratio (B/t), column overall slenderness ratio (L/B) and load eccentricity ratio (e/B).

5.6.1 Effect of concrete compressive strength (f_c')

Figure 5.7 shows the theoretical P-M interaction curves of the tested CFST columns with varying concrete compressive strength. It can be observed from Table 5.10 that, the increase of maximum load P_A is more than the increase of maximum bending moment M_B for specimens with higher f_c'. It indicates that the load resistivity of the specimen is increased with the increase of concrete compressive strength. This is attributed to the fact that the load resisting capability of high strength concrete is much higher than the low strength concrete. Such kind of investigation on square section also implies that for CFST columns with large axial load (P_A) and small bending moment (M_B), the use of high strength concrete will benefit more in term of resistance.

Table 5.10 Comparison between test results and code predictions of CFST specimens with varying concrete compressive strength

Symbol	B x t x L	f_c'	P_A (AISC)	% ΔP_A (AISC)	M_A (AISC)	% ΔM_A (AISC)	P_A (EC4)	% ΔP_A (EC4)	M_A (EC4)	% ΔM_A (EC4)
	(mm x mm x mm)	(Mpa)	(kN)		(kN-m)		(kN)	(kN)	(kN-m)	(kN-m)
E1	100 x 4 x 1000	27	687	–	20.04	–	757	–	21.02	–
E2	100 x 4 x 1000	35	736	+ 7%	20.35	+ 2%	821	+ 8%	21.35	+ 2%
E3	100 x 4 x 1000	44	798	+ 16%	20.68	+ 3%	900	+ 19%	21.70	+ 3%

(a) AISC (2010)   (b) EC4 (2005)
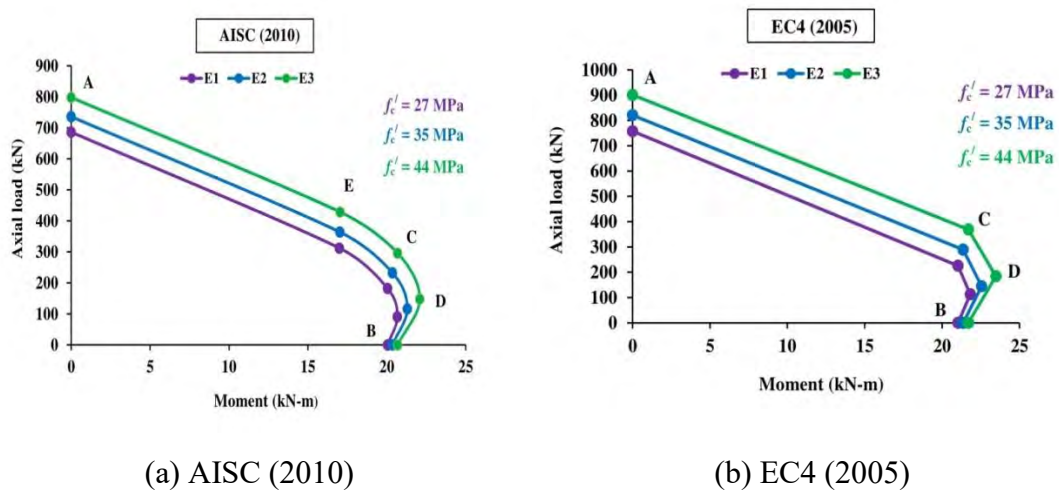
Figure 5.7   P-M Diagrams comparison of CFST columns with varying concrete
compressive strength according to (a) AISC (2010) and (b) EC4 (2005)

It can be seen from Figure 5.8, Table 5.11 and 5.12 that, both codes provide much
safer predictions for the specimens with higher concrete compressive strength.

Table 5.11   Comparison between test results and AISC (2010) of CFST columns
with varying concrete compressive strength

Symbol	B x t x L	$f_c^/$	P_{exp}	P_{AISC}	$\dfrac{P_{AISC}}{P_{exp}}$	M_{exp}	M_{AISC}	$\dfrac{M_{AISC}}{M_{exp}}$
	(mm x mm x mm)	(Mpa)	(kN)	(kN)		(kN-m)	(kN-m)	
E1	100 x 4 x 1000	27	377	418	1.15	13.11	12.75	0.97
E2	100 x 4 x 1000	35	466	444	0.97	15.00	13.54	0.90
E3	100 x 4 x 1000	44	595	488	0.82	19.06	14.67	0.77

Table 5.12   Comparison between test results and EC4 (2005) of CFST columns with
varying concrete compressive strength

Symbol	B x t x L	$f_c^/$	P_{exp}	P_{EC4}	$\dfrac{P_{EC4}}{P_{exp}}$	M_{exp}	M_{EC4}	$\dfrac{M_{EC4}}{M_{exp}}$
	(mm x mm x mm)	(Mpa)	(kN)	(kN)		(kN-m)	(kN-m)	
E1	100 x 4 x 1000	27	377	440	1.17	13.11	13.19	1.01
E2	100 x 4 x 1000	35	466	470	1.01	15.00	14.50	0.97
E3	100 x 4 x 1000	44	595	530	0.89	19.06	16.00	0.84

(a) Column E1 ($f_c^{/}$ = 27 MPa) (b) Column E2 ($f_c^{/}$ = 35 MPa)

(c) Column E3 ($f_c^{/}$ = 44 MPa)
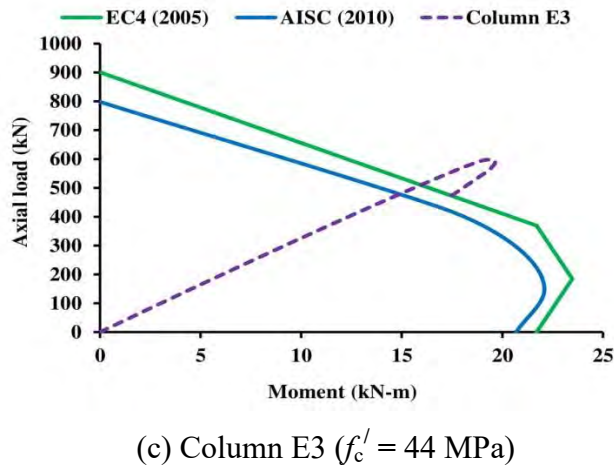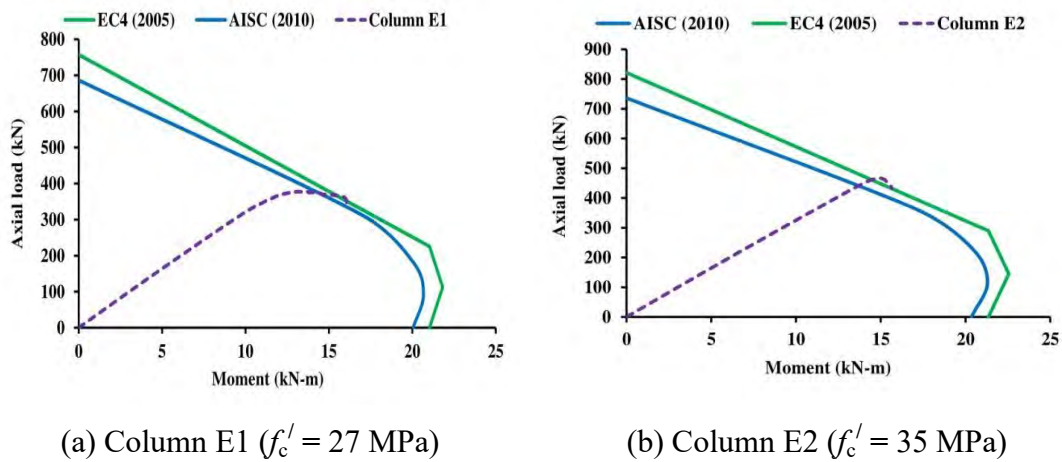
Figure 5.8   Comparison of test and predictions in axial load-bending moment interaction with varying concrete compressive strength

5.6.2   Effect of cross-sectional slenderness ratio (B/t)

It can be noticed from Figure 5.9 and Table 5.13 that, the increase of maximum bending moment M_B is more than the increase of maximum load P_A for specimens with lower B/t ratio. It refers that the moment resisting capability of the specimen is increased with the decrease of cross-sectional slenderness ratio. This is attributed due to the high rigidity and better moment resisting capability of the specimen with thicker steel tube. The use of thicker steel tube or high tensile steel will be beneficial for CFST columns with small axial load (P_A) and large bending moment (M_B).

Table 5.13 Comparison between test results and code predictions of CFST specimens with varying cross-sectional slenderness ratio

Symbol	B x t x L	B/t	P_A (AISC)	$\% \Delta P_A$ (AISC)	M_A (AISC)	$\% \Delta M_A$ (AISC)	P_A (EC4)	$\% \Delta P_A$ (EC4)	M_A (EC4)	$\% \Delta M_A$ (EC4)
	(mm x mm x mm)		(kN)		(kN-m)		(kN)	(kN)	(kN-m)	(kN-m)
E4	125 x 3 x 1000	42	892	–	26.82	–	999	–	31.42	–
E5	125 x 4 x 1000	31	1038	+ 16%	33.03	+ 23%	1147	+ 15%	40.45	+ 29%
E6	125 x 5 x 1000	25	1160	+ 30%	40.37	+ 50%	1270	+ 27%	49.03	+ 56%

(a) AISC (2010)   (b) EC4 (2005)
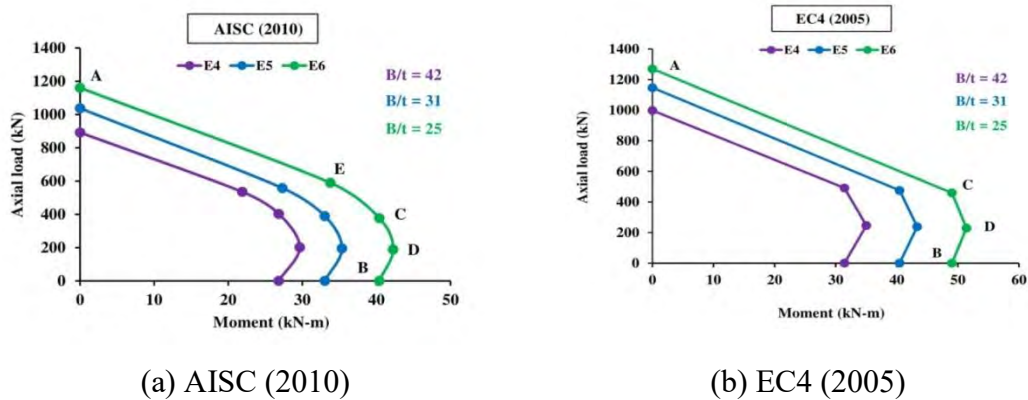
Figure 5.9 P-M Diagrams comparison of CFST columns with varying cross-sectional slenderness ratio according to (a) AISC (2010) and (b) EC4 (2005)

It can be observed from Figure 5.10, Table 5.14 and 5.15 that, conservative prediction of AISC (2010) increases with the decrease of B/t ratio, whilst EC4 remains same with unsafe prediction.

Table 5.14 Comparison between test results and AISC (2010) of CFST columns with varying cross-sectional slenderness ratio

Symbol	B x t x L	B/t	P_{exp}	P_{AISC}	$\dfrac{P_{AISC}}{P_{exp}}$	M_{exp}	M_{AISC}	$\dfrac{M_{AISC}}{M_{exp}}$
	(mm x mm x mm)		(kN)	(kN)		(kN-m)	(kN-m)	
E4	125 x 3 x 1000	42	480	555	1.16	19.87	21.00	1.06
E5	125 x 4 x 1000	31	586	621	1.06	23.88	23.71	0.99
E6	125 x 5 x 1000	25	693	710	1.02	27.90	26.64	0.95

Table 5.15 Comparison between test results and EC4 (2005) of CFST columns with varying cross-sectional slenderness ratio

Symbol	B x t x L	B/t	P_{exp}	P_{EC4}	P_{EC4} / P_{exp}	M_{exp}	M_{EC4}	M_{EC4} / M_{exp}
	(mm x mm x mm)		(kN)	(kN)		(kN-m)	(kN-m)	
E4	125 x 3 x 1000	42	480	631	1.31	19.87	23.71	1.19
E5	125 x 4 x 1000	31	586	710	1.21	23.88	26.87	1.13
E6	125 x 5 x 1000	25	693	791	1.14	27.90	29.35	1.05
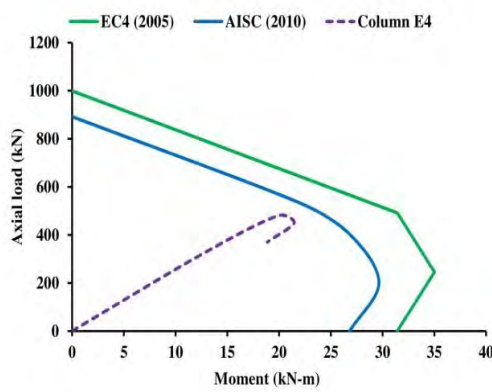
(a) Column E4 (B/t = 42)
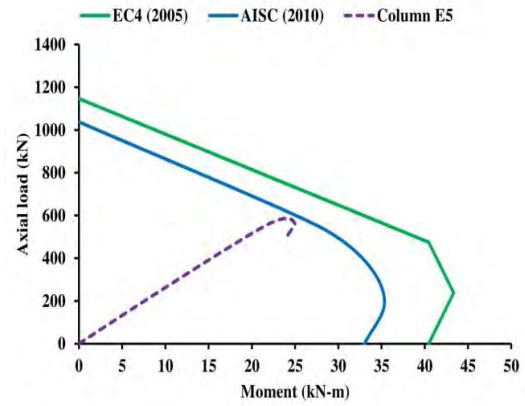
(b) Column E5 (B/t = 31)
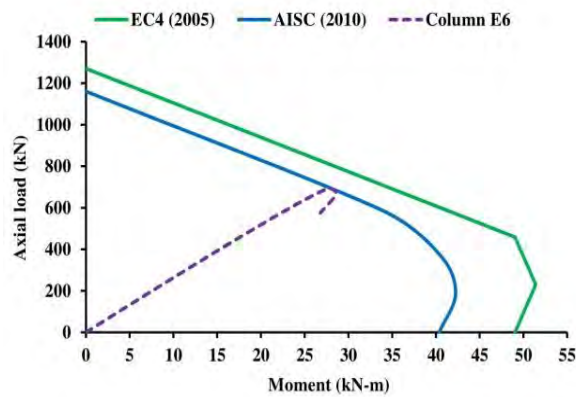
(c) Column E6 (B/t = 25)

Figure 5.10 Comparison of test and predictions in axial load-bending moment interaction with varying cross-sectional slenderness ratio

5.6.3 Effect of global slenderness ratio (L/B)

It can be pointed out from Table 5.16, 5.17 and Figure 5.11 that, safe prediction of both codes increases with the decrease of L/B ratio. This is attributed to the fact that the prediction of EC4 is not accurate for the consideration of global slenderness ratio and full length effect. Further investigation should be needed to modify EC4 with considering such parameters.

Table 5.16 Comparison between test results and AISC (2010) of CFST columns with varying global slenderness ratio

Symbol	B x t x L	L/B	P_{exp}	P_{AISC}	P_{AISC} / P_{exp}	M_{exp}	M_{AISC}	M_{AISC} / M_{exp}
	(mm x mm x mm)		(kN)	(kN)		(kN-m)	(kN-m)	
E3	100 x 4 x 1000	10	595	488	0.82	19.06	14.67	0.77
E7	100 x 4 x 500	5	688	500	0.73	21.92	15.00	0.68
E8	100 x 4 x 300	3	801	515	0.64	25.48	15.35	0.60

Table 5.17 Comparison between test results and EC4 (2005) of CFST columns with varying global slenderness ratio

Symbol	B x t x L	L/B	P_{exp}	P_{EC4}	P_{EC4} / P_{exp}	M_{exp}	M_{EC4}	M_{EC4} / M_{exp}
	(mm x mm x mm)		(kN)	(kN)		(kN-m)	(kN-m)	
E3	100 x 4 x 1000	10	595	530	0.89	19.06	16.00	0.84
E7	100 x 4 x 500	5	688	530	0.77	21.92	16.00	0.73
E8	100 x 4 x 300	3	801	530	0.66	25.48	16.00	0.63
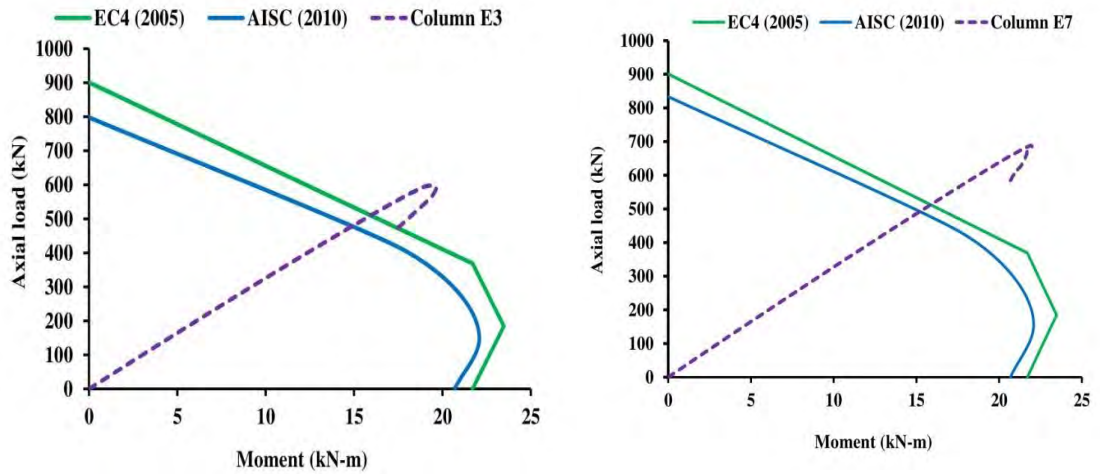
(a) Column E3 (L/B = 10)　　　　　　　(b) Column E7 (L/B = 5)
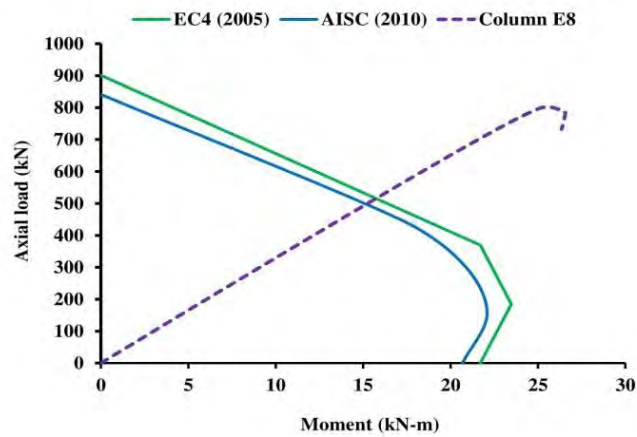
(c) Column E8 (L/B = 3)

Figure 5.11 Comparison of test and predictions in axial load-bending moment interaction with varying global slenderness ratio

5.6.4　Effect of load eccentricity ratio (e/B)

Figure 5.12, Table 5.18 and 5.19 show that both codes remain unsafe for the prediction of the specimen with higher load eccentricity ratio. More investigations should be needed to conduct conservative predictions of AISC (2010) and EC4 (2005) under uniaxial eccentric loading condition.

Table 5.18 Comparison between test results and AISC (2010) of CFST columns with varying load eccentricity ratio

Symbol	B x t x L	e/B	P_{exp}	P_{AISC}	P_{AISC} / P_{exp}	M_{exp}	M_{AISC}	M_{AISC} / M_{exp}
	(mm x mm x mm)		(kN)	(kN)		(kN-m)	(kN-m)	
E9	150 x 5 x 1000	0	1474	1687	1.14	0.00	0.00	0.00
E10	150 x 5 x 1000	0.30	968	1021	1.05	46.83	45.72	0.98
E11	150 x 5 x 1000	0.45	738	844	1.14	53.73	56.45	1.05

Table 5.19 Comparison between test results and EC4 (2005) of CFST columns with varying load eccentricity ratio

Symbol	B x t x L	e/B	P_{exp}	P_{EC4}	P_{EC4} / P_{exp}	M_{exp}	M_{EC4}	M_{EC4} / M_{exp}
	(mm x mm x mm)		(kN)	(kN)		(kN-m)	(kN-m)	
E9	150 x 5 x 1000	0	1474	1859	1.26	0.00	0.00	0.00
E10	150 x 5 x 1000	0.30	968	1078	1.11	46.83	48.54	1.04
E11	150 x 5 x 1000	0.45	738	888	1.20	53.73	59.83	1.11
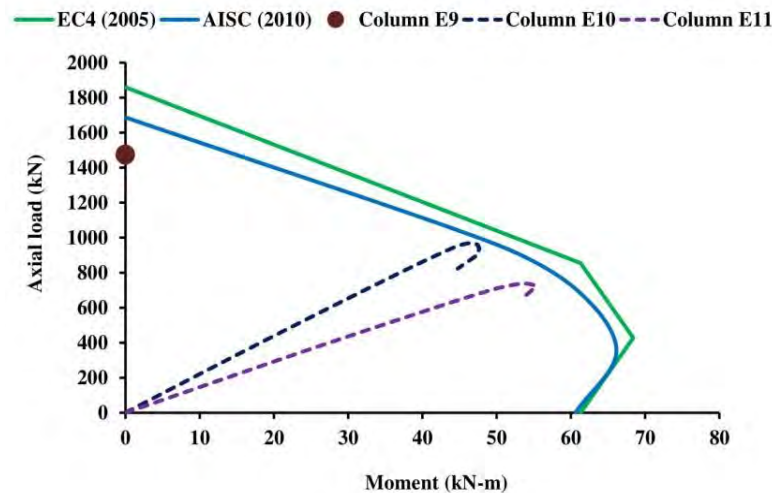
Figure 5.12 Comparison of test and predictions in axial load-bending moment interaction with varying load eccentricity ratio

5.7   Summary

Eurocode 4 (2005) somewhat overestimated the ultimate axial strengths but underestimated the ultimate bending moments of the tested square CFST columns in built-up steel sections, whilst AISC-LFRD (2010) presented the best and safe prediction for both of them. EC4 (2005) predicted higher capacity than the experimental results about 6%. Individually both codes provided much safer predictions for the specimens with higher concrete compressive strength but lower B/t ratio and L/B ratio, whilst both of them remain unsafe with higher load eccentricity ratio. In general, both codes showed good agreement with the experimental results.

Chapter 6
CONCLUSIONS AND RECOMMENDATIONS

6.1 General Conclusions

In this study, eleven square CFST columns with a variety of geometric and material properties were tested under uniaxial eccentric compression. Effects of global slenderness ratio (L/B), cross-sectional slenderness ratio (B/t), concrete compressive strength $(f_c^/)$ and load eccentricity ratio (e/B) on the load strain response, failure behavior, mid-height deflection and performance indices of the test columns were investigated. Comparisons of the test results were also made with several existing design codes. The following conclusions can be drawn within the limited scope of this study:

i. The typical failure mode of the eccentrically loaded specimen with higher global slenderness ratio (L/B = 7 and 10) was characterized by global buckling where buckling was initiated by steel yielding and this was followed by cracking of concrete at the tension side of the eccentrically loaded specimen. Cracking of concrete and steel yielding were also occurred in stockier columns with lower L/B ratio (L/B = 3 and 5).

ii. Stiffness and ultimate capacity of the tested column decreased with the increase of cross-sectional width by tube thickness (B/t) ratio and load eccentricity ratio (e/B), whilst they increased with the increase of concrete compressive strength $(f_c^/)$ and the decrease of global slenderness ratio (L/B) of the specimen.

iii. Axial strain at peak load and ductility index of the tested specimen decreased with the increase of concrete compressive strength, B/t ratio and L/B ratio but increased with the increase of e/B ratio of the specimen. On the other hand, mid-height deflection increased with the increase of B/t, L/B and e/B ratio, whilst decreased with the increase of concrete compressive strength of the tested specimen.

iv. The ultimate axial load of eccentrically loaded (e = 0.03 B) CFST columns was observed to increase by 24% and 58% respectively with the increase of concrete compressive strength from 27 MPa to 35 MPa and 44 MPa respectively. However, these increase in the concrete strength resulted in a significant decrease (19% to 35 MPa and 40% for 44 MPa concrete) in the ductility index of the CFST columns.

v. Increase in the plate slenderness ratio (B/t) from 25 to 32 and 42, resulted in 16% and 31% decrease in the ultimate axial capacity of the CFST columns.

vi. The load eccentricity ratio was found to have significant effect on the axial capacity and failure behavior of CFST columns. Increasing the e/B ratio from 0 to 0.30 and 0.45, resulted in 35% and 50% increase in axial capacity of the columns. On the other hand, similar increase in e/B ratio was found to decrease the ductility index by 29% and 38% respectively. Moreover, as the eccentricity increases the second order moment was found to increase significantly (about 47% and 54% increase was obtained for the change in e/B ratio for 0 to 0.30 and 0.45 respectively).

vii. Eurocode 4 (2005) somewhat overestimated the ultimate axial strengths but underestimated the ultimate bending moments of the tested square CFST columns in built-up steel sections, whilst AISC-LFRD (2010) presented the best and safe prediction for both of them. EC4 (2005) predicted higher capacity than the experimental results about 6%. In general, both codes showed good agreement with the experimental results.

6.2 Recommendations for Future Study

The tests reported as part of this study concentrated on the ultimate load capacity and load-displacement relationships of CFST-HSC columns. In order to derive constitutive models for determining the properties of such columns, detailed examination of the longitudinal and transverse load-strain relationships for all parametric ranges are required. It is considered that in further research studies, the following aspects should be given special attention:

i. The stress-strain relationship of the eccentrically loaded CFST columns and the effective stiffness of the composite sections should be inspected.

ii. Proceeding assessment of the behavior of the CFST column under isolated conditions, studies should be extended to account for the eccentric partial compression and the application of CFST columns as frame elements.

iii. Concrete confinement, interaction between the steel and concrete, cyclic load resistance capacity, different loading condition and the use of stiffeners in different shapes CFST columns should be investigated.

iv. Fire resistance of CFSTs is a common concern, and must be carefully studied before applying these columns in-filled with various high-performance concretes in practice. Future research is necessary to determine the behavior of concentrically and eccentrically loaded CFST columns under elevated temperatures.

REFERENCES

ACI 318R (2014), "Building code requirements for structural concrete." *American Concrete Institute,* ACI, Detroit.

AIJ (2008). "Recommendations for design and construction of concrete filled steel tubular structures." *Architectural Institute of Japan*, Tokyo, Japan.

AISC-LRFD (2010), "AISC manual for steel construction." *American Institute for Steel Construction*, USA.

AS5100 (2004), "Bridge design-steel and composite construction." *Australian Standard*.

ASTM D638-02a (2003), "Standard test method for tensile properties of plastics." *American Society of Testing Materials*.

Bergmann, R. (1994). "Load introduction in composite columns filled with high strength concrete," Tubular Structures VI, *Proceedings of the Sixth International Symposium on Tubular Structures*, 373-380.

BNBC (2016), "Bangladesh national building code." Dhaka, Draft version.

CSA Standard S16 (2009), "Design of steel structures." Published by *Canadian Standards Association*, A not-for-profit private sector organization 5060 Spectrum Way, Suite 100, Mississauga, Ontario, Canada.

DBJ/T 13-51-2010 2010. "Technical specification for concrete-filled steel tubular structures". Department of Housing and Urban-Rural Development of Fujian Province, Fuzhou, China.

Dundu, M. (2012). "Compressive strength of circular concrete filled steel tube columns." *Thin-Walled Structures*, *56*, 62-70.

European Committee for Standardization (1994). "Eurocode 4: Design of Composite Steel and Concrete Structures." CEN.

Fujimoto, T., Mukai, A., Nishiyama, I., and Sakino, K. (2004). "Behavior of eccentrically loaded concrete-filled steel tubular columns." *Journal of Structural Engineering*, 130(2), 203-212.

Gabel, R. J., Carver, R. M., and Gerometta, M. (2015). "The skyscraper surge continues in 2015, The „Year of 100 Supertalls."" 10.

Giakoumelis, G. and Lam, D. (2003). "Axial capacity of circular concrete-filled tube columns," *Journal of Constructional Steel Research*, 60, 1049-1068.

Guo, L., Zhang, S., Kim, W. J., and Ranzi, G. (2007). "Behavior of square hollow steel tubes and steel tubes filled with concrete." *Thin-Walled Structures*, 45(12), 961-973.

Han, L. H. and Yan, S. Z. (2000). "Experimental studies on the strength with high slenderness ratio concrete filled steel tubular columns," Composite and Hybrid Structures, *Proceedings of the Sixth ASCCS International Conference on Steel-Concrete Composite Structures*, 419-426.

Han, L. H., Li, W., and Bjorhovde, R. (2014). "Developments and advanced applications of concrete-filled steel tubular (CFST) structures: Members." *Journal of Constructional Steel Research*, 100, 211–228.

Han, L. H., Ren, Q. X. & Li, W. (2010). "Tests on inclined, tapered and STS concrete-filled steel tubular (CFST) stub columns." *Journal of Constructional Steel Research*, 66(10), 1186–1195.

Ibañez, C., Hernández-Figueirido, D., and Piquer, A. (2018). "Shape effect on axially loaded high strength CFST stub columns." *Journal of Constructional Steel Research*, 147, 247–256.

Kim, C. S., Park, H. G., Choi, I. R., and Chung, K. S. (2017). "Effect of Sustained Load on Ultimate Strength of High-Strength Composite Columns Using 800-MPa Steel and 100-MPa Concrete." *Journal of Structural Engineering*, 143(3), 04016189.

Kim, C. S., Park, H. G., Chung, K. S., and Choi, I. R. (2013). "Eccentric axial load capacity of high-strength steel-concrete composite columns of various sectional shapes." *Journal of Structural Engineering*, 140(4), 04013091.

Knowles, R. B. and Park, R. (1969). "Strength of concrete filled steel tubular columns," *Journal of the Structural Division, ASCE,* 95, 2565-2587.

Lee, H. J., Choi, I. R., and Park, H. G. (2016). "Eccentric compression strength of rectangular concrete-filled tubular columns using high-strength steel thin plates." *Journal of Structural Engineering*, 143(5), 04016228.

Li, W., Han, L. H., Ren, Q. X., and Zhao, X. L. (2013). "Behavior and calculation of tapered CFDST columns under eccentric compression." *Journal of Constructional Steel Research*, 83, 127-136.

Li, W., Ren, Q. X., Han, L. H. and Zhao, X. L. (2012). "Behaviour of tapered concrete-filled double skin steel tubular (CFDST) stub columns." *Thin-Walled Structures*, 57, 37–48.

Liang, Q. Q., Patel, V. I., and Hadi, M. N. S. (2012). "Biaxially loaded high-strength concrete-filled steel tubular slender beam-columns, Part I: Multiscale simulation." *Journal of Constructional Steel Research*, 75, 64–71.

117

Liu, D. (2006). "Behaviour of eccentrically loaded high-strength rectangular concrete-filled steel tubular columns." *Journal of Constructional Steel Research*, 62(8), 839-846.

Luksha, L. K., and Nesterovich, A. P. (1991). "Strength of tubular concrete cylinders under combined loading." *Proceedings of 3rd International Conference on Steel-Concrete Composite Structures*, Fukuoka, Japan, 67–71.

Mahgub, M., Ashour, A., Lam, D., and Dai, X. (2017). "Tests of self-compacting concrete filled elliptical steel tube columns." *Thin-Walled Structures*, 110, 27–34.

Masuo, K., Adachi, M., Kawabata, K., Kobayashi, M., and Konishi, M. (1991). "Buckling behavior of concrete filled circular steel tubular columns using light-weight concrete," *Proceedings of the Third International Conference on Steel-Concrete Composite Structures*, 95-100.

Mursi, M. and Uy, B. (2004). "Strength of slender concrete filled high strength steel box columns." *Journal of Constructional Steel Research*, 60(12), 1825–1848.

O'Shea, M. D. and Bridge, R. Q. (1994). "Tests of thin-walled concrete-filled steel tubes." *Preliminary Report*, Center for Advanced Structural Engineering, University of Sydney, Australia.

O'Shea, M. D. and Bridge, R. Q. (1997). "Behaviour of Thin-Walled Box Sections with Lateral Restraint." *Research Report No. R739*, School of Civil Engineering, University of Sydney, Sydney, Australia, March.

Ouyang, Y., and Kwan, A. K. H. (2018). "Finite element analysis of square concrete-filled steel tube (CFST) columns under axial compressive load." *Engineering Structures*, 156, 443-459.

Ouyang, Y., Kwan, A. K. H., Lo, S. H., and Ho, J. C. M. (2017). "Finite element analysis of concrete-filled steel tube (CFST) columns with circular sections under eccentric load." *Engineering Structures*, 148, 387-398.

Petrus, C., Hamid, H. A., Ibrahim, A., and Nyuin, J. D. (2016). "Behaviour of eccentrically loaded slender concrete filled steel tubes columns." *Jurnal Teknologi*, 78(5-4).

Portolés, J. M., Romero, M. L., Bonet, J. L., and Filippou, F. C. (2011). "Experimental study of high strength concrete-filled circular tubular columns under eccentric loading." *Journal of Constructional Steel Research*, 67(4), 623–633.

Qu, X., Chen, Z., and Sun, G. (2013). "Experimental study of rectangular CFST columns subjected to eccentric loading." *Thin-Walled Structures*, 64, 83-93.

Ren, Q. X., Han, L. H., Lam, D., and Li, W. (2014). "Tests on elliptical concrete filled steel tubular (CFST) beams and columns." *Journal of Constructional Steel Research*, 99, 149-160.

Ren, Q. X., Zhou, K., Hou, C., Tao, Z., and Han, L. H. (2018). "Dune sand concrete-filled steel tubular (CFST) stub columns under axial compression: Experiments." *Thin-Walled Structures*, 124, 291–302.

Sakino, K., Nakahara, H., Morino, S., and Nishiyama, I. (2004). "Behavior of Centrally Loaded Concrete-Filled Steel-Tube Short Columns." *Journal of Structural Engineering*, 130(2), 180–188.

Schneider, S. P. (1998). "Axially loaded concrete-filled steel tubes." *Journal of Structural Engineering*, 124(10), 1125–1138.

Shakir-Khalil, H. and Zeghiche, Z. (1989). "Experimental behavior of concrete-filled rolled rectangular hollow-section columns." *The Structural Engineer*, 67(19), 345-353.

Shanmugam, N. E., and Lakshmi, B. (2001). "State of the art report on steel–concrete composite columns." *Journal of Constructional Steel Research*, 57(10), 1041–1080.

Susantha, K. A. S., Ge, H., and Usami, T. (2001). "A capacity prediction procedure for concrete-filled steel columns." *Journal of Earthquake Engineering*, 5(4), 483–520.

Tam, V. W., Wang, Z. B. and Tao, Z. (2014). "Behaviour of recycled aggregate concrete filled stainless steel stub columns." *Materials and Sructures*, 47(1), 293–310.

Tao, Z., and Han, L. H. (2006). "Behaviour of concrete-filled double skin rectangular steel tubular beam–columns." *Journal of Constructional Steel Research*, 62(7), 631-646.

Tao, Z., and Han, L. H. (2006). "Behaviour of concrete-filled double skin rectangular steel tubular beam–columns." *Journal of Constructional Steel Research*, 62(7), 631-646.

Tao, Z., Han, L. H. and Wang, Z. B. (2005). "Experimental behaviour of stiffened concrete-filled thin-walled hollow steel structural (HSS) stub columns." *Journal of Constructional Steel Research*, 61(7), 962–983.

Tao, Z., Han, L. H. and Zhao, X. L. (2004). " Behaviour of concrete-filled double skin (CHS inner and CHS outer) steel tubular stub columns and beam-columns." *Journal of Constructional Steel Research*, 60(8), 1129–1158.

Tsuda, K., Matsui, C., and Mino, E. (1996). "Strength and Behavior of Slender Concrete Filled Steel Tubular Columns," Stability Problems in Designing, Construction and Rehabilitation of Metal Structures, *Proccedings of the Fifth International Colloquium on Structural Stability*, 489-500.

Uy, B. (2001). "Strength of short concrete filled high strength steel box columns." *Journal of Constructional Steel Research*, 57(2), 113–134.

Uy, B. (2008). "Stability and ductility of high performance steel sections with concrete infill." *Journal of Constructional Steel Research*, 64(7–8), 748–754.

Uy, B., Tao, Z., and Han, L.-H. (2011). "Behaviour of short and slender concrete-filled stainless steel tubular columns." *Journal of Constructional Steel Research*, 67(3), 360–378.

Varma, A. H., Ricles, J. M., Sause, R. and Lu, L. W. (2002). "Experimental behavior of high strength square concrete-filled steel tube beam-columns." *Journal of Structural Engineering*, 128(3), 309–318.

Wang, X., Liu, J., and Zhou, X. (2016). "Behaviour and design method of short square tubed-steel-reinforced-concrete columns under eccentric loading." *Journal of Constructional Steel Research*, 116, 193-203.

Xiamuxi, A., and Hasegawa, A. (2012). "A study on axial compressive behaviors of reinforced concrete filled tubular steel columns." *Journal of Constructional Steel Research*, 76, 144–154.

Xiong, D. X. (2012). "Structural behaviour of concrete filled steel tubes with high strength materials." *PhD thesis*, National University of Singapore.

Yang, Y. F. and Han, L. H. (2006). "Experimental behaviour of recycled aggregate concrete filled steel tubular columns." *Journal of Constructional Steel Research*, 62(12), 1310–1324.

Yang, Y. F., and Han, L. H. (2011). "Behaviour of concrete filled steel tubular (CFST) stub columns under eccentric partial compression." *Thin-Walled Structures*, 49(2), 379-395.

Young, B. and Ellobody, E. (2006). "Experimental investigation of concrete-filled cold-formed high strength stainless steel tube columns." *Journal of Constructional Steel Research*, 62(5), 484–492.

Yu, Q., Tao, Z. and Wu, Y. X. (2008). "Experimental behaviour of high performance concrete-filled steel tubular columns." *Thin-Walled Structures*, 46(4), 362–370.

Zeghiche, J., and Chaoui, K. (2005). "An experimental behaviour of concrete-filled steel tubular columns." *Journal of Constructional Steel Research*, 61(1), 53–66.

Zhang, S. and Zhou, M. (2000). "Stress-strain behavior of concrete-filled square steel tubes," Composite and Hybrid Structures, *Proceedings of the Sixth ASCCS International Conference on Steel-Concrete Composite Structures*, 403-409.

Zhao, X. L. and Grzebieta, R. (2002). "Strength and ductility of concrete filled double skin (SHS inner and SHS outer) tubes." *Thin-Walled Structures*, 40(2), 199–213.

Zhao, XL, Han, LH and Lu, H (2010). "Concrete-filled tubular members and connections," Spon Press London.

Zhong, S. T. and Miao, R. Y. (1988). "Stress-Strain Relationship and Strength of Concrete Filled Tubes," Composite Construction in Steel and Concrete, *Proceedings of the Engineering Foundation Conference*, 773-785.

Zhong-qiu, F., Bo-hai, J., Lei, L., & Wen-jie, Z. (2011). "Behavior of lightweight aggregate concrete filled steel tubular slender columns under axial compression." *ISSN 1816-112X*, 144.

Fu, Z. Q., Ji, B. H., Zhou, Y. & Wang, X. L. (2011). "An Experimental Behavior of Lightweight Aggregate Concrete Filled Steel Tubular Stub under Axial Compression." *In: GeoHunan International Conference 2011*, 24–32.

Zhu, M., Liu, J., Wang, Q., and Feng, X. (2010). "Experimental research on square steel tubular columns filled with steel-reinforced self-consolidating high-strength concrete under axial load." *Engineering Structures*, 32(8), 2278–2286.